Paired fermionic superfluids with s- and p-wave interactions

by

Jesper F. Levinsen

B.A. Physics, University of Copenhagen, 2001

M.S. Physics, University of Copenhagen, 2003

A thesis submitted to the

Faculty of the Graduate School of the

University of Colorado in partial fulfillment

of the requirements for the degree of

Doctor of Philosophy

Department of Physics

2007

This thesis entitled:
Paired fermionic superfluids with s- and p-wave interactions
written by Jesper F. Levinsen
has been approved for the Department of Physics

Victor Gurarie

Eric Cornell

Thomas DeGrand

Andrew Hamilton

James Shepard

Date

The final copy of this thesis has been examined by the signatories, and we find that both the content and the form meet acceptable presentation standards of scholarly work in the above mentioned discipline.

Levinsen, Jesper F. (Ph.D., Physics)

Paired fermionic superfluids with s- and p-wave interactions

Thesis directed by Assistant Professor Victor Gurarie

This thesis presents theoretical work in s- and p-wave resonantly paired Fermi gases at zero temperature. In the BEC regime of the wide-resonance s-wave BCS-BEC crossover, the chemical potential, speed of sound, condensate depletion, and ground state energy are computed. The quantities are calculated in a low density approximation. The bosonic scattering length is computed diagrammatically to be approximately $0.60a$ with a the fermionic scattering length, confirming a well-known result. The perturbative approach breaks down in the intermediate BCS-BEC crossover regime which is not investigated. Quantum corrections are computed in the low density expansion, and the mass-imbalanced two-species Fermi gas is investigated. For identical fermions, it is discussed how p-wave Feshbach resonances naturally fall into two classes of "weak" and "strong", depending on the short-distance physics. It is shown how bound fermionic trimers appear in the strongly-resonant superfluid. The appearance of the trimer under the strengthening of the resonance is investigated, and the lifetime of p-wave diatomic molecules due to collisional relaxation into trimers is estimated.

Acknowledgements

My journey towards becoming a physicist began at a very early age when I accompanied my dad to work at the Niels Bohr Institute. I was immediately captivated by all his different experiments and the magical feel of the place. The magic is still intact all these years later, although somehow I ended up with pen and paper as my primary tools. I guess it is difficult to foresee your future when you are only 7 years old? Having a pastor and a physicist as parents certainly proved an inspiration in my life and gave me a strong desire to discover and understand the world around me. I wish to thank my family for giving me a wonderful home to grow up in.

I enjoyed a very dynamic and exciting physics education at the Niels Bohr Institute with inspirational teachers such as Mogens Dam, Poul Henrik Damgaard, Henrik Smith, Jens Martin Knudsen, Finn Berg, Jan Ambjørn, Andrew Jackson, and many others. In particular, I should thank Poul Henrik Damgaard, not only for his careful guidance of my master's thesis, but also for suggesting that I apply to CU when I considered pursuing my graduate studies in the US. He told me I would love it here, and he was absolutely right!

From the day I arrived in Boulder, Victor has been a great advisor, always full of ideas for new and exciting projects. I have very much appreciated the independence he granted me in working on those projects which I found interesting. Over the past four years I have learned an immense amount from Victor, not only from the many times I would knock on his door to discuss different subjects, but also from his clear way

of approaching physics problems. Thanks a lot for always taking the time to explain difficult subjects to me!

Thanks also go to Jim Shepard who helped me take those important first steps towards solving difficult few-body problems. I should also mention his hugely useful class, through which I learned not to underestimate the power of Fetter and Walecka.

Over the past few years, I have been happy to share F425 with a host of officemates. I thoroughly appreciate our many stimulating discussions. In particular, I enjoyed the company of James McCollough and Quan Zhang, and our many discussions of physics and whatever else came to mind. Many more people have helped make my time in Boulder rich. I would especially like to thank Rune Niclasen, Mike Wilking, Jim Hirschauer, and Sungsoo Choi.

Last but not least I want to mention my girlfriend Klara. Klara continues to make me happy every day. She has taught me a lot about life and through her I have come to realize that life is not only about physics and football. I have immensely enjoyed our walks in the foothills, our trips, and our nights on the sofa watching a good movie. I look forward to every day with her.

Finally, I am grateful for the generous support I have enjoyed from the NSF, the Fulbright Program (through the Danish-American Fulbright Commission), and the Danish Research Agency.

Contents

Chapter

Chapter 1

Introduction

The history of superfluidity dates back to the discovery of superconductivity (charged superfluidity) in mercury by Kamerlingh Onnes [54]. Onnes observed that the electrical resistance of mercury disappears completely as the system is cooled below a critical temperature. A detailed microscopic explanation of the phenomenon of superconductivity proved elusive until the breakthrough in the 1950's by Bardeen, Cooper, and Schrieffer [5, 6]. The work of these authors (BCS theory) described how an arbitrarily weak attractive interaction in a degenerate Fermi gas leads to the formation of Cooper pairs [18], composed of weakly correlated pairs of fermions. The BCS theory explained the resulting appearance of a minimum excitation energy, or energy gap, and proved hugely succesful in understanding properties of superconductors. In particular, the BCS theory was able to correctly describe superfluid ^{3}He (fermionic atoms) but not superfluidity in liquid ^{4}He (bosonic atoms).

The development of the theory of Bose-Einstein condensation (BEC) occurred in parallel. In 1925 Einstein predicted [26] the macroscopic occupation of the single-particle ground state below a critical temperature in systems of particles obeying Bose statistics. This followed ideas by Bose on the quantum statistics of phonons [11]. In 1938 it was proposed by London [51, 52] that superfluidity in ^{4}He appears as a consequence of Bose-Einstein condensation. However, liquid ^{4}He is a strongly interacting system, very different from the weakly interacting limit studied by Einstein. In particular, the

number of particles occupying the single-particle ground state is strongly suppressed even at zero temperature, making the verification of Bose-Einstein condensation in liquid ^{4}He extremely difficult.

Considerable experimental effort was spent on attempting to obtain a BEC in a weakly interacting system. This was first achieved in 1995 in dilute gases of alkali atoms consisting of rubidium [3], sodium [21], and lithium [13]. In these experiments, the gas was cooled to temperatures for which the thermal de Broglie wavelength was of the order of the interparticle spacing and the BEC of weakly interacting atoms could be observed very clearly from the bimodal profile of the momentum distribution of the gas below the critical temperature. For a review of the subject of Bose-Einstein condensation in dilute gases see e.g. Refs. [19, 48, 55].

Soon after the observation of BEC in dilute gases of bosonic atoms, considerable attention was shifted to the study of Fermi gases. Applying the same experimental methods as in the bosonic gases proved challenging, as the s-wave interactions necessary for evaporative cooling are absent in spin-polarized Fermi gases. Thus the cooling of Fermi gases requires the presence of two distinguishable atoms, either in the form of two hyperfine spin components of the same atom or in mixtures of two atomic species. The first realization of a quantum degenerate two-component Fermi gas was obtained in a system of ^{40}K [23] where a temperature of $T \approx 0.2T_F$ was achieved (T_F is the Fermi temperature). Soon experiments followed in which quantum degeneracy was observed in ^{6}Li [72, 66] using sympathetic cooling with the ^{7}Li isotope.

In two-component ultracold Fermi gases, it should be possible to observe superfluidity according to the BCS theory. However, in these first experiments which reached quantum degeneracy, the critical temperature required to enter the superfluid phase was very small due to the diluteness and weak interactions in these gases. It was soon recognized [37, 70] that it is possible to enhance the weak interactions by the use of a scattering resonance known as a Feshbach resonance [27], thereby increasing the critical

temperature.

The use of Feshbach resonances opened up the possibility of studying both BCS superfluidity and BEC in the same system. These resonances are a characteristic of the two-body interactions and they allow for the precise control of the strength of interparticle interactions through the tuning of an applied magnetic field. For a weak and attractive interaction in a two-component Fermi gas, BCS theory is valid and the system is expected to form a BCS superfluid below a critical temperature. If the two-body interaction is made progressively stronger by the tuning of a magnetic field, at some critical strength of the interaction a two-body bound state becomes possible. The bound states are then bosons and form a BEC at sufficiently low temperatures. A BEC in a two-component Fermi gas was first observed in 2003 through the typical bimodal distributions [33, 40, 78]. The observation of the BCS superfluid phase is more subtle as the normal and superfluid phases share many properties. Convincing proof of superfluidity was obtained in 2005 through the observation of quantized vortices on both sides of a Feshbach resonance [77].

The possibility of a BCS-BEC crossover was originally proposed by Eagles in 1969 [24], and later by Leggett [47], and by Nozières and Schmitt-Rink [53]. These authors extended the mean field BCS model, valid in the weakly interacting BCS regime, to an arbitrary interaction strength, i.e. to well outside the regime of the original model's validity. It was discovered that under the strengthening of the interaction, the BCS gap equation, the mean field theory which describes the BCS state, evolves into the Schrödinger equation of a bound pair of fermionic atoms, correctly predicting the binding energy of the diatomic molecule. Furthermore, the results of these authors suggested that no phase transition occurs in the crossover, and thus the BCS and BEC phases are qualitatively the same phase. These results connected the two types of paired superfluidity, within mean field theory, and demonstrated how BCS and BEC are two extreme limits of the same system.

Despite the success of the gap equation in describing the BCS superfluid and the bound pairs in the BEC regime, it remained an open question whether it could correctly predict properties of the many-body system on the BEC side of a Feshbach resonance. The short answer is that it cannot; the gap equation, when applied to the BEC side of the crossover, implicitly assumes that the perturbative parameter is the interaction strength between the Feshbach molecules, i.e. that interactions are weak and scattering proceeds in the Born approximation. However, the Born approximation is known to fail to describe interactions between molecules properly [59]. It follows that while the BCS-BEC gap equation may describe the physics of the BEC regime at a qualitative level due to the lack of a phase transition, it is not to be trusted quantitatively. Thus there is a need for a reliable technique in the BEC regime, beyond mean field theory. This is one of the main subjects of this thesis (see also Ref. [50]).

In this thesis, the small parameter used in the BEC regime is the gas parameter na^3. Here, n is the density of fermions and a the s-wave scattering length between the two components of the Fermi gas. In the gas parameter expansion the chemical potential, ground state energy, speed of sound, and condensate depletion are computed. The results are seen to match the results of the standard dilute Bose gas [1, 29], however with the boson-boson scattering length related to the underlying fermion-fermion scattering length by

$$a_{\rm b} \approx 0.60a. \tag{1.1}$$

This result was first computed in Ref. [59] using a coordinate space formalism and the result is confirmed in this thesis using a diagrammatic technique. While the work reported in Ref. [50] and also in this thesis was in progress, the result (1.1) was computed independently by Brodsky *et al* [14] using essentially the same diagrammatic technique.

At the crossover, the scattering length a diverges. Thus, the parameter na^3 is no longer small, and properties of the gas close to the Feshbach resonance will not be

computed.

In the 1950's, perturbative corrections in powers of na^3 to the chemical potential and ground state energy were computed in the standard dilute Bose gas [45, 46, 76, 65, 38]. It is explicitly demonstrated in this thesis how the fact that the bosons are composed of fermions does not change the first two such corrections, apart from replacing $a_{\rm b}$ by $0.60a$. Even higher order contributions will depend explicitly on the presence of fermions in the problem but will not be considered here.

An interesting system is a two-component Fermi gas where the two components have different masses. For small mass imbalances, this system still displays the usual BCS-BEC crossover physics, with the few-body couplings slightly changed. However, as the mass imbalance is increased, the system becomes less stable until finally above a mass-ratio of 13.6 between the fermion components, the three-body system has been found [57] to contain bound states similar to the Efimov states [25] in systems of bosons. Properties of the mass imbalanced system such as the atom-molecule and molecule-molecule scattering lengths and the loss rate due to collisional relaxation have been calculated in Refs. [56, 57, 59] by use of a real-space technique, and the results will be confirmed in this thesis using a diagrammatic technique.

To date, experiments in ultracold gases of fermionic atoms have primarily studied gases consisting of two hyperfine states of the same atom. However, recently there has been a considerable interest in gases of identical fermionic atoms interacting close to a p-wave Feshbach resonance. The observation of p-wave Feshbach resonances has been reported in ^{40}K [69] and ^{6}Li [67], and theoretical work on the subject includes Refs. [36, 22, 35, 17, 34, 49]. In the p-wave superfluid, the BCS and BEC phases are no longer extreme limits of the same phase, rather they are separated by a genuine phase transition [74, 22], or in some cases a sequence of phase transitions [35, 17, 34]. The phase transition may be topological in some cases [62, 35, 43].

p-wave Feshbach resonances naturally fall into two categories of weak and strong.

Mean field theory in the crossover, as developed in Refs. [35, 17, 34], is only strictly valid for the weak resonances. On the other hand, the p-wave resonance studied in the experiment of Refs. [69, 30] is strong [34]. It is therefore of interest to study the strong resonances. It was first noticed by Y. Castin and collaborators [16] that in this regime, three fermions will form a bound state with angular momentum 1. These trimers are very strongly bound, with a size of the order of the short range physics which led to the formation of the Feshbach molecule. In this thesis, the appearance of the trimer under the strengthening of the resonance will be studied, and the decay rate due to inelastic collisions in which two molecules turn into a trimer and an atom will be estimated.

In this thesis the effects of a trapping potential will not be considered. Of course, the trapping potential is an essential ingredient in the experimental study of ultracold gases. However, the local density approximation has proven quite succesful in describing most properties of the system as long as the trapping potential is sufficiently smooth. For a review of trapped gases see e.g. Ref. [19].

The thesis is organized as follows. Chapter 2 presents some simple properties of the BCS-BEC crossover, and a model of the Feshbach resonance physics is introduced. Chapter 3 contains calculations of properties of the BEC-BCS crossover in the BEC regime, and in chapter 4 higher order corrections to the chemical potential and ground state energy are computed in the gas parameter expansion. The two-component mass-imbalanced Fermi gas in the BEC regime is studied in chapter 5, with emphasis on few body scattering lengths and collisional losses. The focus then shifts to p-wave resonantly coupled superfluids. In chapter 6 the system is described and the model introduced. Chapter 7 investigates the behavior of strongly-resonant p-wave superfluids and the appearance of bound trimer states under the strengthening of the resonance.

For simplicity of notation, Planck's constant $\hbar$ and Boltzmann's constant k_B have been set to 1.

Chapter 2

Physics of the BCS-BEC crossover

Soon after the achievement of Bose-Einstein condensation in dilute gases of bosonic alkali atoms, considerable attention was instead focused on gases comprised by fermionic atoms. The difference in quantum statistics makes these systems quite distinct at ultracold temperatures. As temperature is lowered, a bosonic system goes through a phase-transition to a BEC and this happens even in the absence of interactions. The Pauli principle, on the other hand, prevents two identical fermions from occupying the same single-particle state. Thus, in a non-interacting Fermi gas at zero temperature, the fermions will instead occupy the lowest energy states with exactly one fermion in each state. Hence, superfluidity in a gas of fermions can only stem from the presence of interactions. As the temperature of a Fermi gas is decreased, the crossover from a classical to a quantum behavior is smooth.

Consider a gas of spin 1/2 fermions at low temperature. If the interactions in the spin singlet channel are arbitrarily weak and attractive, the Fermi sea will be destabilized towards the formation of Cooper pairs [18]. The pairing occurs between fermions with equal and opposite momenta, the pairs being weakly correlated in momentum space. The pairs are highly overlapping in real space and should not be thought of as molecules. The ground state of the system is then no longer a Fermi sea, rather it is a superposition of Cooper pairs, the primary contribution arising from fermions close to the Fermi surface. This is explained in the famous work of Bardeen, Cooper

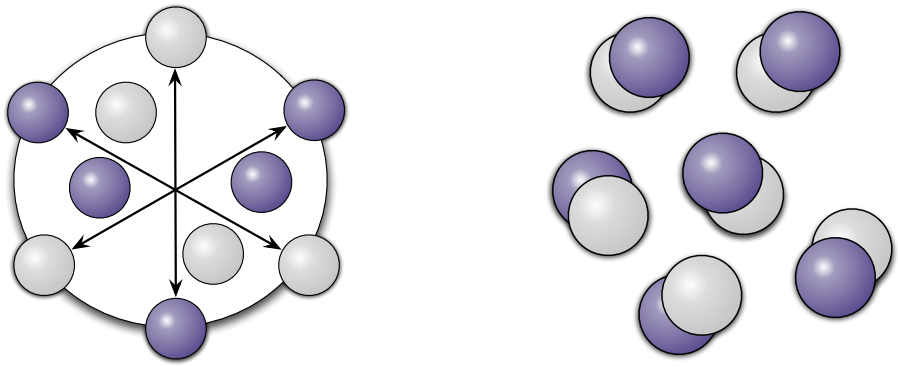

Figure 2.1: An illustration of the BCS-BEC crossover. The BCS regime on the left is illustrated as the pairing in momentum space of fermions, while the BEC regime on the right is illustrated as the real-space pairing of atoms into molecules. Paired fermions in the central regime between the two limits share features with the paired fermions in both limits.

and Schrieffer [5, 6]. The system studied by these authors consisted of pairs of spin-up and spin-down electrons and the resulting many-body system was a superconductor (a charged superfluid). In the context of ultracold two-species Fermi gases, the regime described is known as the BCS regime.

Imagine then that by some means the attractive interaction is increased. As the strength of the interaction is increased, a bound molecular state between two fermions becomes possible. The resulting bound state is then a boson, and a gas of these diatomic molecules may form a BEC. This is the essence of the BCS-BEC crossover; as the interaction between fermions is increased, there will be a continuous crossover from a BCS superfluid to a BEC of diatomic molecules. Thus the BCS and BEC regimes are merely limiting cases of the same system. The crossover is illustrated in Fig. 2.1. In the central region between the two limiting regimes, the bosonic pairs retain some properties of both Cooper pairs and diatomic molecules.

With the advent of BCS theory in the 1950's, the limiting regimes in the BCS-BEC crossover were well understood. However, the connection between these types of superfluids was not appreciated until the work of Eagles in 1969 [24], and the later

works of Leggett [47] as well as Nozières and Schmitt-Rink [53] in the 1980's. These authors started from a BCS mean-field theory which is valid only for weak attractive interactions. They extended the original model to arbitrarily strong attractive interactions, well outside the range of validity of the model. The mean field equation which describes properties of the BCS superfluid is known as the gap equation and it was discovered [47, 53] that the gap equation evolves into the Schrödinger equation of a bound pair of fermions under the strengthening of the interaction. Thus the results of these authors connected the BCS superfluid with the BEC of condensed pairs of fermionic atoms, within a mean field approach. Finite temperature studies [53, 64] further showed that the transition temperature evolves smoothly between the two regimes. The results suggested a smooth crossover without any phase transition. It should be emphasized that the results obtained by this method, while qualitatively correct due to the lack of a phase transition, are not quantitatively correct in the BEC regime, since the mean field approach is not strictly valid. This point will be discussed further in chapter 3.

The crucial tool which allows the experimental control over the interaction strength in a two-component Fermi gas is a *Feshbach resonance* [27, 28, 71]. A Feshbach resonance is an intrinsic two-body phenomenon. Consider the interaction between two fermionic atoms; at short distances the interaction is repulsive, while at large distances it is dominated by the van der Waals attraction which goes as $-C_6/r^6$. In general, the interatomic potentials contain several vibrational bound states. A Feshbach resonance occurs when the energy of a bound state in one scattering channel (usually called the closed channel) coincides with the energy of free particles scattering in another channel (the open channel). The two spin channels will in general have different magnetic moments. Typically, the closed channel is an approximate spin singlet, the open channel an approximate spin triplet, and the (large-distance) splitting between the energy levels is provided by the Zeeman effect. The Zeeman splitting may be tuned by adjusting the magnitude of an external magnetic field. The situation is illustrated in Fig. 2.2. The use

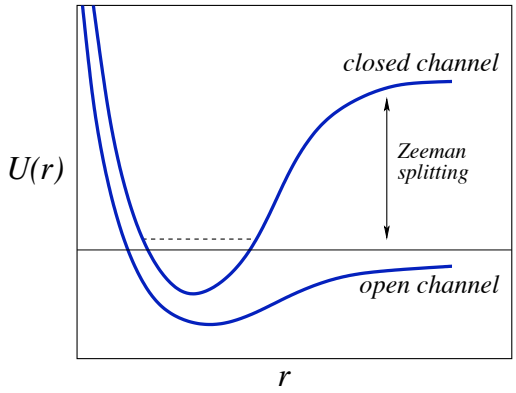

Figure 2.2: A Feshbach resonance occurs as the energy of the bound state in the closed channel crosses the energy of free particles scattering in the open channel.

of Feshbach resonances allows a very precise tuning of the strength of the interaction, which may even be changed in real time.

The presence of the (real or virtual) bound state in the closed channel can significantly alter scattering in the open channel. Across a Feshbach resonance, the (open channel) scattering length behaves as

$$a(B) = a_{\mathrm{nr}} \left[1 + \frac{\Delta B}{B - B_0} \right]. \tag{2.1}$$

Here, a_{nr} is the non-resonant scattering length, the value of the scattering length a far off-resonance, B_0 is the magnetic field position of the resonance, and ΔB is known as the magnetic resonance width (defined as the difference in magnetic field, $B_0 - B$, at which the scattering length becomes zero). The behavior of the scattering length is illustrated in Fig. 2.3.

Below, low-energy scattering properties relevant for the present work will be reviewed. A model of the resonant interactions, the so-called two-channel model, will be considered and its relevance to the Feshbach resonance physics described above will be discussed.

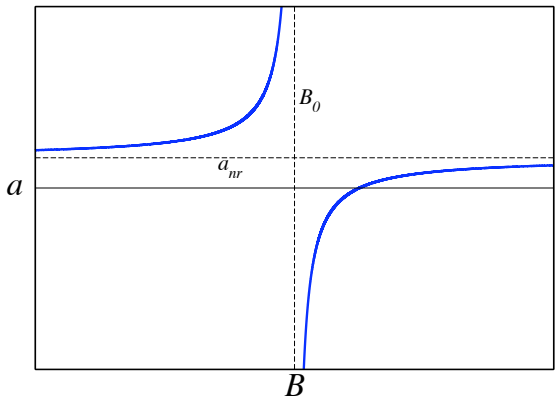

Figure 2.3: The scattering length a across a Feshbach resonance. On the left side of the resonance a real bound state exists.

2.1 Low energy scattering

This section contains a short discussion of the scattering theory relevant for this thesis. For elastic scattering of two particles via a centrally symmetric interaction potential, the scattering amplitude may be written as [44]

$$f(k,\theta) = \sum_{\ell=0}^{\infty} (2\ell+1) P_\ell(\cos\theta) f_\ell(k). \tag{2.2}$$

Here, $|\vec{k}| = |\vec{k}'| \equiv k$ is the magnitude of the incoming, $\pm\vec{k}$, and outgoing, $\pm\vec{k}'$, momenta, while θ is the scattering angle, with $\vec{k}\cdot\vec{k}' = k^2\cos\theta$. The probability of scattering through the solid angle Ω is related to the scattering amplitude by $d\sigma/d\Omega = |f|^2$. A centrally symmetric interaction $U(r)$ conserves the angular momentum ℓ and in this thesis, focus will be on s- and p-wave scattering, with

$$\begin{aligned} f_s(k) &\equiv f_{\ell=0}(k), \\ f_p(k) &\equiv f_{\ell=1}(k). \end{aligned} \tag{2.3}$$

The partial wave amplitudes may also be written in the form [44]

$$f_\ell(k) = \frac{1}{k^{-2\ell} F_\ell(k^2) - ik}. \tag{2.4}$$

The functions $F_\ell(k^2)$ are real and may be Taylor expanded in their arguments. Assuming that all the expansion coefficients take values of the order of some "natural" scale, it is seen that for low-energy scattering (e.g. in ultracold gases) the functions $F_\ell(k^2)$ are well approximated by the first few terms of their Taylor expansions. In particular it is important to note that the scattering amplitude at low energy only depends very weakly on the precise details of the complicated inter-atomic interaction potential $U(r)$.

For s-wave scattering, keeping only one term in the Taylor expansion of $F_\ell(k^2)$ amounts to

$$f_s(k) = \frac{1}{-a^{-1} - ik}, \tag{2.5}$$

where a is the s-wave scattering length. The scattering amplitude has one pole, located at $k_{\text{pole}} = +ia^{-1}$. This pole only corresponds to a real bound state if $a > 0$, otherwise it corresponds to a virtual bound state [44]. For $a > 0$ the real bound state has the energy

$$E = -\frac{1}{2m_{\text{r}}a^2}, \tag{2.6}$$

where m_{r} is the reduced mass in the two body system. The result already nicely matches the Feshbach resonance picture described above. However, the approximation Eq. (2.5) is deficient in one respect, it lacks a true resonance, i.e. a quasistationary state with a finite lifetime [34]. In order to correctly capture the possible existence of such states, the next order expansion

$$F_s(k^2) = -a^{-1} + \frac{1}{2} r_0 k^2 \tag{2.7}$$

is needed. The parameter r_0 is known as the effective range of the interaction potential $U(r)$.

An important energy scale is set by the effective range

$$\Gamma_0 = \frac{4}{mr_0^2}. \tag{2.8}$$

This energy scale is related to the magnetic field width by the approximate relationship $\Gamma_0 \approx 4m\mu_B^2 a_{\rm nr}^2 \Delta B^2$ [34]. The gas contains a finite atom density n, and consequently an additional length scale is set by the average particle spacing $n^{-1/3}$. The corresponding energy scale is the Fermi energy[1] ϵ_F given by

$$\epsilon_F = \frac{k_F^2}{2m}. \tag{2.9}$$

k_F is the Fermi momentum. The two energy scales allow the definition of a dimensionless parameter [34]

$$\gamma_s = \frac{\sqrt{8}}{\pi}\sqrt{\frac{\Gamma_0}{\epsilon_F}}, \tag{2.10}$$

which measures the *width* of the resonance. Resonances for which $\gamma_s \ll 1$ are termed *narrow* while those with $\gamma_s \gg 1$ are called *wide*. The precise criterion for the resonances to be wide was first derived in Ref. [15].

The distinction between wide and narrow resonances is quite important. Since the effective range only varies weakly across a Feshbach resonance, for narrow resonances γ_s provides a small parameter in which a quantitatively correct (in the zero width limit) perturbation theory may be formulated across the whole crossover [34]. In contrast, no such simplification occurs for wide resonances; the other dimensionless parameter which may be constructed from the three length scales a, r_0, and $n^{-1/3}$ is known as the *gas parameter*, $n^{1/3}a$. Since the scattering length diverges across the resonance, no small parameter exists close to a wide Feshbach resonance.

Most current experiments in ultracold two-component Fermi gases are carried out close to wide resonances. As these are the most relevant, the focus in the parts of this thesis concerning s-wave Feshbach resonances (chapters 3, 4, and 5) will be on wide resonances.

[1] In the absence of two-body bound states this would have been the conventional Fermi energy.

It is precisely for the narrow resonances that the two-body problem may display a true resonance (a positive energy state with a finite lifetime) [34]. Since the s-wave Feshbach resonances studied in this thesis are wide, these quasistationary states will be ignored. It is, however, interesting to note that although most experiments are performed close to wide resonances, since $\gamma_s \sim n^{-1/3}$ resonances which are wide in current experiments may become narrow if higher densities are achieved.

2.2 The two-channel model

A model which reflects the physics of the interaction in a two-component Fermi gas interacting close to a Feshbach resonance is provided by the two-channel model. It was first studied by Rumer in 1959 [63] and in the context of atomic Bose-Einstein condensates it was studied by Timmermans *et al* in 1999 [71]. Without interactions, the model describes the open-channel atoms and closed-channel molecules separately. Interaction between atoms and molecules is provided by an interconversion term.

The model is conveniently defined in terms of a functional integral

$$Z = \int \mathcal{D}\bar{\psi}_\uparrow \mathcal{D}\psi_\uparrow \mathcal{D}\bar{\psi}_\downarrow \mathcal{D}\psi_\downarrow \mathcal{D}b\mathcal{D}\bar{b}\; e^{iS_{\rm tc}}. \tag{2.11}$$

$\psi_\uparrow$ and $\psi_\downarrow$ are the fermionic atoms in two different hyperfine states (for simplicity denoted $\uparrow$ and $\downarrow$) and b is the closed-channel molecule. The action $S_{\rm tc}$ consists of three parts, $S_{\rm tc} = S_0 + S_{0\rm b} + S_{\rm fb}$. Of these, S_0 is the free action of fermions

$$S_0 = \sum_{\sigma=\uparrow,\downarrow} \int d^3x\, dt\, \bar{\psi}_\sigma \left(i\frac{\partial}{\partial t} + \frac{1}{2m}\frac{\partial^2}{\partial \mathbf{x}^2} + \mu \right) \psi_\sigma, \tag{2.12}$$

where μ is the chemical potential of the fermions. The free action of the closed-channel molecules is

$$S_{0\rm b} = \int d^3x\, dt\, \bar{b} \left(i\frac{\partial}{\partial t} + \frac{1}{4m}\frac{\partial^2}{\partial \mathbf{x}^2} + 2\mu - \epsilon_0 \right) b. \tag{2.13}$$

ϵ_0 is called the detuning and is the parameter which is typically controlled by a magnetic field in the experimental setup. That is, the detuning controls the proximity to the

Feshbach resonance. The interconversion term between open-channel atoms and the closed-channel molecule is given by

$$S_{\text{fb}} = -g \int d^3x\, dt\, \left[b\, \bar{\psi}_\uparrow \bar{\psi}_\downarrow + \bar{b}\, \psi_\downarrow \psi_\uparrow \right]. \tag{2.14}$$

The coupling g is the probability of converting a b particle to a pair of atoms. In itself, the interaction occurs at a point in space and is unphysical; the action needs to be supplemented by a cut-off, $\Lambda \sim \frac{1}{R_e}$ where R_e denotes the range of the (short-ranged) forces.

It is important to note that the molecule b is only the true bound state in the case of a vanishing coupling between atoms and molecules. Otherwise, the true bound state is the "bare" molecule b surrounded by a cloud of atoms. Thus, while the bare molecule's size is of the range of the forces which led to its creation, R_e, the size of the physical molecule is of the order of the atom-atom scattering length $a \gg R_e$. In fact, the contribution of the bare molecule to the physical molecule effectively disappears for infinitely wide Feshbach resonances, where the two-channel model may be replaced by a one-channel model. This will be discussed in more detail in chapter 3.

The two parameters which characterize the scattering between the atoms are the scattering length and the effective range. These may be calculated in the model and are given by [4]

$$a = -\frac{mg^2}{4\pi \left(\epsilon_0 - \frac{g^2 m \Lambda}{2\pi^2} \right)}, \qquad r_0 = -\frac{8\pi}{m^2 g^2}. \tag{2.15}$$

It is apparent that the position of the resonance is shifted from the "bare" value ϵ_0 to the *physical detuning*,

$$\omega_0 = \epsilon_0 - \frac{g^2 m \Lambda}{2\pi^2}. \tag{2.16}$$

The shift again occurs because the bare molecule does not coincide with the physical molecule.

In terms of the parameters of the model,

$$\gamma_s = \frac{8}{\pi}\frac{1}{k_F|r_0|}. \tag{2.17}$$

In the two-channel model, it is again seen that γ_s is independent of detuning ω_0 and scattering length a. Thus, if $\gamma_s \ll 1$ away from resonance then this is the case across the whole crossover. On the other hand, if r_0 is small then the resonance will be wide. In the next chapter the effective range will be taken to zero in order to model the wide resonances.

Chapter 3

The BCS-BEC crossover in the BEC regime

In the previous chapter some basic properties of the BCS-BEC crossover were described. Consider a two-component Fermi gas with short-ranged interactions. If the interactions between the two components are weak, the fermions will pair into the usual Cooper pairs and the system becomes a BCS superconductor at low temperatures. If the strength of the interaction is then increased by some means, at some point it becomes possible for two fermions to form a bound molecular state. As the strength is tuned further away from resonance, the bosonic molecules will form a regular BEC, and it is properties of this BEC which will be described in the present chapter.

The s-wave scattering length of two different fermionic atoms diverges across the Feshbach resonance. However, the BCS-BEC gap equation which describes the weakly attractive Fermi two-component Fermi gas implicitly assumes that the scattering is weak. Thus, even though the gap equation correctly describes the physics on the BCS side of the resonance there is no reason why the gap equation should be trusted on the BEC side of a Feshbach resonance. Yet, in Refs. [47, 53] it was discovered that under the strengthening of the interaction, the gap equation develops into the Schrödinger equation for the bound pair of fermionic atoms and correctly predicts the binding energy of this bound pair. Studies by these authors furthermore demonstrated that the BCS superfluid evolves into the BEC without undergoing a phase transition. Thus, even though the gap equation is not quantitatively correct on the BEC side of a resonance,

it still yields qualitatively correct results.

In order to systematically investigate the BEC regime of the weakly bound bosonic molecules, it is necessary to identify a small parameter. This is provided by the so-called gas parameter $n^{1/3}a$. n is the density of fermions while $n_{\rm b} = n/2$ is the density of bosonic molecules. The size of a molecule is roughly of order a, as discussed in chapter 2, while the average intermolecular distance is $n_{\rm b}^{-1/3}$. Thus, even though the molecules are rather large compared to the short-distance physics which led to their formation, for small values of the gas parameter the gas is a dilute Bose gas.

Using the low-density (or small gas parameter) expansion allows the computation of the molecular chemical potential $\mu_{\rm b}$, the speed of sound wave propagation u, the condensate depletion, and the ground state energy E_0. In the lowest order these are

$$\mu_{\rm b} = \frac{4\pi n_{\rm b} a_{\rm b}}{m_{\rm b}}, \tag{3.1}$$

$$u = \sqrt{\frac{4\pi n_{\rm b} a_{\rm b}}{m_{\rm b}^2}}, \tag{3.2}$$

$$n_{0,{\rm b}} = n_{\rm b}\left[1 - \frac{8}{3}\sqrt{\frac{n_{\rm b} a_{\rm b}^3}{\pi}}\right], \tag{3.3}$$

$$E_0/V = \frac{2\pi n_{\rm b}^2 a_{\rm b}}{m_{\rm b}}. \tag{3.4}$$

$m_{\rm b} = 2m$ is the mass of a molecule and V is the volume of the system. The molecule-molecule scattering length $a_{\rm b}$ appearing in these equations is proportional to the atom-atom scattering length. The coefficient of proportionality was first calculated by Petrov *et al* [59] who found

$$a_{\rm b} \approx 0.60a. \tag{3.5}$$

This result was later confirmed in Refs. [14, 50] with the calculations of Ref. [50] presented in section 3.6 below. It should be noted that the gap equation predics $a_{\rm b} = 2a$. Hence it is seen how the gap equation does not take interactions between the molecules properly into account.

At the crossover between BEC and BCS physics, the scattering length a diverges. This means that the gas parameter is no longer small, instead the scattering length will be much larger than the inter-molecular distance. The point at which a diverges is known as the unitary point. The physical behavior of the superfluid at zero temperature can only depend on one parameter, the density. The physical properties of the gas in this regime may be obtained by methods such as a large N expansion [73], Monte Carlo techniques (see e.g. the review [32] for references), or other methods. The perturbative approximation employed in this thesis breaks down close to the resonance and here only systems with $n^{1/3}a \ll 1$ will be considered.

In this chapter, wide resonances are investigated. As discussed in chapter 2 this requires $a \gg r_0$. It is important to note that while a diverges across a Feshbach resonance the effective range stays roughly constant. Thus the validity of the low-density expansion is restricted to scattering lengths such that $|r_0| \ll a \ll n^{-1/3}$. This limitation of the model's validity is not too restrictive; typical experimental densities of two-component Fermi gases are of order 10^{13} cm^{-3} corresponding to an interparticle distance of order $10^4 a_0$ (a_0 is the Bohr radius) while r_0 is typically of order $50a_0$.

The fact that the investigated Feshbach resonances are wide implies that the dynamics of the closed-channel molecule is suppressed. In the limit of a vanishing effective range it is then simpler to describe the gas by a one-channel model rather than the two-channel model described in chapter 2. The equivalence of these two approaches will be demonstrated below.

It should be reiterated that all calculations presented in this thesis proceed at zero temperature. A finite temperature extension of these results will not be discussed here. For further references see Ref. [2] and references therein.

The systematic perturbative expansion in the gas parameter may be continued below the lowest order. The first two corrections to the results (3.1) and (3.4) depend only on the gas parameter after which further details of the interaction become impor-

tant. The discussion of these higher order contributions to the chemical potential and ground state energy will be studied in chapter 4.

Another natural extension of the work presented here is to consider a two-component gas with a mass-imbalance. This is treated in chapter 5.

This chapter is organized as follows. First, the one-channel model is introduced and the diagrammatic approach to the BEC regime of the weakly bound molecules is discussed. Next, in section 3.4, physical properties of the BEC are computed in the lowest order gas parameter expansion. Finally, sections 3.5 and 3.6 contain the few-body diagrammatic calculations relevant for the BEC regime.

3.1 The one-channel model

In the previous chapter, the two-channel model was introduced to describe a system where a bound state of two fermions appeared as the magnetic field was tuned across a resonance. The Feshbach resonances described in this thesis (and indeed relevant to most BCS-BEC experiments) are wide, and for wide resonances it is more convenient to treat the gas of weakly bound molecules using what is known as the one-channel model. Below, it will be shown that these two approaches are equivalent in the limit of infinitely wide resonances.

The one-channel model may be expressed by a functional integral

$$Z = \int \mathcal{D}\bar{\psi}_\uparrow \mathcal{D}\psi_\uparrow \mathcal{D}\bar{\psi}_\downarrow \mathcal{D}\psi_\downarrow \; e^{iS_\mathrm{f}}. \tag{3.6}$$

The action $S_\mathrm{f} = S_0 + S_\mathrm{int}$ consists of a free part and an interacting part. The free part is

$$S_0 = \sum_{\sigma=\uparrow,\downarrow} \int d^3x \; dt \; \bar{\psi}_\sigma \left(i\frac{\partial}{\partial t} + \frac{1}{2m}\frac{\partial^2}{\partial \mathbf{x}^2} + \mu \right) \psi_\sigma, \tag{3.7}$$

while the interacting part is

$$S_\mathrm{int} = \lambda \int d^3x \; dt \; \bar{\psi}_\uparrow \bar{\psi}_\downarrow \psi_\downarrow \psi_\uparrow. \tag{3.8}$$

Here λ is chosen positive because the interaction potential is attractive. The interactions described by $S_{\rm int}$ take place at one point in space which by itself is unphysical. The results should be independent of the precise short distance physics and thus $S_{\rm int}$ needs to be supplemented by a cut-off Λ. Note that the one-channel model described by Eqs. (3.6), (3.7), and (3.8) does not explicitly contain the closed channel molecule associated with a Feshbach resonance.

3.1.1 Diagrammatic approach

Consider now the one-channel model of a two-component Fermi gas with $m_\uparrow = m_\downarrow \equiv m$ and $\mu_\uparrow = \mu_\downarrow \equiv \mu$. The propagator of fermions in the model described by Eqs. (3.6), (3.7), and (3.8) is

$$G_0(p,\omega) = \frac{1}{\omega - p^2/2m + \mu + i0}, \tag{3.9}$$

where m is the mass of either one of the fermionic atoms.

The scattering length of fermions in the vacuum may be computed by summing the diagrams shown in Fig. 3.1. The result of this summation is the T-matrix and the relationship between the scattering length and the T-matrix is[1]

$$a = \frac{m_r}{2\pi} T(0) \tag{3.10}$$

with $m_r = m/2$ the reduced mass of two atoms.

In the calculation of the fermionic scattering length it is important to keep $\mu = 0$ since the scattering proceeds in the vacuum. The diagrams in Fig. 3.1 form a geometric series since each loop is independent of the other loops. The T-matrix evaluated at zero incoming and outgoing fermion four-momenta is

$$T(0) = \lambda + \lambda\Pi(0)\lambda + \lambda\Pi(0)\lambda\Pi(0)\lambda + \ldots = \frac{-\lambda}{1 + \lambda\Pi(0)}. \tag{3.11}$$

[1] The T-matrix is a quantity defined for any kind of scattering. In this thesis, scattering between two fermions, a fermion and a bosonic molecule, and between two molecules will be considered. These result in T-matrices $T^{\rm ff}$, $T^{\rm bf}$, and $T^{\rm bb}$. In general the superscripts will be suppressed to ease notation except where any confusion might occur.

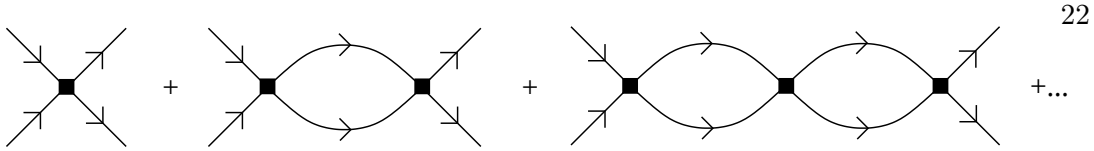

Figure 3.1: The diagrams which sum to give the atom-atom scattering matrix T. The straight line is a propagator of fermions while the square at each vertex is the coupling λ.

The bubble diagram Π consists of two fermion propagators integrated over the free four-momentum in the loop. That is,

$$\Pi(0) = i \int \frac{d^4p}{(2\pi)^4} G_0(p) G_0(-p) = -\frac{m\Lambda}{2\pi^2}. \tag{3.12}$$

Thus, in the one-channel model the atom-atom scattering length is

$$a = \left(-\frac{4\pi}{m\lambda} + \frac{2\Lambda}{\pi} \right)^{-1}. \tag{3.13}$$

In the one-channel model, the dynamics of the closed-channel molecule is suppressed. Instead the propagator of the closed-channel model is constant, equal to $-\lambda$. However, the molecule needs to be "dressed" by the self energy correction due to repeated interactions between the two fermionic components. Fig. 3.2 shows the propagator dressed by the self energy corrections, which consist of fermionic bubble diagrams. The molecular propagator is then

$$D_0(p) = \frac{-\lambda}{1 + \lambda \Pi(p)}, \tag{3.14}$$

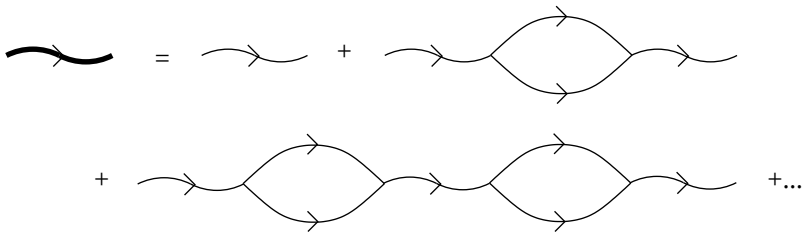

Figure 3.2: The relation between the dressed molecular propagator (thick wavy line) and the bare molecular propagator (thin wavy line). The bare propagator equals $-\lambda$.

where it has been used that the diagrams again form a geometric series. The calculation now proceeds in the medium at a finite chemical potential $\mu \leq 0$. Then the fermionic loop takes the value

$$\begin{aligned} \Pi(p,\omega) &= i\int \frac{d^4q}{(2\pi)^4} G(p+q)G(-q) \\ &= -\frac{m\Lambda}{2\pi^2} + \frac{m^{3/2}}{4\pi}\sqrt{-\omega + p^2/4m - 2\mu - i0}. \end{aligned} \tag{3.15}$$

The infinitesimal is derived from the fermionic propagators and is such that also the molecular propagator is retarded. Note the importance of having $\mu \leq 0$. Had this not been the case, the fermionic propagator would not have been retarded and hole propagation would have occured.

Using the relation (3.13) between the scattering length and the cut-off, the molecular propagator becomes

$$D_0(p,\omega) = \frac{4\pi}{m}\frac{1}{a^{-1} - \sqrt{m}\sqrt{-\omega + p^2/4m - 2\mu - i0}}. \tag{3.16}$$

3.2 BCS-BEC gap equation

In order to derive the BCS-BEC gap equation (the equation for the extremum of the action) from the one-channel model, it is convenient to introduce a Hubbard-Stratonovich field Δ. The one-channel functional integral (3.6) may then be written as

$$Z = \int \mathcal{D}\bar{\psi}_\uparrow \mathcal{D}\psi_\uparrow \mathcal{D}\bar{\psi}_\downarrow \mathcal{D}\psi_\downarrow \mathcal{D}\Delta \mathcal{D}\bar{\Delta}\, e^{iS_{\rm f}}, \tag{3.17}$$

with the action $S_{\rm int}$ replaced by

$$S_{\rm HS} = -\int d^3x\, dt\, \left[\frac{1}{\lambda}\bar{\Delta}\Delta + \left(\Delta\bar{\psi}_\uparrow\bar{\psi}_\downarrow + \bar{\Delta}\psi_\downarrow\psi_\uparrow\right)\right]. \tag{3.18}$$

The advantage of introducing the Hubbard-Stratonovich field is that the action $S_{\rm f}$ becomes quadratic in fermion fields, and these may then be integrated out. The resulting functional integral is

$$Z = \int \mathcal{D}\Delta \mathcal{D}\bar{\Delta}\, e^{iS_\Delta}, \tag{3.19}$$

with

$$S_\Delta = -i \,\mathrm{tr}\, \log \begin{pmatrix} \omega^+ - \frac{p^2}{2m} + \mu & -\Delta \\ -\bar{\Delta} & \omega^+ + \frac{p^2}{2m} - \mu \end{pmatrix} - \frac{1}{\lambda} \int d^3x\, dt\, \bar{\Delta}\Delta. \tag{3.20}$$

Here $\omega^+ = \omega + i0\,\mathrm{sign}\,\omega$.

The gap equation is then derived by assuming that the extremum of the action S_Δ occurs at a constant value Δ_0 of Δ. This results in

$$\frac{1}{\lambda} = \frac{1}{2} \int \frac{d^3p}{(2\pi)^3} \frac{1}{\sqrt{\left(\frac{p^2}{2m} - \mu\right)^2 + \Delta_0^2}}. \tag{3.21}$$

Using Eq. (3.13) the divergence in the momentum integral of Eq. (3.21) at large momenta may be regularized, and the gap equation becomes

$$-\frac{m}{4\pi a} = \frac{1}{2} \int \frac{d^3p}{(2\pi)^3} \left[\frac{1}{\sqrt{\left(\frac{p^2}{2m} - \mu\right)^2 + \Delta_0^2}} - \frac{2m}{p^2} \right]. \tag{3.22}$$

3.3 Equivalence of the one- and two-channel models

The two-channel model described in section 2.2 contains the dynamics of the molecular field. Compared with the one-channel model, this model has an additional parameter, the detuning. This parameter allows for the control of the effective range r_0 independently of the scattering length a. The precise relationships are listed here again for convenience

$$a = -\frac{mg^2}{4\pi\left(\epsilon_0 - \frac{mg^2\Lambda}{2\pi^2}\right)}, \tag{3.23}$$

$$r_0 = -\frac{8\pi}{mg^2}. \tag{3.24}$$

To ensure that a Feshbach resonance is wide, the effective range should be vanishingly small. This means that the interaction strength must be taken to ∞, while at the same time the detuning should be adjusted in such a way that the scattering length remains finite.

This may be achieved as follows. Redefine the bosonic fields of the two-channel model

$$\Delta = gb, \qquad \bar{\Delta} = g\bar{b}. \tag{3.25}$$

Using this definition, the interconversion part of the action, Eq. (2.14), becomes

$$S_{\rm bf} \to -\int d^3x\, dt\, \left[\Delta\bar{\psi}_\uparrow\bar{\psi}_\downarrow + \bar{\Delta}\psi_\downarrow\psi_\uparrow\right]. \tag{3.26}$$

For the free bosonic action use

$$\epsilon_0 = -g^2\left(\frac{m}{4\pi a} - \frac{m\Lambda}{2\pi^2}\right) = -\frac{g^2}{\lambda}, \tag{3.27}$$

which follows from Eqs. (3.13) and (3.23). Then in the limit $g \to \infty$ the free bosonic action (2.13) becomes

$$S_{0\rm b} = -\int d^3x\, dt\, \bar{\Delta}\Delta, \tag{3.28}$$

and the sum $S_{0\rm b} + S_{\rm bf}$ exactly matches the Hubbard-Stratonovich action $S_{\rm HS}$ of the one-channel model, see Eq. (3.18). Thus in the limit of wide resonances, the one-channel model is equivalent to the two-channel model.

In order to ensure that the Feshbach resonance is wide, the interaction strength is taken to the limit $g \to \infty$. Thus it is again seen that it is not possible to treat g as a small coupling and construct a perturbative expansion in powers of g.

3.4 The BEC regime of weakly bound molecules

Having set up the perturbative framework in terms of the gas parameter, the calculation of properties of the BEC of weakly bound bosonic molecules proceeds in a fairly standard manner [1, 29].

It is convenient to trade the expansion in powers of na^3 with a diagrammatic expansion in the number of propagators beginning or ending in the condensate. Each such line is assigned the value Δ_0, the expectation value of the field Δ. Δ_0^2 is not the density of particles in the condensate (the value assigned to condensate lines in the

standard dilute Bose gas) but is proportional to it, with the relation given below. Since the density of bosons in the condensate is lower than the total density, the perturbative expansion in powers of the gas parameter may be viewed as an expansion in the number of condensate lines in the diagrammatic approach.

The presence of the condensate leads to the appearance of both normal (one particle enters, one particle exits) and anomalous (two particles enter and no particles exit or vice versa) propagators. These replace the "bare" propagators G_0 and D_0 and will be denoted $G_{\rm n}$, $G_{\rm a}$ for the fermions and $D_{\rm n}$, $D_{\rm a}$ for the bosons. The fermionic propagators are needed in order to properly compute the particle number while the molecular propagators are needed to determine parameters of the gas. In the systematic perturbative treatment, the low-density approximations to the normal and anomalous propagators must be constructed.

To this end it is convenient to construct the self energy corrections to the propagators. The normal and anomalous fermionic self energies are denoted $\Sigma_{\rm n}$ and $\Sigma_{\rm a}$ while Σ_{11} and Σ_{20} are the normal and anomalous self energies for the molecules. The perturbative expansion in the number of condensate lines then consists in letting $\Sigma = \Sigma^{(1)} + \Sigma^{(2)} + \ldots$ where the superscript denotes the number of condensate lines. However, as discovered by Lee, Huang, and Yang [45, 46] non-trivial orders may be obtained through the summation of certain classes of infinite numbers of diagrams. This does not affect the lowest order results presented in this chapter and is instead the subject of chapter 4.

No normal self energy for the fermions has only one condensate line and thus

$$\Sigma_{\rm n}^{(1)} = 0. \tag{3.29}$$

The anomalous self energy in this order is given by the diagram shown in Fig. 3.3. This has the value

$$\Sigma_{\rm a}^{(1)} = \Delta_0. \tag{3.30}$$

In the next order, the contributions to the normal self energy are as shown in Fig. 3.4.

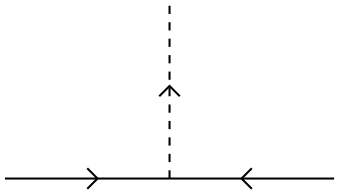

Figure 3.3: Lowest order contribution in the low density approximation to the anomalous fermionic self energy, $\Sigma_{\rm a}$. Straight lines symbolize the fermionic atoms while the dashed line is a condensate line. The external fermion lines *do not* contribute to the self energy, they are present only to guide the eye.

The square block shown in this diagram equals the sum of all diagrams contributing to scattering of an atom and a molecule. There are an infinite number of such diagrams. The computation of such a sum will be discussed in detail in section 3.5 below. Denote by $t^{\rm bf}$ (the atom-molecule scattering matrix) the result of the summation.[2] Then

$$\Sigma_{\rm n}^{(2)} = \Delta_0^2 t^{\rm bf}. \tag{3.31}$$

No diagrams with two condensate lines contribute to the anomalous self energy and thus

$$\Sigma_{\rm a}^{(2)} = 0. \tag{3.32}$$

For the molecular self energies, no diagrams with only one condensate line contribute and therefore

$$\Sigma_{11}^{(1)} = 0, \qquad \Sigma_{20}^{(1)} = 0. \tag{3.33}$$

In the next order, the self energies are shown in Fig. 3.5. The square block is the t-matrix of molecule-molecule scattering calculated in section 3.6. Again this consists of an infinite number of diagrams which may be summed. The self energies are

$$\Sigma_{11}^{(2)} = 2\Delta_0^2 t^{\rm bb}, \tag{3.34}$$

$$\Sigma_{20}^{(2)} = \Delta_0^2 t^{\rm bb}. \tag{3.35}$$

[2] The simplest such diagram consists of $\Sigma_{\rm a}^{(1)}$ repeated twice and should not be included (this is the diagram depicted in Fig. 3.6, excluding external lines). This technical point will not be important for the following discussion.

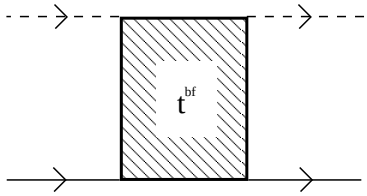

Figure 3.4: Lowest non-vanishing contribution to the normal fermionic self energy, $\Sigma_{\rm n}$. The square block is the sum of all diagrams contributing to atom-molecule scattering.

The factor 2 is due to the symmetry of the diagram.

Using the bosonic self energies Σ_{11} and Σ_{20}, the normal and anomalous propagators of the bosons may be computed. This was first done by Beliaev [8, 9] with the result

$$D_{\rm n}(p,\omega) = \frac{D_0^{-1}(-p,-\omega)-\Sigma_{11}(-p,-\omega)}{D(p,\omega)}, \tag{3.36}$$

$$D_{\rm a}(p,\omega) = \frac{\Sigma_{20}(p,\omega)}{D(p,\omega)}. \tag{3.37}$$

The denominator has the form

$$D(p,\omega) = -\left[\Sigma_{20}(p,\omega)\right]^2 + \left(D_0^{-1}(p,\omega)-\Sigma_{11}(p,\omega)\right)\left(D_0^{-1}(-p,-\omega)-\Sigma_{11}(-p,-\omega)\right). \tag{3.38}$$

In the BEC regime, it was shown by Hugenholtz and Pines [38] that the propagator of bosons must have a pole as the four-momentum tends to zero, corresponding to the presence of a gap-less sound mode in the condensate. This is the crucial observation on which the results of this section depend, and in general the Hugenholtz-Pines relation takes the form

$$D(0,0) = 0. \tag{3.39}$$

In the lowest order in the expansion in powers of Δ_0, the propagator of bosons reduces to the form D_0 obtained in Eq. (3.16). The chemical potential in the lowest order is then

$$\mu = -\frac{1}{2ma^2}. \tag{3.40}$$

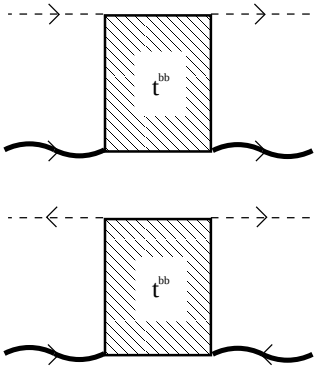

Figure 3.5: Normal (top) and anomalous (bottom) self energy contributions to the bosonic propagator in the lowest non-vanishing order. Wavy lines are molecular propagators. The square blocks are the sum of all diagrams participating in molecule-molecule scattering. As with the fermion self energies, the external molecular propagators are not a part of the self energies. On the other hand, the condensate lines *do* contribute to the self energies.

Thus, in the lowest order of the BEC regime the chemical potential of fermions equals half the binding energy of the molecular state as expected.

It should be noted that the same result for the chemical potential would have been obtained if in the gap equation (3.22) the expectation value Δ_0 had been ignored compared with μ.

The bosonic self energies should be related to the scattering length of the molecules in vacuum, $a_{\rm b}$. The self energies appearing in the Hugenholtz-Pines relation are on the other hand proportional to the molecule-molecule scattering t-matrix in the presence of the medium. In particular the t-matrix is to be evaluated at a finite chemical potential μ. However, as long as corrections to the chemical potential are small, $t^{\rm bb}$ in the medium will approximately equal $t^{\rm bb}$ evaluated in vacuum and will thus (as the four-momentum tends to zero) be proportional to the vacuum scattering length $a_{\rm b}$. The precise relationship is

$$t^{\rm bb} = \frac{2\pi}{mZ} a_{\rm b}. \tag{3.41}$$

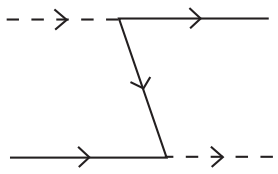

Figure 3.6: The diagram which leads to the lowest order particle number (3.47). As opposed to the self energy diagrams, here the external lines must be included.

Here

$$Z = \frac{8\pi}{m^2 a} \tag{3.42}$$

is the residue of the molecular propagator at its pole and is needed for proper normalization of external propagators [10].

The chemical potential of the bosonic molecules is defined as

$$\mu_{\mathrm{b}} = 2\mu + \frac{1}{ma^2}, \tag{3.43}$$

which vanishes in the lowest order of the low-density approximation. Using this definition of the bosonic chemical potential, the Hugenholtz-Pines relation (3.39) results in

$$\mu_{\mathrm{b}} = Z\left[\Sigma_{11}(0) - \Sigma_{20}(0)\right] - \frac{ma^2 Z^2}{4}\left[\Sigma_{11}(0) - \Sigma_{20}(0)\right]^2. \tag{3.44}$$

Eq. (3.39) will have one additional solution, however this solution is unphysical [1, 29]. In the lowest order in density

$$\begin{aligned} \mu_{\mathrm{b}} &\approx Z\left[\Sigma_{11}(0) - \Sigma_{20}(0)\right] \\ &= \frac{a a_{\mathrm{b}} m \Delta_0^2}{4}, \end{aligned} \tag{3.45}$$

and the relation becomes reminiscent of the Hugenholtz-Pines equation in the standard dilute Bose gas [38].

The particle number may now be computed from the fermionic self energies. The

particle number equation is

$$\begin{aligned} n &= \frac{1}{V}\int d^3x\ \left[\langle\bar{\psi}_\uparrow\psi_\uparrow\rangle + \langle\bar{\psi}_\downarrow\psi_\downarrow\rangle\right] \\ &= -i\int_{\mathcal{C}}\frac{d\omega}{2\pi}\int\frac{d^3p}{(2\pi)^3}\left[G_{n,\uparrow}(p,\omega)+G_{n,\downarrow}(p,\omega)\right], \end{aligned} \tag{3.46}$$

where $\mathcal{C}$ is the contour which includes the real axis and is closed in the upper half plane ensuring that the field operators occur in the proper order. The diagram which contributes to the particle number in the lowest order is shown in Fig. 3.6. Thus the particle number is

$$\begin{aligned} n &= 2i\Delta_0^2\int_{\mathcal{C}}\frac{d\omega}{2\pi}\int\frac{d^3p}{(2\pi)^3}\left[G_0(p,\omega)\right]^2 G_0(-p,-\omega) \\ &= \frac{am^2\Delta_0^2}{4\pi}. \end{aligned} \tag{3.47}$$

The sign of the expression comes from fermionic anti-commutivity and the factor 2 from the two species of fermions. In the evaluation of the integral, the chemical potential has been set to its zero'th order value, Eq. (3.40). With the help of Eq. (3.47) the bosonic chemical potential Eq. (3.45) becomes

$$\mu_{\rm b} = \frac{\pi a_{\rm b} n}{m} = \frac{4\pi a_{\rm b} n_{\rm b}}{m_{\rm b}}. \tag{3.48}$$

The ground state energy E_0 (measured from the binding energy of the molecules, i.e. from $-n_b/ma^2$) is calculated using the standard relation [38, 29]

$$E_0/V - \frac{1}{2}n_{\rm b}\mu_{\rm b} = \frac{i}{2Z}\int_{\mathcal{C}}\frac{d\omega}{2\pi}\int\frac{d^3p}{(2\pi)^3}\left(\omega + p^2/4m\right)D_{\rm n}(p,\omega), \tag{3.49}$$

where the contour $\mathcal{C}$ is again taken in the upper half plane. In the lowest order, the normal molecular propagator reduces to D_0 which is a retarded propagator. Thus with the help of Eq. (3.48) the ground state energy becomes

$$E_0/V = \frac{1}{2}n_{\rm b}\mu_{\rm b} = \frac{2\pi a_{\rm b} n_{\rm b}^2}{m_{\rm b}}. \tag{3.50}$$

The effect of including the higher order molecular propagator (3.36) in the equation for the ground state energy will be discussed in chapter 4.

Even at zero temperature there is still a finite fraction of the bosonic molecules not in the condensate. This phenomenon, caused by the presence of interactions, is known as the condensate depletion. The total density of bosons is

$$n_{\rm b} = n_{0,\rm b} + \frac{i}{Z}\int_{\mathcal{C}} \frac{d\omega}{2\pi} \int \frac{d^3p}{(2\pi)^3} D_{\rm n}(p,\omega), \tag{3.51}$$

with $n_{0,\rm b}$ the density of bosons in the condensate. In the lowest order, the density $n_{\rm b} = n_{0,\rm b}$. Using Eq. (3.36) for $D_{\rm n}(p,\omega)$ it is seen that the frequency and momentum dependence of the molecular self energies $\Sigma_{11}(p,\omega)$ and $\Sigma_{20}(p,\omega)$ is needed. However, considering the integral in Eq. (3.51), it is observed that the integration is dominated by frequencies of order $\omega \sim \mu_{\rm b} \sim \Delta_0^2$ and momenta of order $p^2/4m \sim \Delta_0^2$. For such low frequencies and momenta, the underlying structure of the molecular propagator (3.16) is not important and it reduces to

$$D_0(p,\omega) \approx \frac{Z}{\omega - p^2/4m + \mu_{\rm b} + i0}. \tag{3.52}$$

Also, $Z\Sigma_{11}(0) = 2\mu_{\rm b}$ and $Z\Sigma_{20}(0) = \mu_{\rm b}$ coincide with $\Sigma_{11}(0)$ and $\Sigma_{20}(0)$ in the usual dilute Bose gas. Hence, for small frequencies and momenta, the normal molecular propagator divided by Z coincides with the dilute Bose gas normal propagator at this order in the expansion. The result of evaluating the integral (3.51) then takes the usual form [1, 29]

$$n_{0,\rm b} = n_{\rm b}\left[1 - \frac{8}{3}\sqrt{\frac{n_{\rm b}a_{\rm b}^3}{\pi}}\right]. \tag{3.53}$$

Finally, the speed of sound wave propagation is evaluated by use of the Hugenholtz-Pines relation, Eq. (3.39), at finite p, ω. For small $\omega \lesssim \mu_{\rm b}$ and $p^2/4m \lesssim \mu_{\rm b}$ the self energy terms approximately take the limiting values $\Sigma_{11}^{(2)}(0)$ and $\Sigma_{20}^{(2)}(0)$ in the low density expansion. Imposing the condition

$$D(p,\omega) = 0 \tag{3.54}$$

for the denominator, Eq. (3.38), of the molecular propagators, it is found that

$$\omega^2 = u^2p^2, \qquad u = \sqrt{\frac{4\pi n_{\rm b}a_{\rm b}}{m_{\rm b}^2}}, \tag{3.55}$$

where u is the speed of sound.

The results of this section coincide with the results for the dilute interacting Bose gas [1, 29] with scattering length a_{b}. In order to go beyond these results it is necessary to modify the self energies in a systematic way. This will be further investigated in chapter 4.

3.5 Scattering of a molecule and an atom

In this section, the scattering problem of a fermionic atom with a bound state of fermions is treated. The solution of this scattering process has a long history. It was first solved in the approximation of vanishing effective range by Skorniakov and Ter-Martirosian in 1956 [68] who studied the related problem of a neutron scattering with a deuteron (a neutron-proton bound state). In the context of cold two-component Fermi gases the scattering problem was solved in Ref. [56] for any mass ratio of the fermionic atoms below 13.6. The three-body calculation presented below is a useful exercise before proceeding to more complicated few-body calculations. It is important to note that the calculation below relies on the approximation of a vanishing effective range, i.e. $a \gg |r_0|$ and the results are only valid in this regime.

It should be mentioned that there is a fundamental difference between the fermionic and the bosonic problem. The system of three identical bosons with a large scattering length has an infinite number of bound states, the effect known as the Efimov effect [25]. In this case, to correctly describe the three-body physics, an additional three-body parameter coming from short distance physics is required [20, 7, 12]. This is not the case in the fermionic problem (for mass ratios below 13.6); here the three-body problem is completely describable in terms of the two-body scattering length and the fermionic masses [56].

In the one channel model, the only length scale left is the scattering length between the distinguishable atoms. Since no additional parameters are required in order to

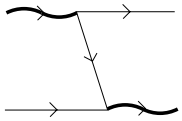

Figure 3.7: The Born approximation to atom-molecule scattering.

describe the three-body problem, the atom-molecule scattering length, $a_{\rm bf}$, must be proportional to the atom-atom scattering length, a.

Apart from the three-body scattering length, it is also interesting to note that the achievable densities for two-component Fermi gases are limited by three-body recombination, a process governed by three-body physics. Here two atoms form a deeply bound state with binding energy of order $1/mR_e^2$ and a third atom escapes the trap as it carries away the released binding energy as kinetic energy. The process requires at least two identical fermionic atoms to approach each other closely (at the order of the range of short distance physics, R_e) and is suppressed by the Pauli principle. The loss rate depends on the precise three-body physics and may be extracted from the three-body calculations below. A precise discussion will be postponed for chapter 5 on mass-imbalanced two-component Fermi gases since the loss-rate depends intimately on the mass ratio.

This is the first of a number of few body problems treated using integral equations and therefore this will be done very carefully. The simplest process contributing to the atom-molecule scattering is that the molecule breaks into its two constituent atoms, one of which forms a bound state with the remaining atom. The process is illustrated in Figure 3.7; had the scattering been weak, this would have been the only contribution to the scattering and thus this diagram will be called the Born contribution. However, as will be discussed below, all of the diagrams contributing to the scattering are of the ladder diagram type shown in Fig. 3.8 and these are all of the same order.

As pointed out above, the vacuum scattering diagrams are exactly those needed

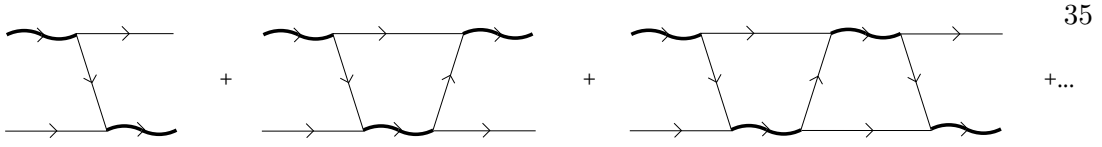

Figure 3.8: The ladder type diagrams contributing to atom-molecule scattering.

for the normal fermionic self energy at next to leading order in the low density expansion and the normal and anomalous molecular self energy at lowest order. That the type of diagrams shown in Fig. 3.8 is the only type contributing to the scattering stems precisely from the fact that this is *vacuum* scattering, i.e. all propagators are retarded and there is no hole propagation. This in turn means diagrammatically that all propagators specify a time direction and the possible diagrams are greatly simplified. In fact, because of the simplicity of the diagrams it is possible to sum all the possible diagrams by using an integral equation of Lippmann-Schwinger type.

Since the scattering proceeds in the vacuum, the chemical potential μ will be taken to vanish in this section.

The scattering t-matrix consists of all diagrams with external incoming and outgoing lines being the scattering particles. The external lines are not included in the t-matrix, however they do affect the overall normalization. The first diagram in Fig. 3.8 thus contributes a single atomic propagator, proportional to ma^2. In general, a diagram with n loops will then contain $2n+1$ fermionic lines of order $(ma^2)^{2n+1}$, n bosonic lines of order $(a/m)^n$, and n integrations over four-momenta $\sim m^{-n}a^{-5n}$. It follows that each diagram will be of order ma^2.

Given the structure of the contributing diagrams it is possible to write an integral equation for the sum of these. The integral equation is shown in Fig. 3.9. In Eq. (3.13) the two-fermion bubble diagrams were summed to yield the atom-atom scattering length by using a geometric series. The reason why the three-body problem is an *integral equation* rather than a geomatric series is that there will be an integral over the free

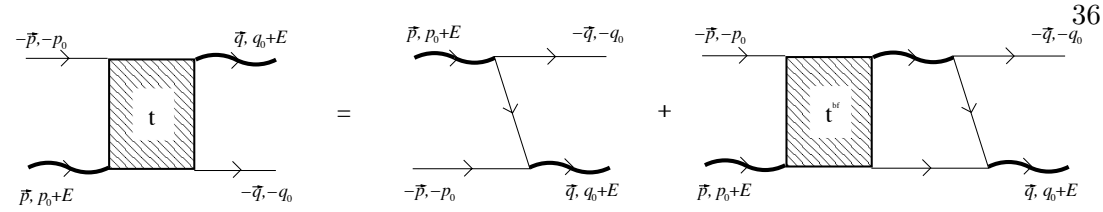

Figure 3.9: The integral equation for the t-matrix (shown as the square block) of atom-molecule scattering.

four-momentum in the loop of the iterated term.

Let the four-momenta be as shown in Fig. 3.9. That is, the incoming molecule and atom have four-momenta $(\vec{p}, p_0+E)$ and $(-\vec{p}, -p_0)$, respectively, while the outgoing molecule and atom have four-momenta $(\vec{q}, q_0+E)$ and $(-\vec{q}, -q_0)$, respectively. E is the total energy going into the scattering and since the initial and final states consist of a bound pair and an atom, it is necessary to restrict the total energy to energies $E \leq E_{\rm b}$. Otherwise, the final scattering state could be three free particles. The scattering t-matrix with these kinematics is denoted $t(\vec{p}, p_0; \vec{q}, q_0)$ (the dependence on total energy is suppressed in this notation). Then the integral equation becomes

$$t(\vec{p}, p_0; \vec{q}, q_0) = -G(p+q+E) - i \int \frac{d^4Q}{(2\pi)^4} G(Q+q+E) G(-Q) D(Q+E) t(\vec{p}, p_0; \vec{Q}, Q_0). \tag{3.56}$$

Here, in a slightly abusive notation, the total energy E is also used as the total four-momentum $(\vec{0}, E)$. To simplify notation further, the four-momentum $(\vec{p}, p_0)$ is abbreviated as p. The propagator of molecules is here given by the expression (3.16) with the chemical potential taken to vanish.

The t-matrix depends on five variables; the two frequencies, the amplitudes of the two momenta, and the angle between incoming and outgoing momenta. However, as the dependence of t on p and p_0 is the same on both sides of the integral equation, the integral equation for t is only a three dimensional problem. Below, it will be discussed how the frequencies q_0 and Q_0 may be integrated out from Eq. (3.56) and in chapter 5

it will be demonstrated how the integral equation may be projected onto each spherical wave component, making the solution of each of these a one-dimensional problem.

$t(\vec{p}, p_0; \vec{q}, q_0)$ is analytic in the upper half planes of both p_0 and q_0. This may be seen from the ladder diagrams contributing to the t-matrix or simply from Eq. (3.56). This in turn means that the integration over Q_0 in Eq. (3.56) may be carried out by closing the contour in the upper half plane, with the only contribution coming from the simple pole of $G(-Q)$, setting $Q_0 = -Q^2/2m$. The solution of the integral equation is then most easily obtained by letting $q_0 \to -q^2/2m$ which means that the momentum dependence of the t-matrix is the same on both sides of the integral equation. Should the value of the t-matrix be desired at a different value of q_0, the result of solving the integral equation at $q_0 = -q^2/2m$ may simply be inserted on the right hand side of Eq. (3.56) and the integration carried out. In this sense the t-matrix with $p_0 = -p^2/2m$ and $q_0 = -q^2/2m$ is quite natural. It is the result of attaching the external atomic propagators to the t-matrix and integrating over their frequencies, closing the contour in the upper half plane (where t is analytic). This will be called the "on-shell" t-matrix and satisfies the integral equation

$$\begin{aligned} t(\vec{p}, -p^2/2m; \vec{q}, -q^2/2m) &= -G(p+q+E) \\ &\quad - \int \frac{d^3Q}{(2\pi)^3} G(Q+q+E) D(Q+E) t(\vec{p}, -p^2/2m; \vec{Q}, -Q^2/2m). \end{aligned} \tag{3.57}$$

The iterative procedure described above for obtaining the solution to the integral equation at the desired values of p_0, q_0 from the on-shell t-matrix is illustrated in Fig. 3.10.

To calculate the s-wave scattering length, the total energy should be set to the two-body binding energy. The scattering length is then found by solving the integral equation, averaging over angles, and taking the limit of vanishing incoming and outgoing four-momenta. Equivalently, the incoming momentum can be taken to vanish prior to solving the integral equation after which there can be no dependence on the angle between incoming and outgoing momentum. Using this second approach yields the

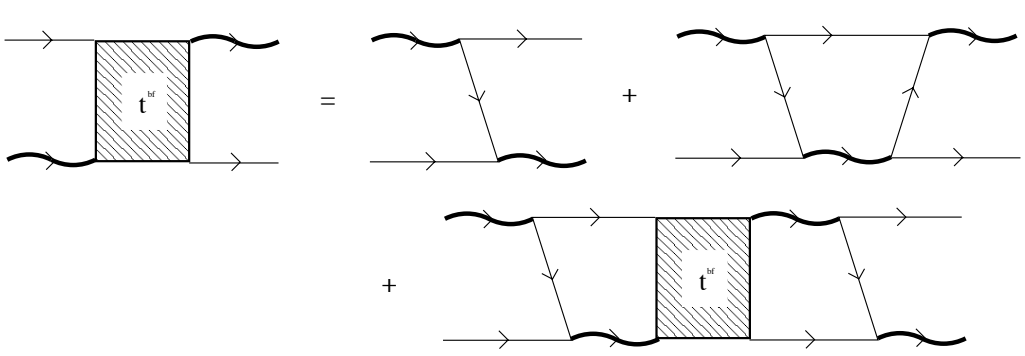

Figure 3.10: The procedure for relating the on-shell t-matrix (the square block on the right hand side) to the t-matrix evaluated at a desired frequency (the left hand side).

integral equation

$$t(p) = \frac{ma^2}{1+p^2} + \frac{1}{\pi p}\int_0^\infty dq \frac{q\,t(q)}{1-\sqrt{1+3q^2/4}} \log\frac{1+p^2+q^2+qp}{1+p^2+q^2-qp}. \tag{3.58}$$

In this equation, momenta are measured in units of inverse scattering length and the "on-shell" s-wave scattering matrix is $t(p) \equiv t(\vec{0}, 0; \vec{p}, -p^2/2m)$.

In general, the integral equations have a form which in matrix notation is

$$t_i = v_i + K_{ij} t_j. \tag{3.59}$$

The matrix equation has the formal solution

$$t_i = (I-K)^{-1}_{ij} v_j. \tag{3.60}$$

The matrix I is the identity matrix. The numerical solution of the t-matrix is then a matter of choosing a discretization and solving the matrix equation. Typically, for purposes of convergence, it is advantageous to perform a change of variable such that the limits of integration become finite [61]. A convenient choice is

$$p = \frac{2}{z+1} - 1, \qquad z \in]-1, 1]. \tag{3.61}$$

All integrals are then performed employing Gauss-Legendre quadrature [61]. Using this method the t-matrix is found to take the shape shown in Fig. 3.11.

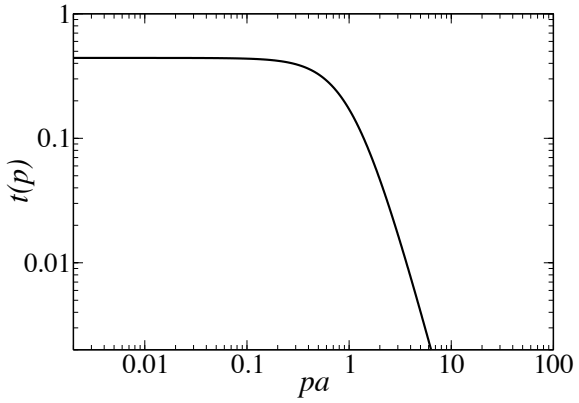

Figure 3.11: The t-matrix $t(p)$ in units of ma^2 calculated by solving Eq. (3.58). For $p \ll a^{-1}$ the t-matrix is approximately constant while for $p \gg a^{-1}$ the t-matrix satisfies a power-law behavior, decaying as $p^{-3.17}$ [7].

The atom-molecule scattering length $a_{\rm bf}$ is proportional to the t-matrix of Eq. (3.58) evaluated at vanishing momentum and energy $E = E_{\rm b}$. To obtain the scattering amplitude from the t-matrix it is necessary to renormalize the external propagators. The fermionic propagators are already free propagators, however the molecular propagators need to be renormalized by the square root of the residue of the molecular propagator at the energy of the bound state [10], i.e.

$$T(0) = Zt(0), \tag{3.62}$$

with Z given by Eq. (3.42). The scattering amplitude is related to the scattering length by

$$T(0) = \frac{2\pi}{m_{3\rm r}} a_{\rm bf} = \frac{3\pi}{m} a_{\rm bf}, \tag{3.63}$$

where $m_{3\rm r}$ is the three-body reduced mass. Using the method described above it is found that

$$a_{\rm bf} \approx 1.18a, \tag{3.64}$$

in perfect agreement with the literature [68, 56].

Bound states in the three-body problem show up as poles of the scattering amplitude. This corresponds to solutions of the homogenous integral equation

$$t_i = K_{ij} t_j, \tag{3.65}$$

or in other words to the integration kernel K having a unit eigenvalue. Bound three-body states will have $E < E_\mathrm{b}$, and writing $E = (1+\epsilon_3)E_\mathrm{b}$ the homogenous equation becomes

$$t(p) = \frac{1}{\pi p}\int_0^\infty dq \frac{q\, t(q)}{1-\sqrt{1+\epsilon_3+3q^2/4}} \log\frac{1+\epsilon_3+p^2+q^2+qp}{1+\epsilon_3+p^2+q^2-qp}. \tag{3.66}$$

It is found that the three-body problem does not have any s-wave bound states. Note that the validity of this statement is limited by the zero effective range approximation. There may still be deeply bound states with binding energies of order $1/mr_0^2$.

3.6 Molecule-molecule scattering

As discussed above, properties of the gas of weakly bound molecules depend intimately on the molecule-molecule scattering length, a_b. Mean field theory gives the result $a_\mathrm{b} = 2a$. This result implicitly assumes that the coupling is weak and that only the diagram shown in Fig. 3.12 contributes to the scattering. An approximate diagrammatic method was developed by Pieri and Strinati in Ref. [60] who found $a_\mathrm{b} \approx 0.75a$. Later the problem was solved exactly by Petrov, Salomon, and Shlyapnikov [59] by solving the quantum mechanical four-body problem using the Bethe-Peierl's method. In this work it was found that $a_\mathrm{b} \approx 0.6a$. This last result is confirmed below by the use of diagrammatic methods. While the work presented in this section and published in Ref. [50] was in progress, the problem was solved by Brodsky *et al* in Ref. [14] by essentially the same diagrammatic method.

The scattering t-matrix consists of all possible diagrams with two incoming and two outgoing molecules, excluding the external propagators. In the atom-molecule

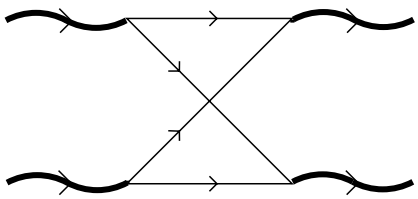

Figure 3.12: The simplest contribution to molecule-molecule scattering.

scattering problem treated above, it was discussed how diagrams contributing to the molecule-molecule scattering do not contain any internal condensate lines nor any hole propagation. This is again the case, since the process considered is scattering in the vacuum. This observation greatly simplifies the diagrams possible in the scattering process. Since all propagators can be assigned a definite time direction, at any time in the scattering of two molecules there will be either two molecules, one molecule and two atoms, or four atoms.

With this observation in mind, consider the different diagrams which contribute to the scattering t-matrix. The simplest possible diagram is the Born diagram shown in Fig. 3.12 where the two molecules exchange their constituent fermionic atoms. Other possible diagrams contributing to the scattering are shown in Fig. 3.13. Fig. 3.13a shows the propagation of an intermediate molecule, Fig. 3.13b a slightly more complicated diagram, and 3.13c a diagram where a pair of molecules propagate at an intermediate step. The crucial observation is that all of these diagrams are of the same order, namely they are all proportinal to m^3a^3. Indeed this is true for all possible vacuum scattering diagrams. Thus the problem of molecule-molecule scattering is not amenable to a perturbative treatment. Instead of considering only the Born diagram, Fig. 3.12, an infinite number of diagrams need to be taken into account.

Fortunately it is possible to perform the summation of all diagrams by using an integral equation. To this end, it is useful to define the concept of a *two-boson irreducible diagram* as a diagram which cannot be cut in two by cutting two molecular

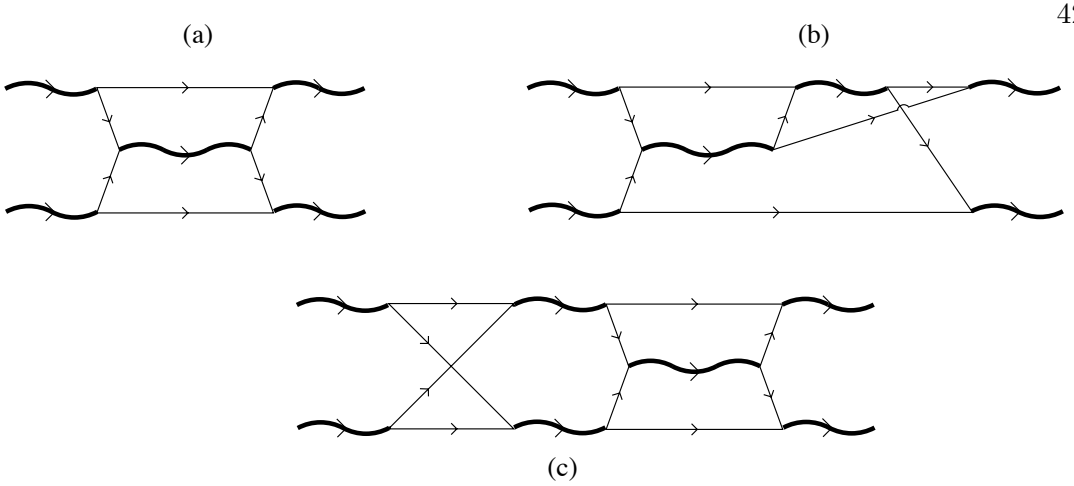

Figure 3.13: Diagrams which contribute to molecule-molecule scattering.

lines only. For instance, the diagrams in Fig. 3.13a and b are two-boson irreducible while the diagram in Fig. 3.13c is not. The scattering t-matrix may then be viewed as the repeated propagation and scattering of two molecules, each pair of molecular propagators separated by the sum of all two boson irreducible diagrams. In this sense, the sum of two-boson irreducible diagrams is similar to the bubble diagram, Π (see Fig. 3.1) occurring in the repeated atom-atom scattering. However, there will be an integral over a free four-momentum and thus the sum does not form a geometric series. Defining Γ as the sum of all two-boson irreducible diagrams, t satisfies an integral equation as shown in Fig. 3.14.

Each diagram contributing to Γ will have a number, n, of molecular propagators, $4+2n$ fermionic propagators, and $n+1$ integrations. The total order of such a diagram is $\left(\frac{a}{m}\right)^n \left(ma^2\right)^{4+2n} \left(\frac{1}{ma^5}\right)^{n+1} = m^3a^3$. Any diagram contributing to t will then have $n+1$ insertions of Γ, $2n$ molecular propagators and n integrations and will be proportional to m^3a^3.

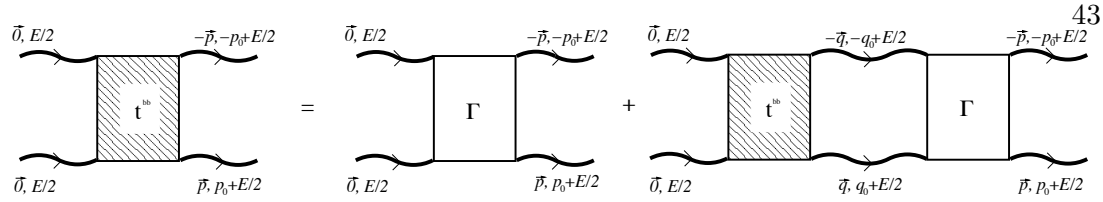

Figure 3.14: Integral equation for the t-matrix (shown as the square block) of molecule-molecule scattering. Here, for simplicity E has been used as the four-momentum $(\vec{0}, E)$.

The integral equation for the t-matrix with kinematics as shown in Fig. 3.14 is

$$t(p,p_0) = \Gamma(0,0;p,p_0) + \frac{i}{4\pi^3}\int q^2 dq\, dq_0 D(q,q_0+E/2)D(q,-q_0+E/2)\Gamma(q,q_0;p,p_0)t(q,q_0). \tag{3.67}$$

The incoming momentum has been taken to zero while the outgoing four-momenta of the molecules are $(\pm\vec{p}, E/2 \pm p_0)$. This choice of kinematics is convenient since ultimately the quantity of interest is the s-wave scattering length, proportional to $t(0,0)$. The scalar $t(\vec{p}, p_0)$ cannot depend on the direction of $\vec{p}$, which is why it is possible to average the sum of two-boson irreducible diagrams over the angle between incoming and outgoing momentum. This average is denoted $\Gamma(p,p_0;q,q_0)$. To determine the scattering length, let $E = 2E_B$, while to search for bound states look for solutions of the homogenous integral equation with $E < -|2E_\mathrm{b}|$.

Because of the symmetry of the problem, it is convenient to slightly redefine what is meant by G and D. Below, *in this section only*, the convention will be used that all atomic propagators have their frequency shifted by a quarter of the energy going into the scattering, while the molecules have their frequency shifted by half the energy. That is

$$G(p,p_0) \equiv \frac{1}{p_0 - p^2/2m + E/4 + i0}, \tag{3.68}$$

$$D(p,p_0) \equiv \frac{4\pi}{m}\frac{1}{a^{-1} - \sqrt{m}\sqrt{-p_0 - E/2 + p^2/4m - i0}}. \tag{3.69}$$

For the purpose of calculating the molecular scattering length a_b, the total energy is $2E_\mathrm{b}$ and in this case each molecule will carry the molecular binding energy.

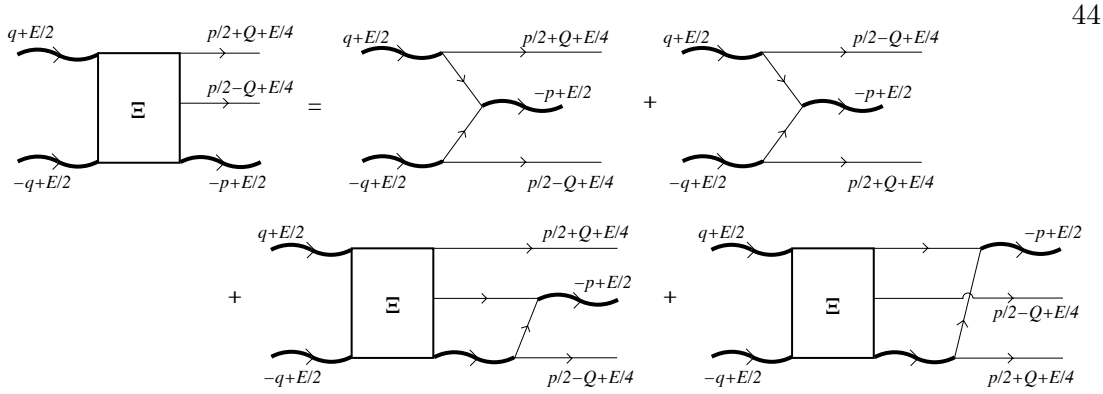

Figure 3.15: Integral equation for the vertex Ξ. Here the notation E has been used to denote the four-momentum $(\vec{0}, E)$.

The integral equation (3.67) is not sufficient to compute the t-matrix. The sum of all two-boson irreducible diagrams still needs to be computed and this sum may again be obtained through the solution of an integral equation. It is not possible to directly write down an integral equation satisfied by Γ. However, it is possible to relate Γ to the solution of an integral equation for the sum, Ξ, of two-boson irreducible diagrams with two incoming molecules, one outgoing molecule and two outgoing fermions. The integral equation to be solved is depicted in Fig. 3.15. This integral equation is quite similar to the equation for atom-molecule scattering, see Fig. 3.9.

Let the kinematics be as shown in Fig. 3.15. Ξ with incoming four-momenta of $(\pm\vec{q}, E/2 \pm q_0)$ for the molecules, $(-\vec{p}, E/2 - p_0)$ for the outgoing molecule, and $(\vec{p}/2 \pm \vec{Q}, E/4 + p_0/2 \pm Q_0)$ for the outgoing fermions is denoted $\Xi(q; p/2+Q; p/2-Q)$. The integral equation for Ξ may then be written as[3]

$$\begin{aligned}\Xi(q; p/2+Q; p/2-Q) &= -\int \frac{d\Omega_{\vec{q}}}{4\pi} \left[G(-p/2-q+Q)G(-p/2+q-Q) + (q \leftrightarrow -q)\right] \\ -i\int \frac{d^4Q'}{(2\pi)^4} \big\{ & G(p/2-Q')G(-3p/2+Q')D(-p-Q+Q')\Xi(q; p/2+Q; p/2-Q') \\ & + G(p/2+Q')G(-3p/2-Q')D(-p+Q-Q')\Xi(q; p/2+Q'; p/2-Q)\big\}. \quad (3.70)\end{aligned}$$

[3] The calculation of the vertex Ξ presented here differs slightly from the formalism in Ref. [50]. The present formalism is better suited to an extension to treating the mass imbalanced problem investigated in chapter 5.

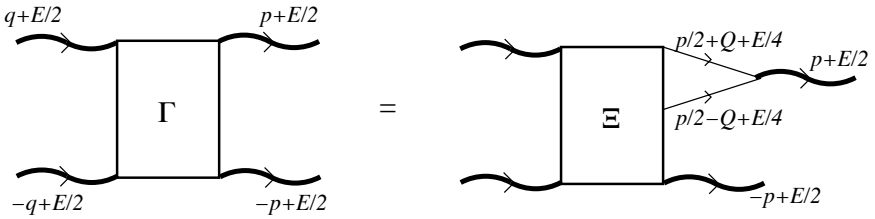

Figure 3.16: The relation between Γ and Ξ.

The integration over directions of $\vec{q}$ (with notation $\int d\Omega_{\vec{q}}$) is the averaging over directions of incoming momentum, i.e. the projection onto the s-wave. Minus signs in front of both the Born terms and the iterated terms all follow from anti-commutivity of the fermionic atoms.

Eq. (3.70) has to be solved at every $|\vec{q}|$ and q_0. It is an integral equation in 5 variables, the length of $\vec{p}$ and $\vec{Q}$, the angle between these vectors, and the corresponding frequencies. As will be shown below, it is possible to integrate out the two frequencies such that the resulting integral equation becomes three-dimensional.

Finally, the two-boson irreducible vertex Γ is related to Ξ by joining the two external fermionic propagators into a molecule as shown in Fig. 3.16. This relation may be written as

$$\Gamma(q,q_0;p,p_0)=\frac{i}{2}\int\frac{d^4Q}{(2\pi)^4}G(p/2+Q)G(p/2-Q)\Xi(q;p/2+Q;p/2-Q). \quad (3.71)$$

The factor $\frac{1}{2}$ ensures that all diagrams enter Γ with the correct weights.

It is advantageous to split $\Xi(q;p/2+Q;p/2-Q)$ into parts $\Xi^+(q;p/2+Q;p/2-Q)$ $[\Xi^-(q;p/2+Q;p/2-Q)]$ analytic in the upper [lower] half planes of Q_0, with

$$\Xi(q;p/2+Q;p/2-Q)=\Xi^+(q;p/2+Q;p/2-Q)+\Xi^-(q;p/2+Q;p/2-Q). \quad (3.72)$$

To this end, note that the iterated terms are already thus split. To split up the Born terms, use the relation

$$G(p)G(q)=\frac{G(p)+G(q)}{G(p)^{-1}+G(q)^{-1}}. \quad (3.73)$$

Then Eq. (3.71) becomes

$$\begin{aligned}\Gamma(q,q_0;p,p_0) \;\; &= \\ &\frac{1}{2}\int\frac{d^3Q}{(2\pi)^3}\Big[G(p/2-Q)\;\Xi^-(q;p/2+Q;p/2-Q)\big|_{Q_0=-p_0/2+(p/2+Q)^2/2m-E/4} \\ &\qquad +G(p/2+Q)\;\Xi^+(q;p/2+Q;p/2-Q)\big|_{Q_0=p_0/2-(p/2-Q)^2/2m+E/4}\Big]\,. \end{aligned} \tag{3.74}$$

In each of the two last terms of Eq. (3.70) it is possible to integrate out Q_0' by closing around the single pole in the lower half plane. The two parts of Ξ appearing in Eq. (3.74) satisfy the coupled integral equations

$$\begin{aligned}&\Xi^-\left(q;\vec{p}/2+\vec{Q},(\vec{p}/2+\vec{Q})^2/2m-E/4;\vec{p}/2-\vec{Q},p_0-(\vec{p}/2+\vec{Q})^2/2m+E/4\right) \\ &\quad= -\int\frac{d\Omega_{\vec{q}}}{4\pi}\left[\frac{G(-p/2+q-Q)}{G^{-1}(-p/2-q+Q)+G^{-1}(-p/2+q-Q)}+(q\leftrightarrow -q)\right] \\ &\qquad -\int\frac{d^3Q'}{(2\pi)^3}G(-3\vec{p}/2+\vec{Q}',-p_0-(p/2-Q')^2/2m+E/4)D(-p-Q+Q') \\ &\qquad\qquad \times\Xi\left(q;\vec{p}/2+\vec{Q},(p/2+Q)^2/2m-E/4;\vec{p}/2-\vec{Q}',(p/2-Q')^2/2m-E/4\right), \\ &\Xi^+\left(q;\vec{p}/2+\vec{Q},p_0-(p/2-Q)^2/2m+E/4;\vec{p}/2-\vec{Q},(p/2-Q)^2/2m-E/4\right) \\ &\quad= -\int\frac{d\Omega_{\vec{q}}}{4\pi}\left[\frac{G(-p/2-q+Q)}{G^{-1}(-p/2-q+Q)+G^{-1}(-p/2+q-Q)}+(q\leftrightarrow -q)\right] \\ &\qquad -\int\frac{d^3Q'}{(2\pi)^3}G(-3\vec{p}/2-\vec{Q}',-p_0-(p/2+Q')^2/2m+E/4)D(-p+Q-Q') \\ &\qquad\qquad \times\Xi\left(q;\vec{p}/2+\vec{Q}',(p/2+Q')^2/2m-E/4;\vec{p}/2-\vec{Q},(p/2-Q)^2/2m-E/4\right). \end{aligned} \tag{3.75}$$

In the first of these equations $Q_0=-p_0/2+(p/2+Q)^2/2m-E/4$ and $Q_0'=p_0/2-(p/2-Q')^2/2m+E/4$. In the second equation $Q_0=p_0/2-(p/2-Q)^2/2m+E/4$ and $Q_0'=-p_0/2+(p/2+Q')^2/2m-E/4$.

On the right hand side of Eqs. (3.75), the vertex Ξ only appears in the form

$$\Xi(q;\vec{p}_1,p_1^2/2m-E/4;\vec{p}_2,p_2^2/2m-E/4)\equiv\chi(q;\vec{p}_1,\vec{p}_2). \tag{3.76}$$

This will be called the "on-shell" vertex. The reason for this terminology is clear; had the propagators $G(p_1)$ and $G(p_2)$ been attached to the vertex $\Xi(q;p_1;p_2)$ and the

frequencies been integrated over using the poles of the propagators, then these on-shell values of the frequencies would have been obtained. In this sense, the on-shell vertex is equivalent to the atom-molecule scattering vertex $t^{\rm bf}(\vec{p},-p^2/2m;\vec{q},-q^2/2m)$ discussed above, see Eq. (3.57).

Solving the integral equations is now possible with the substitution

$$p_0 \to (\vec{p}/2+\vec{Q})^2/2m + (\vec{p}/2-\vec{Q})^2/2m - E/2, \tag{3.77}$$

at which value also the left hand sides of Eqs. (3.75) will be on-shell. Adding the expressions in Eqs. (3.75) at this value of p_0 results in an integral equation in three variables for the total on-shell vertex which may subsequently be inserted on the right hand side of Eqs. (3.75) to find the value of the vertex Ξ at any value of p_0.

After a change of variables to $\vec{p}_1 = \vec{p}/2+\vec{Q}$ and $\vec{p}_2 = \vec{p}/2-\vec{Q}$, the equation for the total on-shell vertex takes the form

$$\begin{aligned}\chi(q;\vec{p}_1,\vec{p}_2) &= -\int \frac{d\Omega_{\vec{q}}}{4\pi}\left[G(q-p_1)G(-q-p_2)+(q\leftrightarrow -q)\right] \\ &\quad -\int \frac{d^3Q}{(2\pi)^3}\left\{ G(-p_1-p_2-Q)D(-Q-p_1)\chi(q;\vec{p}_1,\vec{Q})\Big|_{Q_0=Q^2/2m-E/4}\right. \\ &\qquad \left. + G(-p_1-p_2-Q)D(-Q-p_2)\chi(q;\vec{Q},\vec{p}_2)\Big|_{Q_0=Q^2/2m-E/4}\right\}, \end{aligned}\tag{3.78}$$

where $(p_1)_0 = p_1^2/2m - E/4$ and $(p_2)_0 = p_2^2/2m - E/4$.

Inserting Eq. (3.78) into the right hand sides of Eqs. (3.75) and the resulting expression into the right hand side of Eq. (3.74), the vertex Γ finally becomes

$$\begin{aligned}\Gamma(q,q_0;p,p_0) &= \Gamma^{(0)}(q,q_0;p,p_0) \\ &\quad -\frac{1}{2}\int \frac{d^3p_1}{(2\pi)^3}\frac{d^3p_2}{(2\pi)^3}\left[G(p-p_1)G(-p-p_2)+(p\leftrightarrow -p)\right]D(-p_1-p_2)\chi(q;\vec{p}_1,\vec{p}_2). \end{aligned}\tag{3.79}$$

Here again $(p_1)_0 = p_1^2/2m - E/4$ and $(p_2)_0 = p_1^2/2m - E/4$ while it is important to note that p_0 is a free parameter. This method (3.79) of constructing the two-boson irreducible vertex corresponds diagrammatically to the situation depicted in Fig. 3.17. $\Gamma^{(0)}$ is the result of calculating the Born diagram, shown in Fig. (3.12),

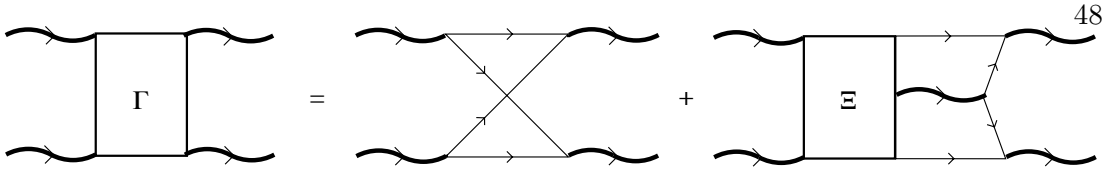

Figure 3.17: An illustration of Eq. (3.79).

$$\begin{aligned}\Gamma^{(0)}(q,q_0;p,p_0) &= -i\int\frac{d\Omega_{\vec{q}}}{4\pi}\int\frac{d^4Q}{(2\pi)^4}G(Q+p/2+q/2)G(Q-p/2-q/2)\\ &\quad\times G(-Q-p/2+q/2)G(-Q+p/2-q/2) \quad (3.80)\\ &= -2\int\frac{d\Omega_{\vec{q}}}{4\pi}\int\frac{d^3Q}{(2\pi)^3}\frac{A}{(A^2-B^2)(A^2-C^2)}, \quad (3.81)\end{aligned}$$

with

$$\begin{aligned}A &= E/2-Q^2/m-p^2/4m-q^2/4m,\\ B &= p_0-\vec{Q}\cdot\vec{q}/m,\\ C &= q_0-\vec{Q}\cdot\vec{p}/m. \quad (3.82)\end{aligned}$$

The angular integrations may be performed independently by first integrating over directions of $\vec{q}$ and then over directions of $\vec{Q}$. The result is

$$\begin{aligned}\Gamma^{(0)}(q,q_0;p,p_0) &= \frac{m^2}{16\pi^2pq}\int_0^\infty\frac{dQ}{-E/2+Q^2/m+p^2/4m+q^2/4m}\\ &\quad\times\log\frac{(-E/2+Q^2/m+p^2/4m+q^2/4m+Qq/2m)^2-p_0^2}{(-E/2+Q^2/m+p^2/4m+q^2/4m-Qq/2m)^2-p_0^2}\\ &\quad\times\log\frac{(-E/2+Q^2/m+p^2/4m+q^2/4m+Qp/2m)^2-q_0^2}{(-E/2+Q^2/m+p^2/4m+q^2/4m-Qp/2m)^2-q_0^2}. \quad (3.83)\end{aligned}$$

The procedure for solving the set of integral equations is now as follows. The integral equation (3.78) for the on-shell χ has to be solved at every $(\vec{q},q_0)$. However, the kernel of this integral equation does not depend on $(\vec{q},q_0)$, an observation which is of great help in the numerical solution, since this means that the identity matrix minus the integration kernel needs to be inverted only once [see Eqs. (3.59) and (3.60)]. With the on-shell χ determined, this should be inserted in Eq. (3.79) to find the two-boson

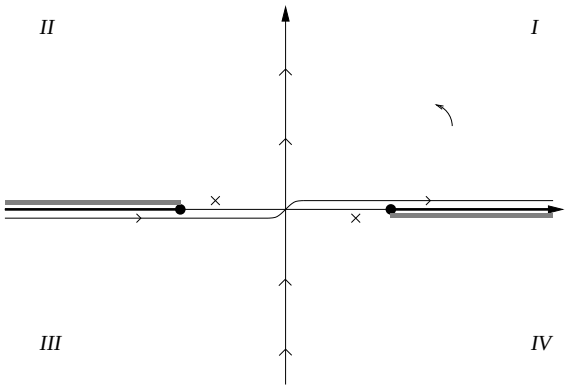

Figure 3.18: The original and rotated contour of frequency integration used in Eq. (3.67). The crosses correspond to poles of the molecular propagators while the black lines correspond to the square root branch cuts. The gray boxes are the areas in which the two-boson irreducible vertex Γ may have non-analytic structure.

irreducible vertex Γ. Finally, Γ may be inserted in Eq. (3.67) to find the scattering t-matrix.

A bit of care needs to be taken in peforming the integration over frequency in Eq. (3.67). Due to the square-root structure of the molecular propagators there will be branch cuts starting at

$$q_0 = -E/2 + q^2/4m \geq 0, \text{ and } q_0 = E/2 - q^2/4m \leq 0 \tag{3.84}$$

and continuing towards $\pm\infty$, respectively. The contour of integration is such that for $\mathrm{Re}(q_0) > 0$ [$\mathrm{Re}(q_0) < 0$] the integration is above [below] the branch cut, which follows from the infinitesimal in the molecular propagator, Eq. (3.16). Furthermore, the molecular propagators have poles at $q_0 = \pm(q^2/4m + E_\mathrm{b} - E/2 - i0)$. It is thus advantageous to perform a Wick rotation as illustrated in Fig. 3.18. This removes the problem of integrating close to the branch cuts and poles. In order to perform such a Wick rotation, the vertex $\Gamma(p, p_0; q, q_0)$ needs to be analytic in quadrants I and III. Eqs. (3.78, 3.79, 3.80) show that this is indeed the case and that any non-analytic structure of Γ must be restricted to the areas marked as gray boxes in Fig. 3.18.

When computing the scattering length, the total energy should be set to $E = 2E_\mathrm{b}$.

Then the simple poles of the molecular propagators present in Eq. (3.67) occur at $q_0 = \pm(q^2/4m - i0)$, i.e. close to both the original and the Wick rotated integration contour. These simple poles are integrable and may be treated by a change of variables to "polar" coordinates,

$$q^2/4m = R^2 \sin\theta, \qquad q_0 = R^2 \cos\theta. \tag{3.85}$$

Here $R \in [0, \infty[$ and $\theta \in [0, \pi]$.

To search for bound states in the four-fermion problem, let $E < 2E_\mathrm{b}$ and look for solutions to the homogenous equation. In a matrix notation this corresponds to the existence of a solution to the equation $t_i = K_{ij} t_j$ or, in other words, the existence of a bound state implies that the kernel of the integral equation, K, has an eigenvalue equal to 1. No bound states are found by using this method. As the one-channel model is employed here, the effective range r_0 has been taken to zero. Thus the validity of this method is only for bound states with binding energies $|E| \ll \frac{1}{mr_0^2}$ and the result does not exclude deeply bound states.

The scattering amplitude is calculated on-shell, with the incoming and outgoing molecules all having four-momentum $(\vec{0}, E_\mathrm{b})$. Thus $E = 2E_\mathrm{b}$. As in the three-body problem above, to calculate the scattering amplitude each external molecular propagator needs to be renormalized by $\sqrt{Z}$, and the relation between the scattering amplitude and the scattering matrix is

$$T(0) = Z^2 t(0,0). \tag{3.86}$$

The scattering length is then found through

$$T(0) = \frac{2\pi}{M_\mathrm{r}} a_\mathrm{b} \tag{3.87}$$

with $M_\mathrm{r} = m$ the molecule-molecule reduced mass. By solving the set of equations described above, it is found that

$$a_\mathrm{b} \approx 0.60a \tag{3.88}$$

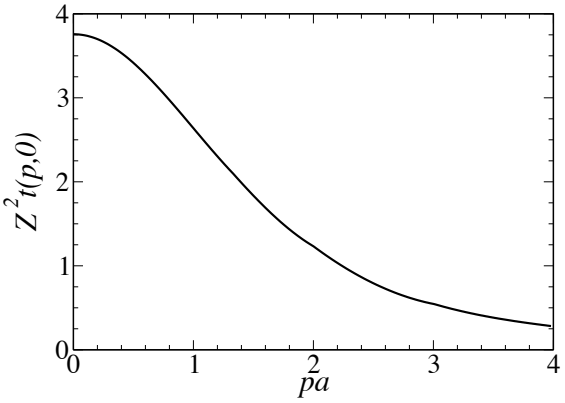

Figure 3.19: The scattering amplitude $Z^2t(p, p_0)$ in unites of a/m evaluated at $p_0 = 0$.

in complete agreement with Refs. [14, 59]. Fig. 3.19 shows the computed t-matrix, from which $t(0, 0)$ may be extracted.

Chapter 4

Quantum corrections

In chapter 3 properties of the BEC regime of the dilute Bose gas consisting of weakly bound molecules were calculated. The calculations were performed in the low density limit and it was seen how this limit corresponds to a diagrammatic expansion in terms of lines beginning or ending in the condensate. The results obtained were seen to exactly match the results of the standard dilute Bose gas [1, 29] with the effect of the fermionic atoms being that the boson-boson scattering length is related to the fermion-fermion scattering length by $a_{\rm b} \approx 0.60a$.

It is possible to extend the low density expansion in order to obtain the chemical potential and ground state energy in higher orders. This involves the determination of the fermionic and bosonic self energies in higher orders. Somewhat surprisingly, the next order self energies for the bosons *do not* involve diagrams such as in Fig. 4.1 which only contributes at even higher order. Rather, they arise due to non-trivial resummations of diagrams occuring because of infrared divergences of the molecular propagator. Lee, Huang, and Yang computed the first correction to the ground state energy [45, 46]. Later, results were obtained in the next order by Wu [76] and Sawada [65] and the results of these authors confirmed by Hugenholtz and Pines [38].

The results in the dilute Bose gas are the following:

$$\mu_{\rm b} = \frac{4\pi a_{\rm b} n_{\rm b}}{m_{\rm b}} \left[1 + \frac{32}{3}\sqrt{\frac{n_{\rm b} a_{\rm b}^3}{\pi}} + 12\pi \left(\frac{4}{3} - \frac{\sqrt{3}}{\pi} \right) n_{\rm b} a_{\rm b}^3 \log n_{\rm b} a_{\rm b}^3 \right], \qquad (4.1)$$

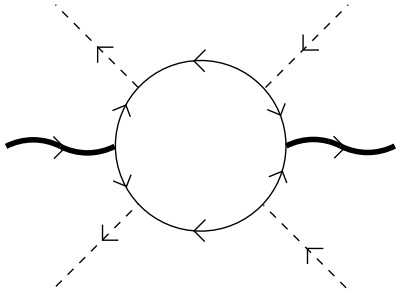

Figure 4.1: A high order contribution to the molecular self energy.

$$\frac{E_0}{V} = \frac{2\pi a_{\rm b} n_{\rm b}^2}{m_{\rm b}} \left[1 + \frac{128}{15}\sqrt{\frac{a_{\rm b}^3 n_{\rm b}}{\pi}} + 8\pi \left(\frac{4}{3} - \frac{\sqrt{3}}{\pi} \right) n_{\rm b} a_{\rm b}^3 \log n_{\rm b} a_{\rm b}^3 \right]. \tag{4.2}$$

Below, it will be shown that these results are also correct in the gas of weakly bound molecules, with the scattering length $a_{\rm b}$ related to the underlying fermion scattering length a.

The first two corrections to the ground state energy and chemical potential are universal in the sense that they only depend on the scattering length $a_{\rm b}$, the density, and the mass of bosons. Higher order corrections will depend on the shape of the interatomic potential, in particular on the effective range r_0. These will not be considered here.

4.1 The molecular propagator at low densities and momenta

Define the chemical potential and particle number as an expansion in Δ_0:

$$\mu_{\rm b} = \mu_{\rm b}^{(2)} + \mu_{\rm b}^{(3)} + \ldots \tag{4.3}$$

$$n_{\rm b} = n_{\rm b}^{(2)} + n_{\rm b}^{(3)} + \ldots \tag{4.4}$$

The superscript denotes powers of Δ_0. In chapter 3 the results

$$\mu_{\rm b}^{(2)} = \frac{a a_{\rm b} m \Delta_0^2}{4}, \tag{4.5}$$

$$n_{\rm b}^{(2)} = \frac{a m^2 \Delta_0^2}{8\pi}, \tag{4.6}$$

were found. Below, the next two orders in the chemical potential will be calculated.

It is useful to consider the molecular propagator at frequencies $\omega \ll 1/ma^2$ and momenta $p \ll a^{-1}$. In the zero density approximation it becomes a free propagator

$$D_0(p,\omega) \approx \frac{Z}{\omega - p^2/2m_\mathrm{b} + i0}, \qquad \left(p \ll a^{-1}, \omega \ll 1/ma^2\right). \tag{4.7}$$

In the first non-trivial order of the low density expansion, the normal and anomalous propagators were similarly seen in section 3.4 to be approximately Z times the usual dilute Bose gas normal and anomalous propagators. The poles of the iterated propagators at low frequencies and momenta may then be separated as [38]

$$D_\mathrm{n}(p,\omega) \approx Z\frac{u_p^2}{\omega - \epsilon(p) + i0} - Z\frac{v_p^2}{\omega + \epsilon(p) - i0}, \qquad \left(p \ll a^{-1}, \omega \ll 1/ma^2\right), \tag{4.8}$$

$$D_\mathrm{a}(p,\omega) \approx Z\frac{-u_p v_p}{\omega - \epsilon(p) + i0} + Z\frac{u_p v_p}{\omega + \epsilon(p) - i0}, \qquad \left(p \ll a^{-1}, \omega \ll 1/ma^2\right), \tag{4.9}$$

with

$$u_p^2 = \frac{\frac{p^2}{2m_\mathrm{b}} + \mu_\mathrm{b}^{(2)} + \epsilon(p)}{2\epsilon(p)}, \tag{4.10}$$

$$v_p^2 = \frac{\frac{p^2}{2m_\mathrm{b}} + \mu_\mathrm{b}^{(2)} - \epsilon(p)}{2\epsilon(p)}. \tag{4.11}$$

Here

$$\epsilon(p) = \sqrt{\left(\frac{p^2}{2m_\mathrm{b}}\right)^2 + \frac{p^2}{m_\mathrm{b}}\mu_\mathrm{b}^{(2)}} \tag{4.12}$$

is the spectrum of low-lying excitations found by solving the Hugenholtz-Pines relation (3.39) at low frequencies and momenta.

For the purpose of computing the vacuum scattering lengths a_bf and a_b in chapter 3 there was only one relevant length scale, namely the atom-atom scattering length a. However, in the BEC regime another length scale is given by the average interparticle spacing $n^{-1/3}$ and na^3 is a dimensionless parameter. It is now seen how another important length scale appears of order $\frac{1}{\sqrt{na}} \gg a$. This scale, known as the healing length, defines a crossover in the excitation spectrum of low-lying excitations; for $p \ll \sqrt{na}$ these behave as sound waves with a constant velocity while for $\sqrt{na} \ll p \ll a^{-1}$ they

are almost free particles. Indeed, for small momenta

$$\epsilon(p) \approx p\sqrt{\frac{\mu_{\rm b}^{(2)}}{m_{\rm b}}}, \qquad p \ll \sqrt{na} \tag{4.13}$$

as found in Eq. (3.55), while for higher momenta

$$\epsilon(p) \approx \frac{p^2}{2m_{\rm b}} + \mu_{\rm b}^{(2)} - \left(\mu_{\rm b}^{(2)}\right)^2 \frac{m_{\rm b}}{p^2}, \qquad \sqrt{na} \ll p \ll a^{-1}. \tag{4.14}$$

Thus there are three regimes of momenta relevant for the problem, small momenta $p \ll \sqrt{na}$, intermediate momenta $\sqrt{na} \ll p \ll a^{-1}$, and large momenta $p \gg a^{-1}$. In the first two [38]

$$u_p^2 \approx v_p^2 \approx \frac{\sqrt{\mu_{\rm b}^{(2)}}}{2p}, \qquad p \ll \sqrt{na}, \tag{4.15}$$

$$u_p^2 \approx 1, \quad v_p^2 = \frac{\left(\mu_{\rm b}^{(2)}\right)^2}{p^4}, \qquad \sqrt{na} \ll p \ll a^{-1}. \tag{4.16}$$

In the limit of large frequencies and momenta, the square root structure of the molecular propagator dominates, and in this limit it will no longer be possible to separate the poles.

4.2 Corrections to the chemical potential and ground state energy

In this section the first corrections to the chemical potential and ground state energy will be calculated in the low density expansion. This will be done by a very direct method, utilizing the particle number equation for the fermionic atoms, Eq. (3.46), and the Hugenholtz-Pines relation, Eq. (3.44).

The chemical potential of the bosonic molecules was found in Eq. (3.44) by requiring a gap-less sound mode in the BEC. The result was

$$\mu_{\rm b} = Z\left[\Sigma_{11}(0) - \Sigma_{20}(0)\right] - \frac{ma^2Z^2}{4}\left[\Sigma_{11}(0) - \Sigma_{20}(0)\right]^2. \tag{4.17}$$

The lowest order contribution to $\mu_{\rm b}$ is of order Δ_0^2. The two non-trivial corrections to the chemical potential considered in this chapter are of order Δ_0^3 and $\Delta_0^4 \log \Delta_0$. Thus

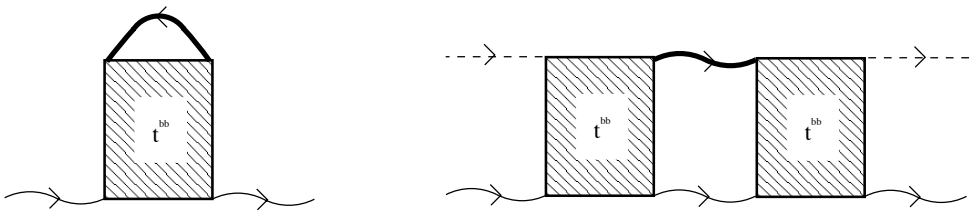

Figure 4.2: The normal self energy at order Δ_0^3. In this chapter, the thin wavy lines are molecular propagators D_0, while the thick wavy lines are the iterated molecular propagators $D_{\rm n}$ and $D_{\rm a}$ [Eqs. (3.36) and (3.37)], distinguished by the directions of arrows.

it is seen that the last term in Eq. (4.17) does not influence these corrections to the chemical potential and the Hugenholtz-Pines relation becomes

$$\mu_{\rm b} \approx Z\left[\Sigma_{11}(0) - \Sigma_{20}(0)\right]. \tag{4.18}$$

The difference between the normal and anomalous self energy of the bosons is needed at order Δ_0^3. The diagrams contributing to the normal self energy in this order are depicted in Fig. 4.2. The diagram in Fig. 4.2a has no analogue in $\Sigma_{11}^{(2)}$. Its value is

$$2i \lim_{\eta\to 0^+} \int \frac{d\omega}{2\pi} e^{i\eta\omega} \int \frac{d^3p}{(2\pi)^3} t^{\rm bb} D_{\rm n}(p,\omega), \tag{4.19}$$

where the factor 2 appears as a combinatorial factor and the exponential factor ensures the correct order of field operators. The four-momentum dependence of $t^{\rm bb}$ has not been made explicit. The t-matrix has the property that it is roughly constant at $\omega \ll 1/ma^2$ and $p \ll a^{-1}$, while it drops quickly to zero for large frequencies and momenta. The value of the integral may then be estimated by assuming that the main contribution is from frequencies and momenta small compared with $|E_b|$ and a^{-1}. Using Eq. (4.8) for the normal propagator, the frequency integration is performed by closing the contour in the upper half plane. The integration picks out the part of the propagator proportional to v_p^2 which is suppressed at momenta $p \gg \sqrt{na}$, and the value of the diagram is

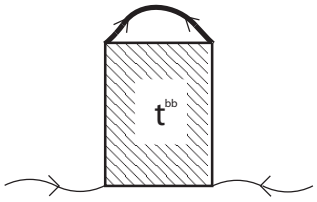

Figure 4.3: The anomalous self energy for the bosons at order Δ_0^3.

approximately

$$t^{\rm bb}\int\frac{d^3p}{(2\pi)^3}\frac{-\epsilon(p)+\frac{p^2}{2m_{\rm b}}+\mu_{\rm b}^{(2)}}{\epsilon(p)}. \tag{4.20}$$

Using the asymptotic forms (4.13) and (4.14) of the excitation spectrum $\epsilon(p)$, the integrand is seen to go as p for $p\ll\sqrt{na}$ and as p^{-2} for $\sqrt{na}\ll a^{-1}$. This means that the integral is dominated by momenta of order $\sqrt{na}\ll a^{-1}$ and the assumption that $t^{\rm bb}$ could be taken constant is justified. The diagram in Fig. 4.2a then has the value

$$\frac{16}{3}Z^{-1}\frac{aa_{\rm b}m\Delta_0^2}{4}\sqrt{\frac{a_{\rm b}^3}{\pi}\frac{am^2\Delta_0^2}{8\pi}}. \tag{4.21}$$

The diagram shown in Fig. 4.2b is already contained in $\Sigma_{11}^{(2)}$ if the iterated normal propagator is replaced by D_0. To compute the contribution to $\Sigma_{11}^{(3)}$ from the diagram, the part proportional to Δ_0^2 must be subtracted and the value of the diagram is

$$\begin{aligned}&4i\Delta_0^2\int\frac{d\omega}{2\pi}\int\frac{d^3p}{(2\pi)^3}t^{\rm bb}\left[D_{\rm n}(p,\omega)-D_0(p,\omega)\right]D_0(-p,-\omega)\\ =\;&16Z^{-1}\frac{aa_{\rm b}m\Delta_0^2}{4}\sqrt{\frac{a_{\rm b}^3}{\pi}\frac{am^2\Delta_0^2}{8\pi}}.\end{aligned} \tag{4.22}$$

Again the integration is dominated by momenta of order $p\sim\sqrt{na}$. The sum of the normal self energies gives

$$Z\Sigma_{11}^{(3)}(0)=\left(\frac{16}{3}+16\right)\frac{aa_{\rm b}m\Delta_0^2}{4}\sqrt{\frac{a_{\rm b}^3}{\pi}\frac{am^2\Delta_0^2}{8\pi}}. \tag{4.23}$$

The only contribution to the anomalous self energy $\Sigma_{11}^{(3)}$ in this order is given by the diagram shown in Fig. 4.3.

$$i\int\frac{d\omega}{2\pi}\int\frac{d^3p}{(2\pi)^3}t^{\rm bb}D_{\rm a}(p,\omega). \tag{4.24}$$

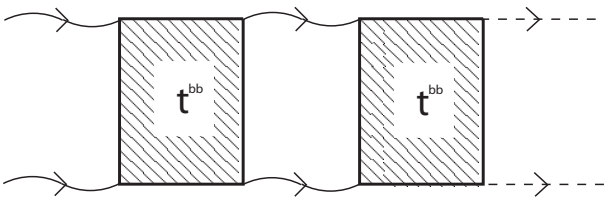

Figure 4.4: A contribution to the anomalous self energy already included at order Δ_0^2.

Assuming that the integration is dominated by small p, ω results in

$$-\frac{Zt^{\rm bb}\mu_{\rm b}^{(2)}}{2}\int\frac{d^3p}{(2\pi)^3}\frac{1}{\epsilon(p)}, \tag{4.25}$$

which is formally divergent at large p. However, the divergence is proportional to Δ_0^2 and arises because the diagram shown in Fig. 4.4, and belonging to $\Sigma_{11}^{(2)}$, is included in the diagram in Fig. 4.3. The diagram should be subtracted and the anomalous self energy at order Δ_0^3 becomes

$$\begin{aligned} Z\Sigma_{20}^{(3)}(0) &= -\frac{Z^2t^{\rm bb}\mu_{\rm b}^{(2)}}{2}\int\frac{d^3p}{(2\pi)^3}\left[\frac{1}{\epsilon(p)}-\frac{2m_{\rm b}}{p^2}\right] \\ &= 8\frac{aa_{\rm b}m\Delta_0^2}{4}\sqrt{\frac{a_{\rm b}^3}{\pi}\frac{am^2\Delta_0^2}{8\pi}}. \end{aligned} \tag{4.26}$$

With the regularization, the diagram is dominated by $p\sim\sqrt{na}$.

The chemical potential up to order Δ_0^3 is found to be

$$\begin{aligned} \mu_{\rm b} &= Z\left[\Sigma_{11}(0)-\Sigma_{20}(0)\right] \\ &= \frac{aa_{\rm b}m\Delta_0^2}{4}\left(1+\frac{40}{3}\sqrt{\frac{a_{\rm b}^3}{\pi}\frac{am^2\Delta_0^2}{8\pi}}\right). \end{aligned} \tag{4.27}$$

The particle number must be determined in the same order. $n_{\rm b}^{(3)}$ originates from only one diagram, shown in Fig. 4.5, with the value

$$\begin{aligned} n_{\rm b}^{(3)} &= \frac{1}{2}2i^2\lim_{\eta\to0^+}\int\frac{dp_0}{2\pi}e^{i\eta p_0}\int\frac{d^3p}{(2\pi)^3}\int\frac{d^4q}{(2\pi^4)}\left[G(p)\right]^2G(-p+q)D_{\rm n}(q) \\ &\approx -2Z\lim_{\eta\to0^+}\int\frac{dp_0}{2\pi}e^{i\eta p_0}\int\frac{d^3p}{(2\pi)^3}\left(\frac{1}{p_0-p^2/2m-1/2ma^2+i0}\right)^2 \\ &\times\int\frac{d^4q}{(2\pi^4)}\frac{1}{-p_0+q_0-(-\vec{p}+\vec{q})^2/2m-1/2ma^2+i0}\frac{q_0+q^2/2m_{\rm b}+\mu_{\rm b}^{(2)}}{q_0^2-\epsilon(q)^2+i0}, \end{aligned} \tag{4.28}$$

Figure 4.5: The diagram giving the particle number at order Δ_0^3.

where it has again been assumed that the integration over q is dominated by $q \ll a^{-1}$. The factor $\frac{1}{2}$ comes from $n_\mathrm{b} = n/2$ while the factor 2 is from the sum on fermion spins. Integrating over frequencies and shifting the momentum $\vec{p} \to \vec{p}+\vec{q}/2$ to get rid of angular dependence, the expression reduces to

$$\begin{aligned} n_\mathrm{b}^{(3)} &= Z \int \frac{d^3p}{(2\pi)^3}\frac{d^3q}{(2\pi)^3}\left(\frac{1}{\epsilon(q)+p^2/m+q^2/2m_\mathrm{b}+1/ma^2}\right)^2 \frac{-\epsilon(q)+q^2/2m_\mathrm{b}+\mu_\mathrm{b}^{(2)}}{\epsilon(q)} \\ &\approx \frac{m^3 a^{3/2} a_\mathrm{b}^{3/2}\Delta_0^3}{3\sqrt{2}\pi^2}. \end{aligned} \tag{4.29}$$

The q integration is indeed dominated by momenta q of order $\sqrt{na}$. The integration also results in terms of order Δ_0^4 and higher which have been ignored.

The particle number to order Δ_0^3 is thus found to be

$$n_\mathrm{b} = \frac{am^2\Delta_0^2}{4\pi}\left(1+\frac{8}{3}\sqrt{\frac{a_\mathrm{b}^3}{\pi}\frac{am^2\Delta_0^2}{8\pi}}\right). \tag{4.30}$$

Combining this result with the result for the chemical potential, Eq. (4.27), results in

$$\mu_\mathrm{b} = \frac{4\pi a_\mathrm{b} n_\mathrm{b}}{m_\mathrm{b}}\left(1+\frac{32}{3}\sqrt{\frac{a_\mathrm{b}^3 n_\mathrm{b}}{\pi}}\right), \tag{4.31}$$

exactly coinciding with the result in the standard dilute Bose gas [45].

The chemical potential is related to the ground state energy by

$$\mu_\mathrm{b} = \frac{1}{V}\frac{\partial E_0}{\partial n_\mathrm{b}}. \tag{4.32}$$

Assuming a form $E_0 = \alpha n_\mathrm{b}^2 + \beta n_\mathrm{b}^{5/2}$ the ground state energy is found to be

$$\frac{E_0}{V} = \frac{2\pi a_\mathrm{b} n_\mathrm{b}^2}{m_\mathrm{b}}\left(1+\frac{128}{15}\sqrt{\frac{a_\mathrm{b}^3 n_\mathrm{b}}{\pi}}\right). \tag{4.33}$$

As this result is computed from the chemical potential it of course also matches the usual dilute Bose gas result.

4.3 Next order corrections

An elegant derivation of the chemical potential and ground state energy in the standard dilute Bose gas was presented by Hugenholtz and Pines in Ref. [38]. These authors noticed that the two quantities are linked by two equations. The first of these was given as Eq. (3.49) and is

$$\frac{E_0}{V} - \frac{1}{2}n_{\rm b}\mu_{\rm b} = \frac{i}{2Z}\lim_{\eta\to 0^+}\int\frac{d\omega}{2\pi}e^{i\eta\omega}\int\frac{d^3p}{(2\pi)^3}\left(\omega + p^2/2m_{\rm b}\right)D_{\rm n}(p,\omega), \tag{4.34}$$

while the second equation is Eq. (4.32). The crucial observation was that given the normal bosonic propagator in some order in the low density expansion, when inserted in Eq. (4.34) the resulting relation between the chemical potential and the ground state energy will be an equation in the next order. This will be demonstrated below.

The method may be used to compute the results of section 4.2 above. Inserting the propagator $D_{\rm n}$ from Eq. (4.8), correct up to order Δ_0^2 in Eq. (4.34), results in

$$\frac{E_0}{V} - \frac{1}{2}n_{\rm b}\mu_{\rm b} = -\frac{i}{2}\lim_{\eta\to 0^+}\int\frac{d\omega}{2\pi}e^{i\eta\omega}\int\frac{d^3p}{(2\pi)^3}\left(\omega + p^2/2m_{\rm b}\right)\frac{v_p^2}{\omega+\epsilon(p)-i0}, \tag{4.35}$$

where it has been assumed that only small p,ω contribute to the integral. Carrying out the integration, the assumption is seen to be valid, and the result is

$$\begin{aligned}\frac{E_0}{V} - \frac{1}{2}n_{\rm b}\mu_{\rm b} &= -\frac{2}{15\pi^2 m_{\rm b}}(4\pi a_{\rm b})^{5/2}\left(\frac{am_{\rm b}^2\Delta_0^2}{32\pi}\right)^{5/2} \\ &= -\frac{2}{15\pi^2 m_{\rm b}}(4\pi a_{\rm b})^{5/2}n_{\rm b}^{5/2}.\end{aligned} \tag{4.36}$$

In the last step, Δ_0^2 has been traded for $n_{\rm b}$ using Eq. (3.47). This is correct at the current order in na^3. Now assume the following forms for the ground state energy and chemical potential

$$\frac{E_0}{V} = \frac{2\pi a_{\rm b}n_{\rm b}^2}{m_{\rm b}} + \alpha\frac{a_{\rm b}^{5/2}n_{\rm b}^{5/2}}{m_{\rm b}}, \tag{4.37}$$

$$\mu_{\rm b} = \frac{4\pi a_{\rm b} n_{\rm b}}{m_{\rm b}} + \beta \frac{a_{\rm b}^{5/2} n_{\rm b}^{3/2}}{m_{\rm b}}. \tag{4.38}$$

Performing the differentiation in Eq. (4.32) gives

$$\mu_{\rm b} = \frac{4\pi a_{\rm b} n_{\rm b}}{m_{\rm b}} + \frac{5}{2}\alpha \frac{a_{\rm b}^{5/2} n_{\rm b}^{3/2}}{m_{\rm b}}, \tag{4.39}$$

from which it is seen that $\beta = \frac{5}{2}\alpha$. A second linear equation is provided by comparing powers of $n_{\rm b}$ in Eq. (4.36). Solving the equation gives $\alpha = \frac{256\sqrt{\pi}}{15}$, and inserting α and β in the equations for $\mu_{\rm b}$ and E_0, the resulting ground state energy and chemical potential are seen to exactly match the results in Sec. 4.2 above.

4.3.1 The logarithmic contributions

In the low density expansion, the next order contribution (computed by Wu and Sawada [76, 65] and denoted below by WS) to the chemical potential and ground state energy is logarithmic, proportional to $\log \frac{a^{-1}}{\sqrt{na}}$. This in turn means that the correction arises from momenta in the range $\sqrt{na} \ll p \ll a^{-1}$. It should thus not come as a great surprise that the BEC of weakly bound molecules also at this order coincides with the standard dilute Bose gas since the precise structure of $t^{\rm bb}$ will not be probed by these momenta.

As above, the normal molecular propagator is needed. Define

$$D_{\rm n}(p,\omega) = D_{\rm n}^{(1)}(p,\omega) + D_{\rm n}^{(2)}(p,\omega) + \ldots \tag{4.40}$$

The propagator $D_{\rm n}^{(1)}(p,\omega)$ is the one considered above in calculating the Lee-Huang-Yang (LHY) ground state energy (4.33), and is correct to order Δ_0^2. $D_{\rm n}^{(2)}(p,\omega)$ is the part of the molecular propagator leading to the logarithmic corrections while the dots correspond to even higher order parts of the normal propagator. The anomalous propagator $D_{\rm a}^{(2)}(p,\omega)$ is defined in the same manner.

In Eqs. (3.36) and (3.37) the normal and anomalous molecular propagators were related to the "bare" propagator D_0 and the exact self energies, the result of Beliaev

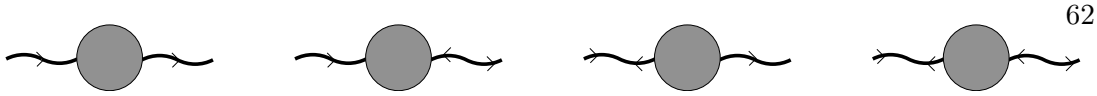

Figure 4.6: The expansion of the normal propagator, Eq. (4.43). The circles are the effective self energies Σ'_{11} and Σ'_{20}.

[8]. It is possible to derive an analogous expression relating the exact propagators not to the bare propagator but to $D^{(1)}_{\rm n}(p,\omega)$ and $D^{(1)}_{\rm a}(p,\omega)$ [38]. This requires the definition of new effective self energies

$$\Sigma'_{11}(p,\omega) \equiv \Sigma_{11}(p,\omega) - \Sigma^{(2)}_{11}(0,0), \tag{4.41}$$

$$\Sigma'_{20}(p,\omega) \equiv \Sigma_{20}(p,\omega) - \Sigma^{(2)}_{20}(0,0), \tag{4.42}$$

since the self energies (at zero four-momentum) $\Sigma^{(2)}_{11}$ and $\Sigma^{(2)}_{20}$ are already included in the LHY propagators $D^{(1)}_{\rm n}$ and $D^{(1)}_{\rm a}$. In order to compute the WS order, it is sufficient to approximate the normal molecular propagator by [38]

$$\begin{aligned} D^{(2)}_{\rm n}(p,\omega) &= D^{(1)}_{\rm n}(p,\omega)\Sigma'_{11}(p,\omega)D^{(1)}_{\rm n}(p,\omega) + D^{(1)}_{\rm n}(p,\omega)\Sigma'_{20}(p,\omega)D^{(1)}_{\rm a}(p,\omega) \\ &\quad + D^{(1)}_{\rm a}(p,\omega)\Sigma'_{20}(p,\omega)D^{(1)}_{\rm n}(p,\omega) + D^{(1)}_{\rm a}(p,\omega)\Sigma'_{11}(-p,-\omega)D^{(1)}_{\rm a}(p,\omega). \end{aligned} \tag{4.43}$$

Diagrammatically, the expansion is shown in Fig. 4.6. Because of the range of momenta relevant to the problem ($p \gg \sqrt{na}$), the propagators may be expanded in powers of the density and become

$$\begin{aligned} D^{(1)}_{\rm n}(p,\omega) &\approx D_0(p,\omega) \approx \frac{Z}{\omega - p^2/2m_{\rm b} + i0}, \\ D^{(1)}_{\rm a}(p,\omega) &\approx \Delta_0^2 t^{\rm bb} D_0(p,\omega) D_0(-p,-\omega) \approx \frac{Z\mu^{(2)}_{\rm b}}{\omega - p^2/2m_{\rm b} + i0}\frac{1}{-\omega - p^2/2m_{\rm b} + i0}. \end{aligned} \tag{4.44}$$

Inserting the resulting normal molecular propagator $D^{(2)}_{\rm n}$ in Eq. (4.34) results in an equation between the ground state energy and the chemical potential in WS order

$$\frac{\tilde{E}_0}{V} - \frac{1}{2}n_{\rm b}\tilde{\mu}_{\rm b} = \frac{iZ}{2}\lim_{\eta\to 0^+}\int\frac{d\omega}{2\pi}e^{i\eta\omega}\int\frac{d^3p}{(2\pi)^3}\left[\frac{\Sigma_{11}(p,\omega)(\omega + p^2/2m_{\rm b})}{\omega - p^2/2m_{\rm b} + i0}\right.$$

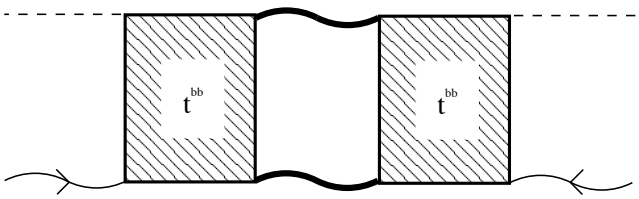

Figure 4.7: The class of diagrams which must be considered in the anomalous self energy.

$$-\frac{2\Sigma'_{20}(p,\omega)\mu_{\rm b}^{(2)}}{(\omega-p^2/2m_{\rm b}+i0)^2}+\frac{\Sigma'_{11}(-p,-\omega)\mu_{\rm b}^{(2)}}{(\omega-p^2/2m_{\rm b}+i0)^2(\omega+p^2/2m_{\rm b}+i0)}\Bigg]. \quad (4.45)$$

The quantity in square brackets is $(\omega+p^2/2m_{\rm b})D_{\rm n}^{(2)}(p,\omega)$ and the normal propagator has the property that any poles must lie slightly above the negative real ω axis or slightly below the positive real ω axis. Looking at the ω integration, which must be closed in the upper half plane, it is then concluded that the following contributions to the self energies need to be considered:

- poles of $\Sigma'_{20}(p,\omega)$ above the negative real axis
- poles of $\Sigma'_{11}(p,\omega)$ above the negative real axis, and
- poles of $\Sigma'_{11}(-p,-\omega)$ above the negative real axis as well as the momentum dependence of $\Sigma_{11}^{(2)}(p,p^2/2)$.

The simplest class of diagrams entering the anomalous self energy sum to give the molecule-molecule scattering t-matrix. This reduces to a constant at $p\ll a^{-1}$ and this class of diagrams does not have any poles at relevant momenta. Poles above the negative real exis become possible if, in the molecule-molecule scattering problem, a pair of bare molecular propagators are replaced by the iterated propagators $D^{(1)}$, thus all diagrams of the form depicted in Fig. 4.7 must be taken into account. The leading of these diagrams is shown in Fig. 4.8. Carrying out the frequency integration, anticipating that the main contribution will be from $p\ll a^{-1}$ and $\omega\ll 1/ma^2$, results in

$$\tilde{\Sigma}'_{20}(p,\omega)=4\Delta_0^2Z^2\mu_{\rm b}^{(2)}\left(t^{\rm bb}\right)^2\int\frac{d^3q}{(2\pi)^3}\frac{m_{\rm b}}{q^2\left(\omega+q^2/2m_{\rm b}+k^2/2m_{\rm b}-i0\right)}. \quad (4.46)$$

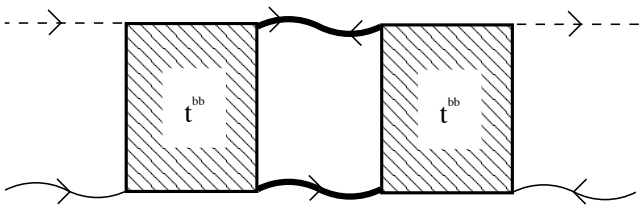

Figure 4.8: The diagram belonging to $\Sigma'_{20}(p,\omega)$ which gives the leading contribution in Eq. (4.45).

For simplicity $\vec{k} \equiv \vec{p} + \vec{q}$. The tilde signifies that this is the only relevant part of the self energy at WS order. In the prefactor, the factor 4 comes from combinatorics, $Z^2\mu_{\rm b}^{(2)}$ from propagators, Δ_0^2 from condensate lines, and $\left(t^{\rm bb}\right)^2$ from the two t-matrices evaluated at low momenta.

The normal self energy is constructed in the same way. The two leading diagrams relevant for computing the poles of $\Sigma'_{11}(p,\omega)$ above the negative real ω axis are shown in Fig. 4.9. The sum of these diagrams is

$$\tilde{\Sigma}'_{11}(p,\omega) = -4\Delta_0^2 Z^2 \left(\mu_{\rm b}^{(2)}\right)^2 \left(t^{\rm bb}\right)^2 \int \frac{d^3q}{(2\pi)^3} \left(\frac{1}{q^2k^2} + \frac{1}{k^4}\right) \frac{m_{\rm b}^2}{\omega + q^2/2m_{\rm b} + k^2/2m_{\rm b} - i0}, \tag{4.47}$$

where it is again anticipated that only momenta small compared with the inverse scattering length are relevant.

The final contribution from molecular self energies comes from $\Sigma'_{11}(-p,-\omega)$ and here it is important to include the momentum dependence of the self energy. This

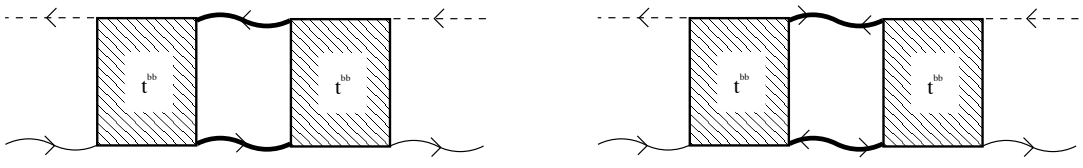

Figure 4.9: The diagrams belonging to $\Sigma'_{11}(p,\omega)$ which result in the leading terms in the low density expansion of Eq. (4.45).

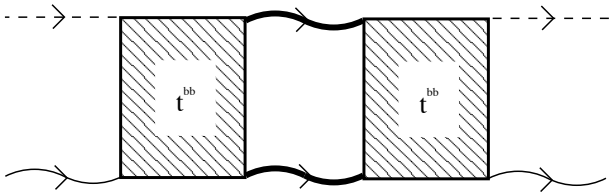

Figure 4.10: A contribution from $\Sigma'_{11}(-p,-\omega)$.

may be included by considering the relation between the normal self energy and the scattering amplitude. This relation was first derived by Beliaev [8, 9] (and similar results for fermion scattering by Galitskii [31]) and at relevant momenta it takes the approximate form [38]

$$\begin{aligned}\Sigma_{11}(p,\omega) &\approx 2\Delta_0^2 \mathrm{Im} f_s(p/2,p/2) \\ &+2Z^2\Delta_0^2\left(t^{\mathrm{bb}}\right)^2\int\frac{d^3q}{(2\pi)^3}\left(\frac{1}{\omega-p^2/4m_{\mathrm{b}}-q^2/m_{\mathrm{b}}+i0}+\frac{1}{q^2/m_{\mathrm{b}}-p^2/4m_{\mathrm{b}}-i0}\right).\end{aligned} \quad (4.48)$$

Here $f_s(p,q) \equiv \left(f(p,q)+f(-q,p)\right)/2$ is a symmetrized scattering amplitude and reduces at small momenta to t^{bb}. Note how the first term under the integral simply corresponds to the diagram of Fig. 4.10 while the second term under the integral is a kinematic term. The reasoning behind Eq. (4.48) is that while the scattering amplitude between two particles contains the possibility of multiple scattering, it is still an intrinsic two-body quantity in the sense that it is assumed that after the scattering the two particles are in the vacuum and on-shell which is certainly not true in the many-body case. The proof by Beliaev of this equation is for a dilute gas of bosons but it goes through in exactly the same way in the problem of the weakly bound bosonic molecules, since the assumption is that the potential between the bosons (which in the case of the fermion problem is replaced by the two-boson irreducible diagram Γ, see chapter 3) reduces to a constant at momenta $p \ll a^{-1}$.

The imaginary part in the first term of Eq. (4.48) may be written in a different

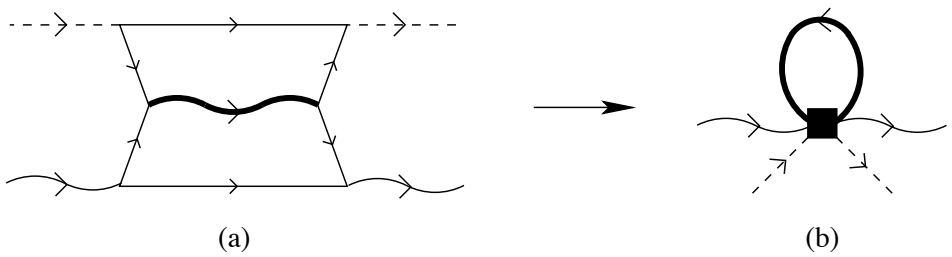

Figure 4.11: An illustration of how fermions may be thought of as constants at low momenta. Fermions lines are drawn as straight thin lines.

way, as also found by Beliaev,

$$\mathrm{Im} f_s(p/2, p/2) = -Z^2 \left(t^{\mathrm{bb}}\right)^2 \mathrm{Im} \int \frac{d^3q}{(2\pi)^3} \frac{1}{q^2/m_{\mathrm{b}} - p^2/4m_{\mathrm{b}} - i0}. \tag{4.49}$$

The real part of the first term in Eq. (4.48) is simply the scattering matrix t^{bb} which reduces to a constant and does not contribute to the ground state energy.

At this point it is important to investigate whether the presence of the fermionic atoms affects self energies at the current order. The effect of replacing a bare molecular propagator insde the two-boson irreducible diagram by an iterated propagator $D_{\mathrm{n}}^{(1)}$ must be examined. As an example, consider the diagrams in Fig. 4.11. The fermionic propagators in this diagram all have chemical potential $\mu = -1/2ma^2$ in the BEC regime of the gas, see Eq. (3.40). Equivalently, when a molecule in the vacuum breaks into two atoms they equally share the binding energy $-1/ma^2$. For momenta small compared with the inverse scattering length, the fermionic propagators are thus approximately constant and the diagram shown in Fig. 4.11a effectively shrinks to that of Fig. 4.11b. The integration over the normal propagator closed on itself was performed in Eq. (4.21) and goes as Δ_0^3. Thus the diagram in Fig. 4.11a goes as Δ_0^5 and is of higher order than the WS order. The same argument goes through for all two-boson irreducible diagrams with molecular propagators replaced by iterated propagators.

The fermionic atoms are also modified by their self energies. The anomalous fermion self energy at lowest order is simply two fermions coming in and a condensate

line going out. Such anomalous self energies must come in pairs and thus modifying the two-boson irreducible diagram by the simplest two such anomalous self energies simply corresponds to adding the possibility of three boson scattering. This in turn only contributes at order Δ_0^4. The normal fermion self energy consists of atom-molecule scattering. Replacing a fermion propagator with the atom-molecule scattering process inside the two-boson irreducible diagram again results in a diagram belonging to the class of three boson scattering. Furthermore, the atom-molecule diagram reduces to a constant at $p \ll a^{-1}$. Thus the presence of this self energy does not change the pole structure of the two-boson irreducible diagram in the range of momenta and energies under consideration.

Each two-boson irreducible diagram will contain exactly one fermion loop. The external four-momentum going into the two-boson irreducible diagram may be contained completely inside the loop and since the fermionic propagators are constant at $p \ll a^{-1}$, the pole structure of the molecular self energies at small momenta is completely unchanged by the presence of fermions in the problem.

The conclusion to this discussion is that the presence of fermionic atoms does not change the chemical potential and ground state energy from the results of the standard dilute Bose gas beyond replacing the scattering length a_b with $0.60a$.

The rest is mathematics. Inserting the self energies, Eqs. (4.46), (4.47), and (4.48) in Eq. (4.45) and performing the integrals, the result is [38]

$$\frac{\tilde{E}_0}{V} - \frac{1}{2} n_\mathrm{b} \tilde{\mu}_\mathrm{b} = Z \Delta_0^2 \left(\mu_\mathrm{b}^{(2)}\right)^2 \frac{1}{32\pi^2} \left(\frac{4}{3} - \frac{\sqrt{3}}{\pi}\right) \int \frac{dp}{p}. \tag{4.50}$$

The range of integration is determined by p being in the range $\sqrt{na} \ll p \ll a^{-1}$ and with logarithmic accuracy $\sqrt{na}$ and a^{-1} may be used as the actual limits of integration.

Using the relation (4.32) between the ground state energy and the chemical potential as well as the particle number equation (4.30) the result of the usual dilute Bose

gas [76, 65] is reproduced

$$\frac{\tilde{E}_0}{V} = 16\pi^2 \frac{n_{\rm b}^3 a_{\rm b}^4}{m_{\rm b}} \left(\frac{4}{3} - \frac{\sqrt{3}}{\pi} \right) \log(n_{\rm b} a_{\rm b}^3), \tag{4.51}$$

$$\tilde{\mu}_{\rm b} = 48\pi^2 \frac{n_{\rm b}^2 a_{\rm b}^4}{m_{\rm b}} \left(\frac{4}{3} - \frac{\sqrt{3}}{\pi} \right) \log(n_{\rm b} a_{\rm b}^3). \tag{4.52}$$

It has been assumed that $n_{\rm b}$ does not contain terms of order $\Delta_0^4 \log \Delta_0$. Arguments similar to those given above show that this assumption is indeed correct.

In conclusion, the LHY and WS terms in the low density expansion arise from non-trivial renormalizations due to the infrared divergences of molecular propagators. At low momenta the fermionic atoms in the BEC regime are nearly constants and their dynamics do not affect the low-density expansion of the chemical potential and ground state energy at the order considered here. However, from the above discussion, and also from the Hugenholtz-Pines relation (3.44), it is obvious that the presence of fermions will affect next order quantities in a non-trivial way.

Chapter 5

Two-component Fermi gases with a mass imbalance

Since the experimental discovery of the BCS-BEC crossover in ultracold mixtures of atoms in two different hyperfine states of e.g. ^{40}K [69], a major effort has gone into creating other more exotic superfluids. An example is a system with a mass imbalance, where instead of studying two different hyperfine states of the same fermionic atom, a mixture of two different atomic species is used. While experiments in these mixtures are still in their infancy, these systems have received considerable theoretical attention [56, 59, 39]. The interest in these systems has several reasons. For instance, the advent of the use of optical lattices in ultracold gases has opened up the possibility of continuously changing the effective mass of one of the species independently of the other, since the resonant frequencies of the atomic species will be different.

One might naively expect that the presence of a mass imbalance would serve only to modify the few-body coupling constants computed in chapter 3. However, it turns out that beyond a certain mass ratio, the physical picture becomes quite different. It was discovered in Ref. [57] that, as the mass imbalance is increased, collisional losses of the Fermi gas also increase. For small mass imbalances, the gas becomes more stable as a Feshbach resonance is approached. Conversely, beyond a mass ratio of 12.33 the system becomes less stable as a Feshbach resonance is approached and finally, beyond the mass ratio 13.6, the three body system was found to display bound states in a manner very similar to the Efimov phenomenon in systems of three bosons [25].

For moderate mass ratios, the main effect of introducing a mass imbalance is indeed to change the few-body coupling constants. Results for the three and four fermion problems, calculated in coordinate space using the Bethe-Peirls method, have been obtained in Refs. [56, 58]. The results for four fermions have been confirmed by Monte Carlo methods in Ref. [75]. Thus, the results in this chapter for three- and four-body scattering calculated using the momentum space formalism are not new, rather they confirm already known results by the use of a complimentary method.

Even though the Fermi energies will be different, in heteronuclear mixtures with equal densities of the two atomic species, the Fermi momenta will be equal. This means that the usual Cooper pairing is still taking place on the BCS side and the picture of a BCS-BEC crossover is valid. In this chapter the BEC regime with equal densities will be examined.

5.1 Molecular propagator

The formalism presented here is very similar to that presented in chapter 3. Consider two species of fermionic atoms interacting close to a heteronuclear Feshbach resonance. For simplicity of notation, even though the particles are not different hyperfine states of the same isotope, the particles will be called $\uparrow$ and $\downarrow$. Let the particles have masses

$$m_\uparrow \equiv \gamma m, \qquad m_\downarrow \equiv m \tag{5.1}$$

and chemical potentials $\mu_\uparrow, \mu_\downarrow < 0$.

To calculate the molecular propagator, the polarization bubble which appears in the repeated scattering between the two species of atoms is needed (see Fig. 3.1). The polarization bubble has the value

$$\begin{aligned} \Pi(p,\omega) &= i\int \frac{d^4q}{(2\pi)^4} G_\uparrow(q+p/2)G_\downarrow(-q+p/2) \\ &= \int \frac{d^3q}{(2\pi)^3} \frac{1}{\omega - (q+p/2)^2/2m_\uparrow - (q-p/2)^2/2m_\downarrow + \mu_\uparrow + \mu_\downarrow + i0} \end{aligned}$$

$$= -\frac{m_{\rm r}\Lambda^2}{\pi^2} + \frac{m_{\rm r}^{3/2}}{\sqrt{2}\pi}\sqrt{-\omega + p^2/2m_{\rm b} - \mu_\uparrow - \mu_\downarrow - i0}, \tag{5.2}$$

where it has been used that q can be shifted such that the angular integration becomes trivial (let $q \to q + \frac{1}{2}\frac{m_\uparrow - m_\downarrow}{m_\uparrow + m_\downarrow}p$). Here

$$m_{\rm r} = \frac{m_\uparrow m_\downarrow}{m_\uparrow + m_\downarrow} \tag{5.3}$$

is the reduced mass and $m_{\rm b} = m_\uparrow + m_\downarrow$ is the mass of the molecule.

The scattering length between the two species of atoms is related to the *vacuum* polarization bubble (for which $\mu_\uparrow = \mu_\downarrow = 0$) by

$$a = \frac{m_{\rm r}}{2\pi}T(0) = \frac{m_{\rm r}}{2\pi}\frac{-\lambda}{1 + \lambda\Pi(0)} = \left(-\frac{2\pi}{m_{\rm r}\lambda} + \frac{2\Lambda}{\pi}\right)^{-1}. \tag{5.4}$$

The molecular propagator is then given by

$$D(p,\omega) = \frac{-\lambda}{1 + \lambda\Pi(p,\omega)} = \frac{2\pi}{m_{\rm r}}\frac{1}{a^{-1} - \sqrt{2m_{\rm r}}\sqrt{-\omega + p^2/2m_{\rm b} - \mu_\uparrow - \mu_\downarrow - i0}}, \tag{5.5}$$

which reduces to the usual form (3.16) in the limit of equal masses. According to Hugenholtz and Pines [38], the molecular propagator should have a pole at $p, \omega = 0$. This leads to the relation

$$E_{\rm b} = \mu_\uparrow + \mu_\downarrow = -\frac{1}{2m_{\rm r}a^2} \tag{5.6}$$

for the binding energy of the molecule.

In the limit of small momenta and energies, $p \ll a^{-1}$ and $\omega \ll 1/2m_{\rm r}a^2$, the underlying structure of the molecule is not probed. In this limit the propagator reduces to

$$D(p,\omega) \approx \frac{Z}{\omega - p^2/2m_{\rm b} + i0}. \tag{5.7}$$

$Z = \frac{2\pi}{m_{\rm r}^2 a}$ is the residue and the remainder is the free propagator of a particle with mass $m_{\rm b} = m_\uparrow + m_\downarrow$ as expected.

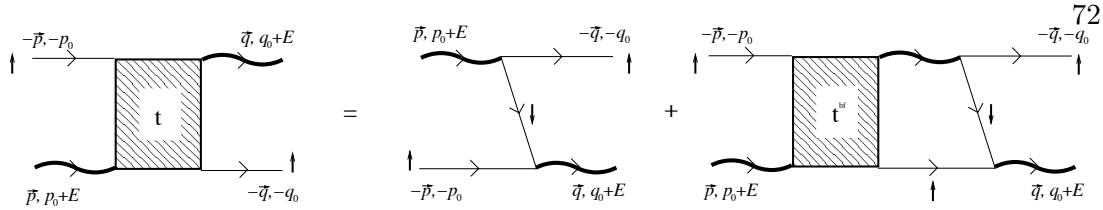

Figure 5.1: The integral equation satisfied by the atom-molecule scattering t-matrix.

5.2 Three-body problem

Assume an atom of type $\uparrow$ scatters off the bound molecular state. The general integral equation for the atom-molecule scattering matrix with kinematics as shown in Fig. 5.1 is given by

$$t(\vec{p},p_0;\vec{q},q_0) = -G_\downarrow(p+q+E) - i\int \frac{d^4Q}{(2\pi)^4} G_\downarrow(Q+q+E)G_\uparrow(-Q)D(Q+E)t(\vec{p},p_0;\vec{Q},Q_0). \tag{5.8}$$

E is here used both as the total energy and as the total four-momentum $(\vec{0},E)$. The symmetry factors are the same as in the mass-balanced case.

As in chapter 3, in the notation for the t-matrix the dependence on the total energy has been suppressed. Also, $E \leq E_\mathrm{b}$ in order for processes in which the molecule and atom scatters into a final state of three free atoms to be forbidden.

The frequency Q_0 can be integrated out by closing the contour in the upper half plane, where the only pole is the pole of $G_\uparrow(-Q)$. This results in

$$t(\vec{p},p_0;\vec{q},q_0) = -G_\downarrow(p+q+E) - \int \frac{d^3Q}{(2\pi)^3} G_\downarrow(Q+q+E)D(Q+E)t(\vec{p},p_0;\vec{Q},Q_0), \tag{5.9}$$

where $Q_0 = -Q^2/2m_\uparrow$.

Consider first the s-wave scattering length which is proportional to $t(\vec{0},0;\vec{0},0)$ evaluated at $E = E_\mathrm{b}$. The incoming momentum and frequency may be taken to vanish but the outgoing should be kept finite in order to have a solvable integral equation. The

result is the equation

$$\begin{aligned} t(p) &= \frac{2m_{\rm r}a^2}{1+p^2} \\ &+\frac{1+\gamma^{-1}}{2\pi p}\int_0^\infty dq \frac{q\,t(q)}{1-\sqrt{1+q^2\left[1-\gamma^2/(1+\gamma)^2\right]}}\log\frac{1+p^2+q^2+2qp/\left(1+\gamma^{-1}\right)}{1+p^2+q^2-2qp/\left(1+\gamma^{-1}\right)}, \end{aligned} \tag{5.10}$$

where momenta are measure in units of inverse scattering length. Here the integral equation for $t(p) \equiv t(\vec{0},0;\vec{p},-p^2/2m_\uparrow)$ is solved with $p_0 = -p^2/2m_\uparrow$ to make the dependence on momentum the same on both sides of the equation. This point has been discussed in detail in section 3.5.

Having solved Eq. (5.10) at a certain mass ratio, to calculate the scattering amplitude each external molecular propagator has to be renormalized by the square root of the residue of the pole of the molecular propagator. The scattering amplitude at vanishing momentum is thus

$$T(0) = Z\,t(0). \tag{5.11}$$

The relationship between the scattering amplitude and the scattering length is

$$T(0) = \frac{2\pi}{m_{3\rm r}}a_{\rm bf}, \tag{5.12}$$

with $m_{3\rm r} = \frac{m_{\rm b}m_\uparrow}{m_{\rm b}+m_\uparrow}$ being the three-body reduced mass. The three-body scattering length is found to be

$$a_{\rm bf} = \frac{m_{3\rm r}}{m_{\rm r}}\frac{t(0)}{m_{\rm r}a^2}a. \tag{5.13}$$

The result is shown in Fig. 5.2 and exactly matches the result of Petrov [56].

5.2.1 p-wave scattering and collisional relaxation

Up to now the only bound molecular two-atom state considered has been the weakly bound and large state of size comparable with the scattering length a. This state is the state appearing at a Feshbach resonance and is the highest ro-vibrational

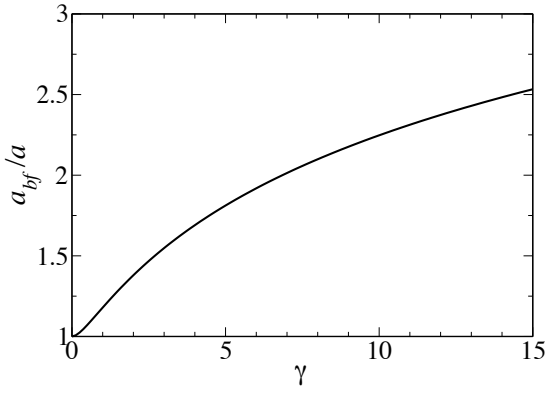

Figure 5.2: $a_{\rm bf}/a$ as a function of $\gamma \equiv m_\uparrow/m_\downarrow$.

state. Additionally, in the two body problem there are tightly bound states of size R_e, the scale at which short distance physics becomes important. Through collisions the weakly bound molecules can fall into these deeply lying states and in the process a binding energy of order $1/(mR_e^2)$ is converted into kinetic energy. The released energy is quite large and the colliding atoms will escape the system. This process is called collisional relaxation and is the process which determines the lifetime of the Bose gas of weakly bound molecules [57].

The rate at which the collisional relaxation occurs is conventionally written as either

$$\dot{n}_{\rm b} = -\alpha_{\rm rel} n_{\rm b}^2 \tag{5.14}$$

or

$$\dot{n}_{\rm b} = -\beta_{\rm rel} n_{\rm b}. \tag{5.15}$$

Both versions are natural; for the first, two molecules need to approach each other closely for the relaxation process to occur and $\alpha_{\rm rel}$ is the probability for this to occur. For the second $\beta_{\rm rel}^{-1}$ is the characteristic relaxation time. Below, the result will be presented in the form (5.14).

For equal masses of the constituent fermions the relaxation rate $\alpha_{\rm rel}$ decreases with increasing a as [57]

$$\alpha_{\rm rel} \propto \frac{R_e}{m}\left(\frac{R_e}{a}\right)^{2.55}. \tag{5.16}$$

This ensures the stability of the Fermi gas in the vicinity of a Feshbach resonance as opposed to the case of Bose gases which become unstable close to a Feshbach resonance. The reason for the stability of the Fermi gas is that the relaxation process requires three particles to approach each other within a distance of order R_e, while the remaining particle in the molecule-molecule scattering will typically be at a distance of order a. The probability for three fermions to approach each other is suppressed because of the Pauli principle, since two of the fermions will necessarily be identical.

It was shown in Ref. [56] that the leading relaxation channel at large a is scattering through the p-wave channel. In general the relaxation rate may be written as

$$\alpha_{\rm rel} \propto \frac{R_e}{m}\left(\frac{R_e}{a}\right)^{s}. \tag{5.17}$$

The power s is a function of the mass imbalance. s is related to the power-law behavior $\psi \sim \rho^{\nu-1}$ satisfied by (the p-wave part of) the three-body wave function in the range $R_e \ll \rho \ll a$ by $s = 2\nu + 1$. This can be seen from estimating the probability for the three particles to be within a distance of R_e of each other. This probability is

$$\frac{\int_0^{R_e} d^3\rho\, |\psi(\rho)|^2}{\int_0^{a} d^3\rho\, |\psi(\rho)|^2} = \left(\frac{R_e}{a}\right)^{2\nu+1}. \tag{5.18}$$

The relation between the outgoing part of the wavefunction and (the p-wave part of) the t-matrix is

$$\begin{aligned}\psi_{\rm out}(\vec{r}_1,\vec{r}_2,\vec{r}_3) &= \int \frac{d^4p}{(2\pi)^4}\int \frac{d^4q}{(2\pi)^4} D(p+E)t\left(\vec{0},0;\vec{p},p_0\right)\\ &\quad\times G_\uparrow(p-q+E)G_\uparrow(-p)G_\downarrow(q)e^{i\vec{r}_1\cdot(\vec{p}_1+\vec{p}_2)+i\vec{r}_2\cdot\vec{p}_2-i\vec{r}_3\cdot\vec{p}_1}.\end{aligned} \tag{5.19}$$

This relation is illustrated in Fig. 5.3. If the t-matrix scales as $t(p) \propto p^\delta$ at large momenta, $p \gg a^{-1}$, then

$$s = -3 - 2\delta. \tag{5.20}$$

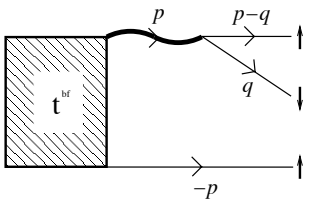

Figure 5.3: Relation between the scattering matrix and the scattered wave function.

The collisional relaxation rate may be calculated by noting that the scattering t-matrix can be written as the sum over partial waves

$$t(\vec{p}, p_0; \vec{q}, q_0) = \sum_{\ell=0}^{\infty} (2\ell + 1) P_\ell(\cos\theta) t^{(\ell)}(p, p_0; q, q_0). \tag{5.21}$$

Here θ is the angle between $\vec{p}$ and $\vec{q}$. $P_\ell(\cos\theta)$ are the Legendre polynomials of which the first few are

$$\begin{aligned} P_0(x) &= 1, \\ P_1(x) &= x, \\ P_2(x) &= \frac{1}{2}(3x^2 - 1). \end{aligned}$$

These satisfy the orthogonality relation

$$\int_{-1}^{1} P_{\ell'}(x) P_\ell(x)\, dx = \frac{2}{2\ell + 1} \delta_{\ell'\ell}. \tag{5.22}$$

To see that the integral equations for the partial waves decouple, consider the general integral equation, Eq. (5.8). Let θ denote the angle between $\vec{p}$ and $\vec{q}$ and likewise ϕ the angle between $\vec{q}$ and $\vec{Q}$. Then the angle γ between $\vec{p}$ and $\vec{Q}$ satisfies $\cos\gamma = \cos\theta\cos\phi + \sin\theta\sin\phi\cos\lambda$. With this definition of angles, only the t-matrix under the integral depends on the azimuthal angle and the corresponding integration may be carried out as

$$\int_0^{2\pi} \frac{d\lambda}{2\pi}\, t(\vec{p}, p_0; \vec{Q}, Q_0) = \sum_{\ell=0}^{\infty} P_\ell(\cos\theta) P_\ell(\cos\phi) t^{(\ell)}(p, p_0; Q, Q_0). \tag{5.23}$$

Here the addition theorem for Legendre polynomials [44]

$$P_\ell(\cos\gamma) = P_\ell(\cos\theta)P_\ell(\cos\phi) + \sum_{m=1}^{\ell} 2\frac{(\ell-m)!}{(\ell+m)!}P_\ell^m(\cos\theta)P_\ell^m(\cos\phi)\cos m\lambda \qquad (5.24)$$

has been used. The integral equations are now decoupled by using the orthogonality relation 5.22 with the result

$$\begin{aligned} t^{(\ell)}(p,p_0;q,q_0) &= -\frac{1}{2}\int_{-1}^{1} d(\cos\theta)\, P_\ell(\cos\theta)G_\downarrow(p+q+E) \\ &-\frac{1}{4\pi^2}\int_0^\infty Q^2 dQ t^{(\ell)}(p,p_0;Q,Q_0)D(Q+E)\int_{-1}^{1} d(\cos\phi)\, P_\ell(\cos\phi)G_\downarrow(q+Q+E), \end{aligned} \qquad (5.25)$$

where $Q_0 = -Q^2/2m_\uparrow$.

To solve the integral equation for the p-wave contribution, let $q_0 \to -q^2/2m_\uparrow$. For simplicity let also $p_0 \to -p^2/2m_\uparrow$. The p-wave contribution to the t-matrix satisfies

$$\begin{aligned} &t^p(p,-p^2/2m_\uparrow;q,-q^2/2m_\uparrow) \\ &\quad = ma^2\left(\frac{1}{pq} - \frac{(1+\gamma^{-1})(1+p^2+q^2)}{4p^2q^2}\log\frac{1+p^2+q^2+2pq/(1+\gamma^{-1})}{1+p^2+q^2-2pq/(1+\gamma^{-1})}\right) \\ &\quad\quad + \frac{1+\gamma^{-1}}{\pi}\int_0^\infty Q^2 dQ \frac{t(p,-p^2/2m_\uparrow;Q,-Q^2/2m_\uparrow)}{1-\sqrt{1+Q^2\left[1-\gamma^2/(1+\gamma)^2\right]}} \\ &\quad\quad \times\left(\frac{1}{qQ} - \frac{(1+\gamma^{-1})(1+q^2+Q^2)}{4q^2Q^2}\log\frac{1+q^2+Q^2+2qQ/(1+\gamma^{-1})}{1+q^2+Q^2-2qQ/(1+\gamma^{-1})}\right) \end{aligned} \qquad (5.26)$$

at $E = E_\mathrm{b}$. Fig. 5.4 shows the dependence of s on the mass imbalance found by solving Eq. (5.26). The curve matches the result of Ref. [58].

It is seen that above a mass ratio of $m_\uparrow/m_\downarrow \approx 12.3$ the relaxation rate *increases* with increasing scattering length. This is nicely explained in the Born-Oppenheimer picture [58]; in the case of a large mass ratio, if the two heavy atoms are separated by a distance much smaller than a, then the presence of the light atom will mediate an effective attractive $\frac{1}{r^2}$ potential between the heavy atoms. On the other hand, the Pauli principle results in the centrifugal barrier, which is a repulsive $\frac{1}{r^2}$ potential. The mass imbalance of 12.3 corresponds to the cancellation of these potentials in the Born-Oppenheimer picture. As the mass ratio is further increased, the attractive potential is

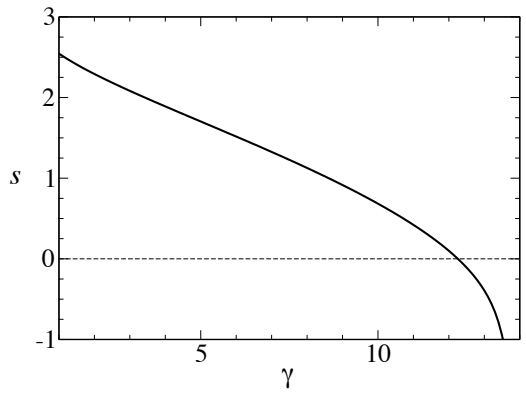

Figure 5.4: The power s appearing in the relaxation rate, Eq. (5.17), as a function of γ.

also increased and at a mass ratio of approximately 13.6 one encounters the phenomenon of the fall to the centre [44]: The system displays a behavior characteristic of the Efimov phenomenon[25] where a hierarchy of three-body bound states appear [58]. The short distance physics becomes very important and a short range three-body parameter is needed in order to accurately describe the physics, see e.g. Refs. [7, 12].

5.3 Scattering of composite molecules

Consider now the 4-body problem with a mass imbalance. The present calculation follows closely the mass-balanced molecule-molecule scattering calculation presented in section 3.6. Thus some intermediate steps in the calculation will be skipped.

The governing integral equation is formally identical to the problem of equal masses, Eq. (3.67), that is

$$t(p,p_0)=\Gamma(0,0;p,p_0)+\frac{i}{4\pi^3}\int q^2 dq\, dq_0 D(q,q_0+E/2)D(q,-q_0+E/2)\Gamma(q,q_0;p,p_0)t(q,q_0). \tag{5.27}$$

The difference from the previous calculation is that now both the molecular propagator and the two-boson irreducible vertex, Γ, depend on the mass-ratio.

Below, the convention is used that all atomic propagators have their frequency shifted by a quarter of the energy going into the scattering, while the molecules have their frequency shifted by half the energy. That is

$$G_{\uparrow,\downarrow}(p,p_0) \equiv \frac{1}{p_0 - p^2/2m_{\uparrow,\downarrow} + E/4 + i0}, \tag{5.28}$$

$$D(p,p_0) = \frac{2\pi}{m_{\rm r}} \frac{1}{a^{-1} - \sqrt{2m_{\rm r}}\sqrt{-p_0 - E/2 + p^2/2m_{\rm b} - i0}}. \tag{5.29}$$

The relation between Γ and Ξ is

$$\Gamma(q,q_0;p,p_0) = \frac{i}{2}\int \frac{d^4Q}{(2\pi)^4} G_\uparrow(p/2+Q)G_\downarrow(p/2-Q)\Xi(q;p/2+Q;p/2-Q), \tag{5.30}$$

and the vertex Ξ satisfies

$$\begin{aligned}\Xi(q;p/2+Q;p/2-Q) &= -\int \frac{d\Omega_{\vec{q}}}{4\pi}\left[G_\uparrow(-p/2-q+Q)G_\downarrow(-p/2+q-Q) + (q \leftrightarrow -q)\right] \\ &-i\int \frac{d^4Q'}{(2\pi)^4}\left\{G_\downarrow(p/2-Q')G_\uparrow(-3p/2+Q')D(-p-Q+Q')\Xi(q;p/2+Q;p/2-Q')\right. \\ &\left.+G_\uparrow(p/2+Q')G_\downarrow(-3p/2-Q')D(-p+Q-Q')\Xi(q;p/2+Q';p/2-Q)\right\}. \end{aligned} \tag{5.31}$$

The vertex $\Xi(q;p/2+Q;p/2-Q)$ may again be split into parts $\Xi^+(q;p/2+Q;p/2-Q)$ $[\Xi^-(q;p/2+Q;p/2-Q)]$ analytic in the upper [lower] half planes of Q_0, with

$$\Xi(q;p/2+Q;p/2-Q) = \Xi^+(q;p/2+Q;p/2-Q) + \Xi^-(q;p/2+Q;p/2-Q). \tag{5.32}$$

To achieve this use Eq. (3.73). Now insert Eq. (5.32) into Eq. (5.30) and perform the frequency integrations over simple poles (fermionic propagators). The iterated terms in the integral equations for $\Xi^\pm$ evaluated at the values of frequency dictated by the simple poles will then only depend on an on-shell vertex

$$\Xi(q;\vec{p}_1,p_1^2/2m_\uparrow - E/4;\vec{p}_2,p_2^2/2m_\downarrow - E/4) \equiv \chi(q;\vec{p}_1,\vec{p}_2). \tag{5.33}$$

Again, as in section 3.6, the on-shell frequencies would have been obtained had $G_\uparrow(p_1)$ and $G_\downarrow(p_2)$ been attached to the vertex $\Xi(q;p_1;p_2)$ and their frequencies been integrated out using a contour around their simple poles.

The solution of the integral equation for the on-shell vertex χ is now possible with the substitution

$$p_0 \to (\vec{p}/2+\vec{Q})^2/2m_\uparrow + (\vec{p}/2-\vec{Q})^2/2m_\downarrow - E/2. \tag{5.34}$$

The equation for the on-shell vertex is

$$\begin{aligned}\chi(q;\vec{p}_1,\vec{p}_2) &= -\int \frac{d\Omega_{\vec{q}}}{4\pi}\left[G_\downarrow(q-p_1)G_\uparrow(-q-p_2)+(q\leftrightarrow -q)\right] \\ &\quad -\int \frac{d^3Q}{(2\pi)^3}\left\{ G_\uparrow(-p_1-p_2-Q)D(-Q-p_1)\chi(q;\vec{p}_1,\vec{Q})\Big|_{Q_0=Q^2/2m_\downarrow-E/4}\right. \\ &\quad \left. + G_\downarrow(-p_1-p_2-Q)D(-Q-p_2)\chi(q;\vec{Q},\vec{p}_2)\Big|_{Q_0=Q^2/2m_\uparrow-E/4}\right\}, \end{aligned}\tag{5.35}$$

where $(p_1)_0 = p_1^2/2m_\uparrow - E/4$ and $(p_2)_0 = p_2^2/2m_\downarrow - E/4$.

The relation between Γ and χ is

$$\begin{aligned}\Gamma(q,q_0;p,p_0) &= \Gamma^{(0)}(q,q_0;p,p_0) \\ &\quad -\frac{1}{2}\int \frac{d^3p_1}{(2\pi)^3}\frac{d^3p_2}{(2\pi)^3}\left[G_\downarrow(p-p_1)G_\uparrow(-p-p_2)+(p\leftrightarrow -p)\right]D(-p_1-p_2)\chi(q;\vec{p}_1,\vec{p}_2). \end{aligned}\tag{5.36}$$

Again $(p_1)_0 = p_1^2/2m_\uparrow - E/4$ and $(p_2)_0 = p_1^2/2m_\downarrow - E/4$ and p_0 is a free parameter. $\Gamma^{(0)}$ is the result of calculating the Born diagram,

$$\begin{aligned}\Gamma^{(0)}(q,q_0;p,p_0) &= -i\int \frac{d\Omega_{\vec{q}}}{4\pi}\int \frac{d^4Q}{(2\pi)^4} G_\uparrow(Q+p/2+q/2)G_\uparrow(Q-p/2-q/2) \\ &\qquad \times G_\downarrow(-Q-p/2+q/2)G_\downarrow(-Q+p/2-q/2) \\ &= -2\int \frac{d\Omega_{\vec{q}}}{4\pi}\int \frac{d^3Q}{(2\pi)^3}\frac{A}{(A^2-B^2)(A^2-C^2)}, \end{aligned}\tag{5.37}$$

with

$$A = E/2 - Q^2/2m_{\rm r} - p^2/8m_{\rm r} - q^2/8m_{\rm r} - \vec{p}\cdot\vec{q}/4m_\uparrow + \vec{p}\cdot\vec{q}/4m_\downarrow, \tag{5.38}$$

$$B = p_0 - \vec{Q}\cdot\vec{p}/2m_\uparrow + \vec{Q}\cdot\vec{p}/2m_\downarrow - \vec{Q}\cdot\vec{q}/2m_{\rm r}, \tag{5.39}$$

$$C = q_0 - \vec{Q}\cdot\vec{q}/2m_\uparrow + \vec{Q}\cdot\vec{q}/2m_\downarrow - \vec{Q}\cdot\vec{p}/2m_{\rm r}. \tag{5.40}$$

Finally, to relate the scattering amplitude to the scattering t-matrix at vanishing incoming energy and momentum use

$$T(0) = Z^2 t(0), \tag{5.41}$$

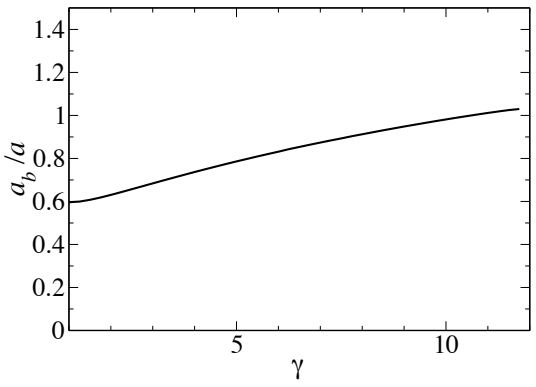

Figure 5.5: The scattering length a_b as a function of mass-imbalance, $\gamma = m_\uparrow/m_\downarrow$. Above a mass ratio of about $\gamma \approx 10$ convergence becomes very slow and numerical errors quite large. The curve is thus only plotted to $\gamma = 12$.

while the scattering amplitude is related to the scattering length by

$$T(0) = \frac{2\pi}{M_\mathrm{r}} a_b. \tag{5.42}$$

$M_\mathrm{r} = \frac{1+\gamma}{2} m$ is the reduced molecular-molecular mass. The result is shown in Fig. 5.5 and matches the result of Refs. [58, 75].

Chapter 6

Superfluidity close to a p-wave resonance

Attention will now be turned to atomic Fermi gases interacting close to a p-wave Feshbach resonance. At low energies, because of the angular momentum barrier, typically s-wave scattering will dominate. However, in gases consisting of identical fermionic atoms, the Pauli exclusion principle prevents s-wave scattering. At low temperatures in these systems, p-wave scattering will dominate over higher angular momentum scattering, and the study of p-wave resonantly paired Fermi gases is therefore of fundamental interest.

The p-wave resonantly coupled superfluid state has not yet been observed experimentally in degenerate atomic gases, but p-wave Feshbach resonances have been observed in both ^{40}K [69] and ^{6}Li [67]. Considerable theoretical attention has been given to the subject [36, 22, 35, 17, 34], particularly since it was pointed out [35] that the two-dimensional p-wave superfluids may display phases which are candidates for quantum computing systems. Below, only three-dimensional systems will be considered.

The gas of p-wave resonantly paired fermions is in many ways a richer system than the s-wave system considered in the previous chapters. In the s-wave paired superfluid, the BCS and BEC phases were merely different limits of the same phase, but this is no longer true in p-wave systems. The order parameters now correspond to different projections of angular momentum and distinct symmetries. This allows for

the possibility of genuine phase transitions which in some cases can even be topological [74, 62, 22, 35] and the phase diagram becomes much richer.

An interesting theoretical feature of the p-wave Feshbach resonances is that they are naturally narrow, whereas most s-wave resonances studied in experiments are wide. This means that a quantitatively correct perturbative approach may be used across the whole crossover [34]. However, as discussed below, the Feshbach resonances fall into categories of weak and strong, and while the weak resonances are amenable to a mean field treatment, as performed in Ref. [34], the strong resonances must be treated more carefully. In particular, it will be shown in chapter 7 that the system close to a strong resonance will contain three-body bound states (trimers), an effect first noticed by Y. Castin and co-workers [16].

In this chapter, the two-channel model for p-wave Feshbach resonances will be introduced and its parameters related to those of basic scattering theory. Next the important distinctions between wide and narrow and between weak and strong Feshbach resonances will be discussed.

6.1 A two-channel model for p-wave resonances

Consider a system of N identical (atoms in the same hyperfine state) spin-less fermions of mass m. At low energies, the scattering will proceed entirely in the p-wave channel, since s-wave scattering is excluded due to the Pauli principle and higher order scattering is suppressed. As in the s-wave problem, it is convenient to describe the system by a two-channel model. For the p-wave resonantly coupled superfluid the two-channel Hamiltonian is given by [71, 70, 37, 35, 17, 34]

$$H = \sum_{p} \frac{p^2}{2m} \hat{a}^{\dagger}_{\vec{p}} \hat{a}_{\vec{p}} + \sum_{\vec{q},\mu} \left(\epsilon_0 + \frac{q^2}{4m} \right) \hat{b}^{\dagger}_{\mu,\,\vec{q}} \hat{b}_{\mu,\,\vec{q}} + \sum_{\vec{p},\vec{q},\mu} \frac{g(|\vec{p}|)}{\sqrt{V}} \left(\hat{b}_{\mu,\,\vec{q}}\; p_{\mu}\; \hat{a}^{\dagger}_{\frac{\vec{q}}{2}+\vec{p}}\; \hat{a}^{\dagger}_{\frac{\vec{q}}{2}-\vec{p}} + h.c. \right). \tag{6.1}$$

The operators $\hat{a}^\dagger_{\vec{p}}$, $\hat{a}_{\vec{p}}$ are creation and annihilation operators of the fermionic atoms of momentum $\vec{p}$. Similarly, $\hat{b}^\dagger_{\mu,\vec{p}}$, $\hat{b}_{\mu,\vec{p}}$ are creation and annihilation operators of the bosonic spin 1 molecules with the vector index μ being the spin projection on some axis. The coupling $g(|\vec{p}|)$ appears as the amplitude for the transition from a pair of identical fermions with relative momentum $\vec{p}$ and orbital angular momentum 1 into the bare closed-channel molecular state with internal angular momentum 1.

The superfluid described by the two-channel Hamiltonian (6.1) is controlled by four parameters. The first of these is the bare detuning ϵ_0. This may in principle have a directional dependence, however for simplicity it will be taken constant in this thesis. The second parameter is the particle number N, which is the expectation value of the operator

$$\hat{N} = \sum_p \hat{a}^\dagger_{\vec{p}}\hat{a}_{\vec{p}} + 2\sum_{\mu,\vec{q}} \hat{b}^\dagger_{\mu,\vec{q}}\hat{b}_{\mu,\vec{q}}. \tag{6.2}$$

It is convenient to trade the particle number for the energy scale

$$\epsilon_F = \left(\frac{6\pi^2 N}{V}\right)^{2/3}/2m. \tag{6.3}$$

In the absence of the Feshbach molecules this would have been the Fermi energy. The remaining two parameters are contained in the coupling constant $g(|\vec{p}|)$. Taking g constant would imply that the interactions take place at a point in space, as if the molecules were infinitesimally small. However, in practice the molecules have a finite size set by the range of the interactions, R_e. $g(|\vec{p}|)$ is in turn proportional to the wave function of the molecule in momentum space and should be taken approximately constant for $p \ll \Lambda \sim \frac{1}{R_e}$ while quickly dropping to zero for $p \gg \Lambda$. Thus define a cut-off function

$$g(|\vec{p}|) \equiv g\,\xi(|\vec{p}|). \tag{6.4}$$

In this introductory chapter to the physics of p-wave resonantly coupled superfluids, the simplest cut-off function, a step function, will be used. This choice is

$$\xi(|\vec{p}|) = \Theta(1 - |\vec{p}|/\Lambda), \tag{6.5}$$

which is 1 for $|\vec{p}| < \Lambda$ and 0 above. In chapter 7 both this and a "softer" cut-off will be investigated.

6.1.1 The diagrammatic approach

The propagator of fermionic atoms is

$$G(p,\omega) = \frac{1}{\omega - p^2/2m + i0}. \tag{6.6}$$

From the Hamiltonian (6.1), the propagator of the bare closed-channel molecule may be read off to be

$$D_{0,\mu\nu}(p,\omega) = \frac{\delta_{\mu\nu}}{\omega - \epsilon_0 - p^2/4m + i0}. \tag{6.7}$$

As in chapter 3, the bare molecular propagator needs to be corrected by self energy insertions as shown in Fig. 3.2. The physical dressed propagator is then

$$D_{\mu\nu}(p,\omega) = \left(\frac{1}{D_0^{-1}(p,\omega) - \Sigma(p,\omega)}\right)_{\mu\nu}. \tag{6.8}$$

The value of the self energy bubble is

$$\Sigma_{\mu\nu}(p,\omega) \;=\; 2ig^2 \int \frac{dq_0}{2\pi}\frac{d^3q}{(2\pi)^3}\frac{q_\mu q_\nu\, \xi^2(|\vec{q}|)}{[\omega/2 + q_0 - (q+p/2)^2/2m + i0]\,[\omega/2 - q_0 - (q-p/2)^2/2m + i0]}. \tag{6.9}$$

The factor 2 appears as the appropriate combinatorial factor; in the s-wave problem, the operators giving the propagators of the two distinguishable fermionic atoms inside the bubble could be contracted in only one way, in the present case there are two possible ways. Notice how the physical molecular propagator will in general depend on the chosen method of cut-off. To proceed, the cut-off function needs to be specified. Using the simplest cut-off, Eq. (6.5), the self energy becomes

$$\Sigma_{\mu\nu}(p,\omega) \;=\; \frac{2}{3}g^2\delta_{\mu\nu}\frac{1}{2\pi^2}\int_0^\Lambda dq \frac{q^4}{\omega - q^2/m - p^2/4m + i0}$$

$$= \quad \delta_{\mu\nu}\left\{-c_1 + c_2(q^2/4m - q_0 - i0) \right.$$
$$\left. -c_2\frac{\sqrt{m}}{\Lambda}(q^2/4m - q_0 - i0)^{3/2}\tan^{-1}\frac{\Lambda}{\sqrt{q^2/4 - mq_0 - i0}}\right\}. \quad (6.10)$$

The integral scales as q^3 for large momenta. Thus, two cut-off dependent parameters have been defined,

$$c_1 = \frac{mg^2\Lambda^3}{9\pi^2}, \qquad c_2 = \frac{m^2g^2\Lambda}{3\pi^2}. \quad (6.11)$$

c_1 has dimensions of energy while c_2 is a very important dimensionless parameter as will become clear below.

The propagator of bosons becomes

$$D_{\mu\nu}(q, q_0) \quad =$$
$$\frac{\delta_{\mu\nu}}{(1+c_2)(q_0 - q^2/4m - \omega_0 + i0) + c_2\frac{\sqrt{m}}{\Lambda}(q^2/4m - q_0 - i0)^{3/2}\tan^{-1}\frac{\Lambda}{\sqrt{q^2/4 - mq_0}}}, \quad (6.12)$$

which is diagonal in spin indices. It is seen that c_1 disappears from the theory, it is absorbed in the *physical detuning*[1] as

$$\omega_0 = \frac{\epsilon_0 - c_1}{1 + c_2} \leq 0. \quad (6.13)$$

ω_0 is an important parameter in the theory; a negative ω_0 implies the presence of a physical bound state in the two-body system. On going through $\omega_0 = 0$ the bound state disappears and is replaced by a resonance.

6.1.2 p-wave scattering

At low energies, the scattering amplitude between two identical fermionic atoms may be approximated by [see Eq. (2.4)]

$$f_p(k) = \frac{k^2}{-v^{-1} + \frac{1}{2}k_0k^2 - ik^3}, \quad (6.14)$$

[1] In the two-channel s-wave model, a coefficient proportional to the cut-off appeared to shift the bare detuning to the physical detuning, see Eq. (2.16). No analogue of c_2 is present in the s-wave problem.

with k being the relative momentum of the two scattering atoms. Whereas the s-wave scattering amplitude $f_s(k) \to -a$ as $k \to 0$, $f_p(k) \to 0$ in the low-energy limit, demonstrating how s-wave scattering, if allowed, would dominate the scattering problem. The scattering volume v is the analogue of the s-wave scattering length, diverging and changing sign across the Feshbach resonance. The parameter k_0 is a characteristic momentum and is analogous to the effective range r_0.

In the model above, with the choice of cut-off function Eq. (6.4), the scattering amplitude is [35, 34]

$$f_p(k) = \frac{1}{\frac{6\pi}{mg^2k^2}(1+c_2)\left(\omega_0 - \frac{k^2}{m}\right) - ik}, \tag{6.15}$$

from which it is possible to identify

$$v = -\frac{mg^2}{6\pi\,(1+c_2)\,\omega_0}, \qquad k_0 = -\frac{4\Lambda\,(1+c_2)}{\pi c_2}. \tag{6.16}$$

Again it is seen how $\omega_0 = 0$ is the physical position of the resonance, the point at which the scattering volume changes sign. For $\omega_0 < 0$ the system has a low-lying bound state and as ω_0 changes sign, the bound state turns into a resonance.

6.2 Properties of p-wave Feshbach resonances

In the finite density atomic gas there will be three length scales, and thus it is possible to construct two dimensionless parameters. The interparticle separation is of order $1/\sqrt{m\epsilon_F}$, a second length scale is provided by m^2g^2, while a third is the range of the forces $R_e \sim 1/\Lambda$. The first dimensionless parameter is c_2 defined in Eq. (6.11). The second is

$$\gamma_{\rm p} = m^{3/2} g^2 \sqrt{\epsilon_F}. \tag{6.17}$$

In order for the results to be independent of the precise nature of short-distance physics, the interparticle separation must be greater than R_e. This translates into the requirement

$$\gamma_{\rm p} \ll c_2. \tag{6.18}$$

The value of $\gamma_{\rm p}$ determines the width of the Feshbach resonance in the same manner as $\gamma_{\rm s}$ determines the width of s-wave resonances. The main difference between these is that while $\gamma_{\rm s}$ increases with decreasing density, the opposite is true for $\gamma_{\rm p}$. Thus, p-wave resonances may be made arbitrarily narrow by reducing the particle density and it is possible to construct a pertubative theory, accurate across the Feshbach resonance, for densities achievable in current experiments.

That the p-wave resonances are intrinsically narrow comes from the presence of the centrifugal barrier, which adds a long ranged $1/r^2$ tail to the interatomic potential, as in $U_{\rm eff}(r) = U(r) + 1/m_r r^2$. The width of a low lying resonance may then be estimated by computing the decay rate through the effective potential and is found to be dominated by the presence of the long-ranged tail [34].

Note how, even after the shift to a physical detuning, the scattering amplitude (6.15) still depends on the regularization scheme through the parameter c_2. If $c_2 \ll 1$ then the ultraviolet cut-off indeed drops out of the problem. However, if $c_2 \gg 1$ then $k_0 \sim -\Lambda$ and the bare molecule may be integrated out, resulting in a p-wave single channel model. Feshbach resonances with $c_2 \ll 1$ are called *weak* while those with $c_2 \gg 1$ are termed the *strong* resonances. Unlike $\gamma_{\rm p}$, c_2 is an intrinsic property of the Feshbach resonance in question and depends only on the physics of the resonance, it cannot be changed simply by changing the density.

Both of the parameters c_2 and $\gamma_{\rm p}$ control the perturbative expansion in powers of the coupling constant g. The usual approach is to apply mean field theory to the system described by the Hamiltonian (6.1). This approach has been used in Refs. [35, 17, 34]. The mean field approach relies on the smallness of the coupling g which means that both $\gamma_{\rm p}$ and c_2 must be small. This is not necessarily the case since c_2 is an uncontrollable parameter.

The breakdown of mean field theory for strong p-wave resonances does not imply that no other techniques exist with which to investigate the system. Fluctuational

corrections arise from two distinct regimes of momenta, of the order of the inverse interparticle spacing and of the order of the ultraviolet cut-off. Corrections to the many-body problem are governed by the former and are small as long as $\gamma_{\rm p}$ is small. At momenta of the order of the ultraviolet cut-off only virtual particles propagate and thus corrections to mean field theory from large momenta must be few-body, resulting in a renormalization of the few-body coupling constants.

The situation is quite similar to the wide resonance s-wave superfluid studied in chapter 3. Here, the interactions between fermions were strong (and the scattering problems studied dominated by momenta of order a^{-1}) and led to non-trivial renormalizations of the few-body coupling constants, in particular it was seen how $a_{\rm b} \approx 0.60$. However, the many-body physics was dominated by physics at small momenta ($p \ll a^{-1}$) in a perturbative expansion in the gas parameter. As long as the gas parameter was small, the mean field theory remained essentially valid, with the few-body couplings non-trivially renormalized.

Finally, it should be mentioned that the p-wave Feshbach resonance investigated in the experiment [30] is narrow and strong. This estimate was performed in Ref. [34]. The existing mean field theory is valid for the narrow and weak Feshbach resonances, and is in principle not valid for this particular Feshbach resonance. The few-body physics leads to a non-trivial renormalization of coupling constants, and indeed it also leads to bound states of three identical fermionic atoms interacting close to a strong Feshbach resonance [49, 41]. A reliable method with which to investigate the strongly resonant p-wave condensates is thus needed and this is the subject of the next chapter.

Chapter 7

Strongly resonant p-wave condensates

While the weak and narrow Feshbach resonances are amenable to a mean field treatment [35, 17, 34], it is the strong and narrow p-wave Feshbach resonances which are most relevant to current experiments and properties of these are calculated in this chapter. The main results of this chapter were presented in Ref. [49].

An interesting effect in the vicinity of a strong resonance is the appearance of bound molecule-atom (trimer) states with angular momentum 1. This effect was first noticed by Y. Castin and collaborators [16]. These trimer states are quite unusual. They are very strongly bound, with a size of the order of the short-disance physics, R_e, the same as the closed-channel molecule. The binding energy is very large (of the order of Λ^2/m) and only weakly dependent on detuning from the resonance. Below, the binding energy of the trimer as a function of the strength of the resonance is found. In particular, the critical value of the strength of the resonance at which the trimer state appears is calculated.

The two-channel Hamiltonian (6.1) is valid both for weak and strong resonances. In a manner similar to the s-wave case (see chapter 3) it reduces to a one-channel model in the limit of infinitely strong resonces, i.e. as $c_2 \to \infty$. However, it is interesting to investigate the manner in which the physics evolves under the strengthening of the Feshbach resonance, in particular the appearance of three-body bound states for strong resonances. Thus the starting point will be the two-channel Hamiltonian.

As discussed in the previous chapter, in order to study the two-channel Hamiltonian (6.1), the coupling constant between the open and closed channels needs to reflect the suppression of the molecule wave-function outside the range of short-distance physics. Different regularization schemes are possible. The two choices of cut-off functions used below give results which are in qualitative agreement, although they do not completely agree quantitatively. Arguments will be given as to why the results are still qualitatively trustworthy.

A recent experiment [30] studied a gas of p-wave Feshbach molecules in ^{40}K. Unfortunately, the gas was found to be quite short-lived, with a lifetime of about 2 ms. Ref. [30] studied whether the short lifetime might be due to dipolar relaxation but found that the lifetime was shorter than predicted from losses due to dipolar relaxation alone. The presence of the trimer state opens up for the possibility of inelastic collisions in which the scattering of two molecules results in an atom and a trimer with large kinetic energies. The lifetime of the p-wave superfluid due to these decay processes is estimated below.

One question which is not addressed below is the nature of the true ground state of the system. In order to properly answer this question, the molecule-molecule scattering problem needs to be studied and the few-body coupling constants computed, as in Ref. [34] for weak resonances. A diagrammatic technique similar to the one studied in section 3.6 may be employed, but the solution of the resulting set of integral equations will be technically very difficult.

In this chapter, first the diagrammatical expansion used to study few-body problems will be discussed. Next, the three-body problem will be solved for different choices of the ultraviolet cut-off and it will be studied how the system evolves under the strengthening of the Feshbach resonance. Finally, the stability of the gas will be considered.

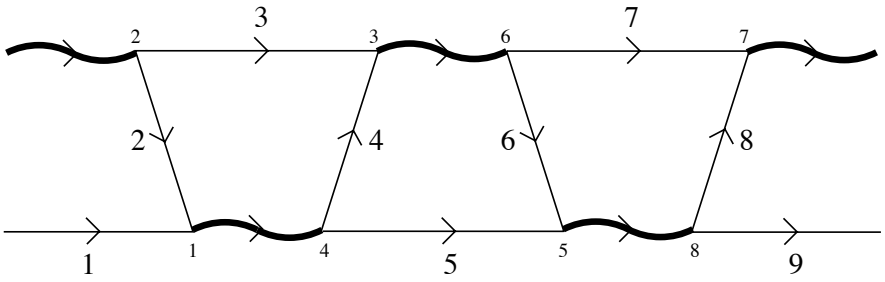

Figure 7.1: The numbering of fermion propagators and vertices as explained in the text.

7.1 The three-body problem

In this section, the three-body problem consisting of three identical fermionic atoms interacting close to a Feshbach resonance is studied. It will be assumed that the system is tuned to the BEC side of the resonance, that is

$$\omega_0 = \frac{\epsilon_0 - c_1}{1 + c_2} \leq 0, \tag{7.1}$$

and thus a physical bound two-body state exists.

It is convenient to explicitly write down the Feynman rules governing the diagrammatic expansion. These may be derived from the Hamiltonian, Eq. (6.1). In the Hamiltonian, each vertex converting two atoms into a molecule (or vice versa) contains two fermionic operators. Thus the vertices commute and they may be arranged in any desired order. The atom-molecule scattering problem contains precisely one line of fermion propagators.[1] Associate a number with each fermion line, from incoming to outgoing, and also a number with each vertex, as illustrated in Fig. 7.1. Then the Feynman rules are read off from the Hamiltonian:

(i) At vertex i where a molecule of spin μ is created associate a factor of $(p_{i+1} - p_i)_\mu/2$ where p_i is the numbered fermion momentum. At vertex i where a molecule is annihilated, associate a factor $-(p_{i+1} - p_i)_\mu/2$.

[1] This is also true for the two-boson irreducible vertex Γ appearing in the molecule-molecule scattering problem of section 3.6. The Feynman rules derived here apply equally well to molecule-molecule scattering.

(ii) Fermion contractions give the same signs as in the s-wave problem. In the three-body problem this is a factor $(-1)^{n+1}$ where n is the number of loops.

(iii) Each vertex gives a combinatorial factor of 2 arising from indistinguishability of the fermions.

(iv) Each fermion line gives a factor iG and each molecule a factor of $iD_{\mu\nu}$.

(v) Finally, each vertex joining fermions of momenta p_i and p_{i+1} gives rise to a factor $ig(|\vec{p}_i - p_{i+1}|/2) \equiv ig\,\xi(|\vec{p}_i - \vec{p}_{i+1}|/2\Lambda)$.

The atom-molecule scattering problem is studied in a similar manner to the corresponding s-wave problem of section 3.5. The kinematics is chosen as follows: An incoming molecule of spin μ has four-momentum $\left(\vec{0}, E\right)$ and the incoming fermion $(\vec{0}, 0)$. The outgoing molecule has spin ν and four-momentum $(\vec{p}, p_0 + E)$ and the outgoing atom $(-\vec{p}, -p_0)$. To calculate the s-wave scattering length, the total energy E reduces to a function $\kappa_0(\omega_0) \leq 0$ (this ensures that the molecular propagator is on-shell and will be defined precisely below) and to look for bound states the total energy must be taken less than κ_0. This is similar to the s-wave problem where $E \leq E_{\rm b} = -\frac{1}{ma^2}$.

According to the Feynman rules above, the contribution to the scattering amplitude from the Born diagram of Fig. 7.2a has the value

$$-iT^{(1)}_{\mu\nu}(\vec{p}, p_0) = 2iZ\, g^2 p_\mu p_\nu G(\vec{p}, p_0 + E)\xi\left(|\vec{p}|/\Lambda\right)\xi\left(|\vec{p}|/2\Lambda\right). \tag{7.2}$$

For proper normalization of the external propagators in the scattering amplitude, the residue Z of the molecular propagator at its pole is included (as in the s-wave three-body problem, see section 3.5). The Born diagram is proportional to $p_\mu p_\nu$ and goes to zero as $\vec{p}, p_0 \to 0$ (except in the case of scattering at zero energy with vanishing detuning).

The first loop diagram, shown in Fig. 7.2b, takes the value

$$-iT^{(2)}_{\mu\nu}(\vec{p}, p_0) \quad = \quad 8Z\, g^4 \int \frac{d^4q}{(2\pi)^4} q_\mu q_\alpha G(\vec{q}, q_0 + E)G(-\vec{q}, -q_0)\xi\left(|\vec{q}|/\Lambda\right)\xi\left(|\vec{q}|/2\Lambda\right)$$

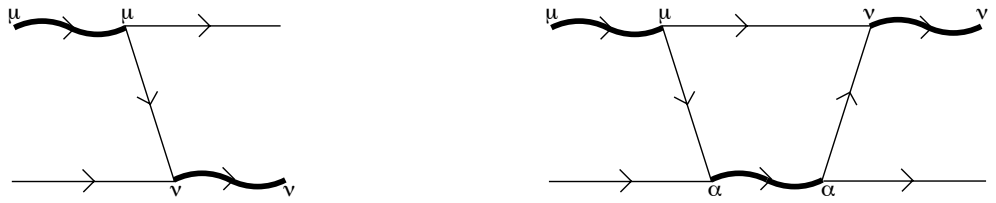

Figure 7.2: The Born diagram (a) and the first loop diagram (b) contributing to atom-molecule scattering. The molecular spin has been made explicit while the kinematics is explained in the text.

$$\times D(\vec{q}, q_0 + E) G(\vec{p} + \vec{q}, p_0 + q_0 + E)$$
$$\times (p + q/2)_\alpha (p/2 + q)_\nu \xi\left(|\vec{p} + \vec{q}/2|/\Lambda\right) \xi\left(|\vec{p}/2 + \vec{q}|/\Lambda\right). \qquad (7.3)$$

Repeated spin indices indicate a summation over the corresponding spin. The propagator of molecules has been defined as $D_{\mu\nu}(q, q_0) \equiv \delta_{\mu\nu} D(q, q_0)$ where it has been used that the molecular propagator is diagonal in spin indices (independent of the particular choice of regularization).

Using the Feynman rules above, it is seen that the generalization to an integral equation is

$$\begin{aligned} T_{\mu\nu}(\vec{p}, p_0) &= -2Z\, g^2 G(\vec{p}, p_0 + E) p_\mu p_\nu \xi\left(|\vec{p}|/\Lambda\right) \xi\left(|\vec{p}|/2\Lambda\right) \\ &-4ig^2 \int \frac{d^4q}{(2\pi)^4} T_{\mu\alpha}(\vec{q}, q_0) D(\vec{q}, q_0 + E) G(-\vec{q}, -q_0) \\ &\times G(\vec{p} + \vec{q}, p_0 + q_0 + E)(p + q/2)_\alpha (p/2 + q)_\nu \xi\left(|\vec{p} + \vec{q}/2|/\Lambda\right) \xi\left(|\vec{p}/2 + \vec{q}|/\Lambda\right). \end{aligned} \qquad (7.4)$$

Exactly as in the s-wave problem, it is possible to integrate over the loop frequency with the result $q_0 = -q^2/2m$. Let $p_0 = -p^2/2m$ to achieve the same frequency dependence in both T-matrices of the equation. Define the "on-shell" scattering amplitude $T_{\mu\nu}(\vec{p}) \equiv T_{\mu\nu}(\vec{p}, -p^2/2m)$. In order to proceed, it is advantageous to scale out the cut-off by measuring momenta in units of the cut-off, Λ. Additionally, measure the total energy

in units of Λ^2/m. Then the integral equation is

$$\begin{aligned} T_{\mu\nu}(\vec{p}) &= -2Z\, g^2 m\, G(\vec{p}, -p^2/2 + E) p_\mu p_\nu \\ &\quad -\frac{2m^2 g^2 \Lambda}{\pi^2} \int_0^\infty q^2 dq \int \frac{d\Omega_{\vec{q}}}{4\pi} T_{\mu\alpha}(\vec{q}) D(\vec{q}, -q^2/2 + E) G(\vec{p} + \vec{q}, -p^2/2 - q^2/2 + E) \\ &\quad \times (p + q/2)_\alpha (p/2 + q)_\nu \xi\left(|\vec{p} + \vec{q}/2|\right) \xi\left(|\vec{p}/2 + \vec{q}|\right). \end{aligned} \tag{7.5}$$

In writing this equation, for simplicity the dimensions of the propagators G and D have been extracted and the remaining G and D are dimensionless. The integration $\int d\Omega_{\vec{q}}$ denotes an integration over directions of $\vec{q}$.

The tensor $T_{\mu\nu}(\vec{p})$ must have the general form

$$T_{\mu\nu}(\vec{p}) = T^1(p)\delta_{\mu\nu} + T^2(p)\frac{p_\mu p_\nu}{p^2} \equiv \sum_{i=1,2} T^i(p) u^i_{\mu\nu}(\vec{p}), \tag{7.6}$$

with a set of basis tensors defined as $u^1_{\mu\nu}(\vec{p}) = \delta_{\mu\nu}$ and $u^2_{\mu\nu}(\vec{p}) = p_\mu p_\nu / p^2$. It is then possible to derive two coupled integral equations for the coefficients T^1 and T^2. Multiply Eq. (7.5) by $u^j_{\mu\nu}(\vec{p})$ and sum over spin indices. On the left hand side a product of basis tensors appears:

$$u^j_{\mu\nu}(\vec{p}) u^i_{\mu\nu}(\vec{p}) = \begin{pmatrix} 3 & 1 \\ 1 & 1 \end{pmatrix}_{ji} \equiv U_{ji}. \tag{7.7}$$

The matrix U is clearly invertible. Upon further multiplying the integral equation by the inverse matrix it becomes

$$\begin{aligned} T^j(p) &= -2Z\, g^2 m\, G(\vec{p}, -p^2/2 + E) p^2 \delta_{2,j} \\ &\quad -\frac{2m^2 g^2 \Lambda}{\pi^2} \int_0^\infty q^2 dq D(\vec{q}, -q^2/2 + E) a_{ji}(p, q, E) T^i(q), \end{aligned} \tag{7.8}$$

which is a set of two coupled integral equations. The matrix a is dimensionless and is given by

$$\begin{aligned} a_{ji}(p, q, E) &= U^{-1}_{jk} \int \frac{d\Omega_{\vec{q}}}{4\pi} G(\vec{p} + \vec{q}, -p^2/2 - q^2/2 + E) u^k_{\mu\nu}(\vec{p}) u^i_{\mu\alpha}(\vec{q}) \\ &\quad \times (p + q/2)_\alpha (p/2 + q)_\nu \xi\left(|\vec{p} + \vec{q}/2|\right) \xi\left(|\vec{p}/2 + \vec{q}|\right). \end{aligned} \tag{7.9}$$

In order to proceed, it is necessary to specify the precise form of the cut-off function ξ, as this affects both the integration kernel, through the matrix a, and the molecular propagator.

7.1.1 The hard cut-off

The coupling constant is now assumed to be constant up to the ultraviolet cut-off after which it drops to zero. That is,

$$g(|\vec{p}|) \equiv g\,\Theta(\Lambda - |\vec{p}|), \tag{7.10}$$

where Θ is the usual step function, and properties of the gas calculated with this assumption.

With the hard cut-off, the molecular propagator was found in Eq. (6.12) to be

$$D(q,q_0)=\frac{\delta_{\mu\nu}}{(1+c_2)(q_0-q^2/4m-\omega_0+i0)+\frac{c_2\sqrt{m}}{\Lambda}(q^2/4m-q_0-i0)^{3/2}\tan^{-1}\frac{\Lambda}{\sqrt{q^2/4-mq_0}}}. \tag{7.11}$$

The physical on-shell molecule in the presence of the medium must have a pole as its four-momentum vanishes [38]. That is, the molecule is affected by the detuning ω_0 and should be evaluated at a four-momentum $(\vec{q}, q_0 + \kappa_0(\omega_0))$ such that $D^{-1}\left(\vec{0}, \kappa_0(\omega_0)\right) = 0$. From Eq. (6.12) it is seen that $\kappa_0(\omega_0)$ satisfies the implicit relation

$$\omega_0 = \kappa_0(\omega_0) + \frac{c_2}{1+c_2}\frac{\sqrt{m}}{\Lambda}\left(-\kappa_0(\omega_0)\right)^{3/2}\tan^{-1}\frac{\Lambda}{\sqrt{-m\kappa_0(\omega_0)}}. \tag{7.12}$$

For $\omega_0 \ll \frac{\Lambda^2}{m}$ the function κ_0 reduces to the physical detuning.

The residue of the molecular propagator at its pole is also found from the molecular propagator. It takes the value

$$Z = \left[1 + c_2 - \frac{1}{2}\frac{c_2\kappa_0}{\Lambda^2/m - \kappa_0} - \frac{3c_2\sqrt{-m\kappa_0}}{2\Lambda}\tan^{-1}\frac{\Lambda}{\sqrt{-m\kappa_0}}\right]^{-1}, \tag{7.13}$$

and reduces to $Z \approx 1/(1+c_2)$ as $\omega_0 \to 0$.

7.1.1.1 The simplest hard cut-off

The solution of the integral equation (7.8) requires the determination of the matrix a, Eq. (7.9). Note that this matrix *does not* depend on the strength of the resonance, c_2. It is instructive to first consider the approximation in which the momenta appearing in the integral equation are cut off at the value Λ. Strictly speaking this approach is not correct, as the momenta going through the vertices are not treated in a manner invariant under Galilean transformations. Instead it corresponds to the approximation $\xi\left(|\vec{p}+\vec{q}/2|\right)\xi\left(|\vec{p}/2+\vec{q}|\right) \to \xi(|\vec{p}|)\xi(|\vec{q}|)$ in Eq. (7.9).

Using this approximation, the matrix a may be evaluated to give

$$\begin{aligned}
a_{11}(p,q,E) &= \frac{E-p^2-q^2}{4p^2} \\
&\quad -\frac{(p^2-pq+q^2-E)(p^2+pq+q^2-E)}{8p^3q}\log\frac{p^2-pq+q^2-E}{p^2+pq+q^2-E}, \\
a_{12}(p,q,E) &= \frac{6p^4+p^2(5q^2-12E)+3(q^2-E)(q^2-2E)}{12p^2q^2} \\
&\quad +\frac{(2p^2+q^2-2E)(p^2-pq+q^2-E)(p^2+pq+q^2-E)}{8p^3q^3}\log\frac{p^2-pq+q^2-E}{p^2+pq+q^2-E}, \\
a_{21}(p,q,E) &= \frac{-3E-2p^2+3q^2}{4p^2}+\frac{3(q^2-E)^2-p^2E}{8p^3q}\log\frac{p^2-pq+q^2-E}{p^2+pq+q^2-E}, \\
a_{22}(p,q,E) &= \frac{2E-2p^2-q^2}{8p^3q^3}\left[2pq(2p^2+3q^2-3E)\right. \\
&\quad \left.+\left(p^2(2p^2+4q^2-5E)+3(q^2-E)^2\right)\log\frac{p^2-pq+q^2-E}{p^2+pq+q^2-E}\right]. \qquad (7.14)
\end{aligned}$$

Note that since the total energy $E \leq 0$ there are no poles in the angular integration.

The integral equation (7.8) may then be solved at any given value of the strength of the Feshbach resonance, c_2, the total energy, E, and the detuning ω_0. Fig. 7.3 shows the functions $T^1(p)$ and $T^2(p)$ in the limit of very strong resonances with a small detuning. The s-wave scattering length is determined from

$$a_{\rm bf} = \frac{m}{3\pi}T^1(0) \qquad (7.15)$$

evaluated at $E = \kappa_0(\omega_0)$. For the specific choice of parameters

$$a_{\rm bf} \approx 3\Lambda^{-1}, \qquad \text{at } c_2 \to \infty,\ \omega_0 = -10^{-5}\Lambda^2/m. \qquad (7.16)$$

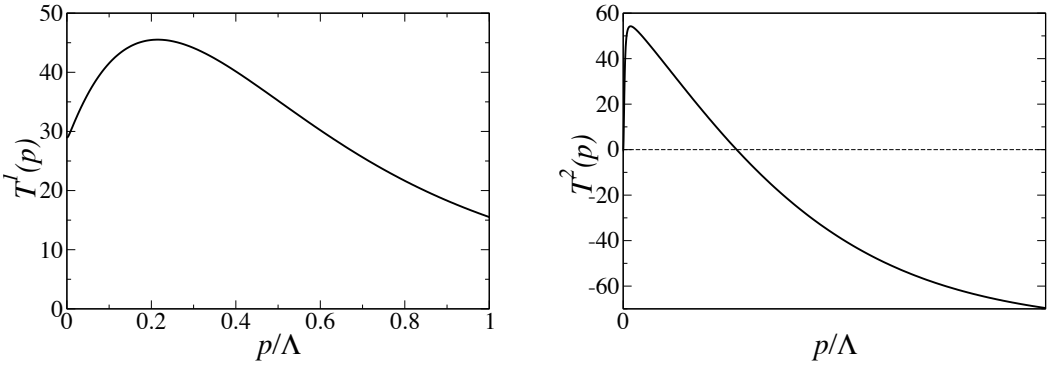

Figure 7.3: The functions $T^1(p)$ and $T^2(p)$ in units of $\frac{1}{m\Lambda}$ evaluated using the simplest hard cut-off.

The scattering length only weakly depends on the detuning as will be discussed below.

Bound trimer states are found as solutions to the homogenous integral equation at $E < \kappa_0$. One bound state is found in the problem, at

$$E_3 \approx -0.04\Lambda^2/m, \qquad \text{at } c_2 \to \infty, \omega_0 = -10^{-5}\Lambda^2/m. \tag{7.17}$$

The binding energy is seen to be proportional to Λ^2, thus this three-body bound state is of size of the order of R_e. The method used to find the binding energy is the following (also discussed in chapter 3): A bound state in the problem shows up as a pole of the scattering amplitude at a negative total energy, the binding energy E_3. This in turn corresponds to a solution of the homogenous integral equation at that energy, thus to an eigenvalue equal to 1 of the integration kernel. Fig. 7.4 shows the behavior of the largest eigenvalues as functions of the total energy E. It is seen that an eigenvalue equal to 1 is obtained for a total energy of $E_\mathrm{b} \approx -0.04\Lambda^2/m$.

7.1.1.2 The invariant hard cut-off

It is now interesting to see if the simplified approach above indeed captured the correct physics. Therefore, the matrix a of Eq. (7.9) is now evaluated in an invariant

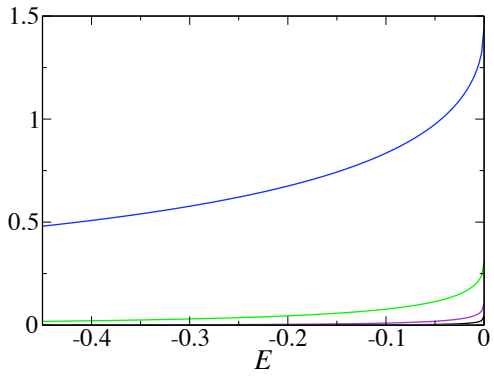

Figure 7.4: The largest eigenvalues of the integration kernel in Eq. (7.8) as a function of total energy E in units of Λ^2/m. The eigenvalues are evaluated at $c_2 \to \infty$ and $\omega_0 = -10^{-5}\Lambda^2/m$. The largest eigenvalue is seen to go through 1 at $E \approx -0.04\Lambda^2/m$, corresponding to the appearance of the bound trimer.

way, using

$$\xi\left(|\vec{p}+\vec{q}/2|\right)\xi\left(|\vec{p}/2+\vec{q}|\right) = \Theta\left(\Lambda - p^2 - q^2/4 - \vec{p}\cdot\vec{q}\right)\Theta\left(\Lambda - q^2 - p^2/4 - \vec{p}\cdot\vec{q}\right). \quad (7.18)$$

It is seen that the maximum possible value of the momenta is now 2Λ and the integral equation is solved on the interval $p \in [0, 2]$. The matrix a may again be obtained exactly. For $p, q \leq \Lambda$ it reduces to the result (7.14) above. For larger p, q the limits of angular integration depend on the cut-off and, although the integration is simple to perform, the resulting expressions are not very enlightening and will not be written here.

In the limit of very strong resonances ($c_2 \to \infty$) the integral equation (7.8) reduces to

$$\begin{aligned} T^j(p) &= -2Z\, g^2 m\, G(\vec{p}, -p^2/2 + E) p^2 \delta_{2,j} \\ &- \frac{6}{\pi^2}\int_0^\infty q^2 dq \frac{1}{E - 3q^2/4 - \omega_0 + (3q^2/4 - E)^{3/2}\tan^{-1}\frac{1}{\sqrt{3q^2/4 - E}}} a_{ji}(p, q, E) T^i(q). \end{aligned} \quad (7.19)$$

It is of interest to study the behavior of the physics as the strength of the resonance is increased. Had c_2 been zero, the only diagram which would have contributed is the Born diagram whose value was computed in Eq. (7.2) above. The Born contribution

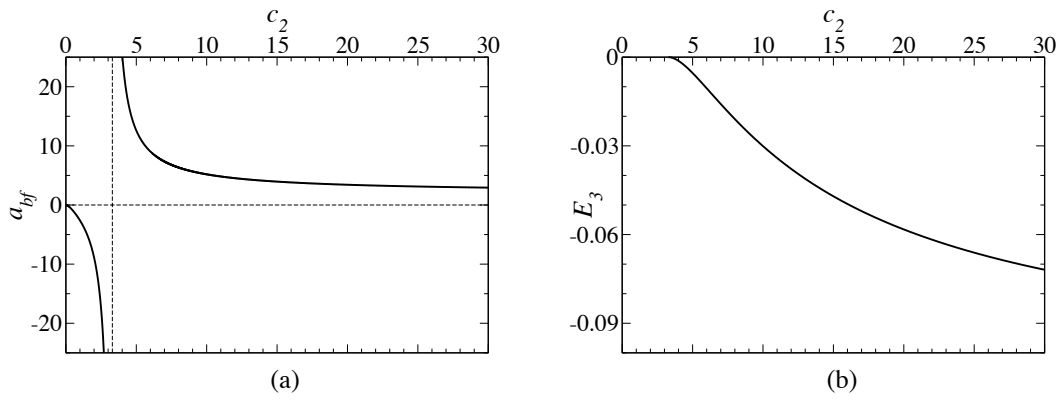

Figure 7.5: (a) The atom-molecule scattering length in units of Λ^{-1} and (b) the binding energy in units of Λ^2/m, both as functions of c_2. The position of the appearance of the bound state is seen to be at $c_{2,\mathrm{crit}} \approx 3.3$.

does not have a pole at a negative energy and thus the bound state is absent for weak resonances. It follows that the bound state found for strong resonances must develop at a certain critical value of c_2. This is indeed the case as depicted in Fig. 7.5. The scattering length a_{bf} vanishes for $c_2 = 0$ since the Born term is purely proportional to $p_\mu p_\nu$, see Eq. (7.2). a_{bf} becomes negative for small values of c_2 and diverges to $-\infty$ at the critical value

$$c_{2,\mathrm{crit}} \approx 3.3. \tag{7.20}$$

The scattering length then reemerges from $+\infty$ to go asymptotically towards the value of

$$a_{\mathrm{bf}} \approx 1.9\Lambda^{-1}, \tag{7.21}$$

as c_2 approaches ∞. The critical value of $c_2 \approx 3.3$ is exactly the value at which the bound state appears. For large values of c_2 the binding energy saturates at

$$E_3 \approx -0.11\Lambda^2/m. \tag{7.22}$$

The values obtained here in the large c_2 limit are somewhat different from the ones obtained above using the simplified hard cut-off, but the results are still qualitatively

consistent.

7.1.2 Softening the cut-off

The above results may be tested by applying a different cut-off function. In this section, the coupling constant $g(|\vec{p}|) \equiv g\,\xi(|\vec{p}|)$ is chosen to be

$$g(|\vec{p}|) = g\,\exp\left(-p^2/\Lambda^2\right), \tag{7.23}$$

which is more smooth than the hard cut-off used above.

The first order of the day is to compute the propagator of molecules using the new cut-off. To this end, the fermionic loop Σ is needed and according to Eq. (6.10) it becomes

$$\begin{aligned}
\Sigma_{\mu\nu}(p,p_0) &= \delta_{\mu\nu}\frac{g^2}{3\pi^2}\int dq \frac{q^4\exp\left(-2q^2/\Lambda^2\right)}{p_0 - q^2/m - p^2/4 + i0} \\
&= -\frac{mg^2}{3\pi^2}\delta_{\mu\nu}\left\{\frac{\sqrt{2\pi}}{16}\Lambda^3 - \frac{\sqrt{2\pi}}{4}m\Lambda(q^2/4m - q_0 - i0)\right. \\
&\qquad \left. + \frac{\pi}{2}m^{3/2}(q^2/4m - q^0 - i0)^{3/2}\exp\left(2\frac{q^2/4m - q_0}{\Lambda^2/m}\right)\mathrm{Erfc}\sqrt{2\frac{q^2/4m - q_0}{\Lambda^2/m}}\right\} \\
&\equiv \delta_{\mu\nu}\left\{-c_1' + c_2'(q^2/4m - q_0 - i0) - c_2'\frac{\sqrt{m}}{\Lambda}(q^2/4m - q_0 - i0)^{3/2}F\left(\frac{q^2/4m - q_0}{\Lambda^2/m}\right)\right\}.
\end{aligned} \tag{7.24}$$

The coefficients c_1' and c_2' are the analogues of c_1 and c_2 calculated in chapter 6 for the hard cut-off. They are slightly changed and take the values

$$c_1' = \frac{mg^2\Lambda^3}{12(2\pi)^{3/2}}, \qquad c_2' = \frac{m^2g^2\Lambda}{3(2\pi)^{3/2}}. \tag{7.25}$$

The function F replaces the arctan present in the hard cut-off propagator and is given by

$$F(x) = \sqrt{2\pi}\exp(2x)\mathrm{Erfc}\sqrt{2x}. \tag{7.26}$$

Erfc is the complementary error function

$$\mathrm{Erfc}(x) \equiv 1 - \frac{2}{\sqrt{\pi}}\int_0^x e^{-t^2}dt. \tag{7.27}$$

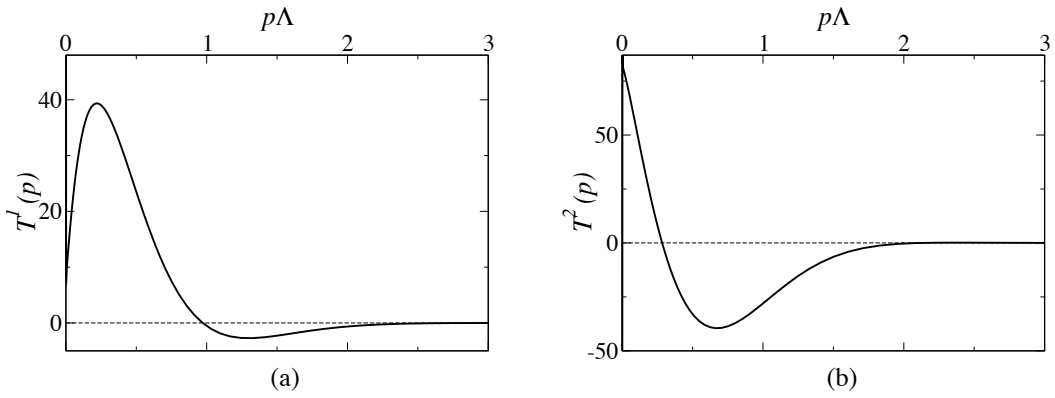

Figure 7.6: The functions $T^1(p)$ and $T^2(p)$ in units of $\frac{1}{m\Lambda}$ evaluated using the "soft" cut-off.

Note that $F(x)_{x\to 0} \approx \sqrt{2\pi}$ while $F(x)_{x\to\infty} \approx x^{-1/2}$.

Using Eq. (6.8) the molecular propagator becomes

$$D_{\mu\nu}(\vec{q}, q_0) = \frac{\delta_{\mu\nu}}{(1+c_2')(q_0 - q^2/4m - \omega_0) + c_2'\frac{\sqrt{m}}{\Lambda}(q^2/4m - q_0 - i0)^{3/2} F\left(\frac{q^2/4m - q_0}{\Lambda^2/m}\right)}. \tag{7.28}$$

As above, $\omega_0 = \frac{\epsilon_0 - c_1'}{1+c_2'}$. The on-shell molecular propagators must be evaluated at $D(\vec{q}, q_0 + \kappa_0(\omega_0))$ with κ_0 satisfying the implicit relation

$$\omega_0 = \kappa_0(\omega_0) + \frac{c_2'}{1+c_2'}\frac{\sqrt{m}}{\Lambda}(-\kappa_0(\omega_0))^{3/2} F\left(-\frac{m\kappa_0(\omega_0)}{\Lambda^2}\right). \tag{7.29}$$

The residue of the molecular propagator at its pole takes the value

$$Z = \left[1 + c_2' - \frac{2c_2'}{\sqrt{\pi}}\frac{m\kappa_0(\omega_0)}{\Lambda^2} - c_2'\left(\frac{3}{2} - \frac{2m\kappa_0(\omega_0)}{\Lambda^2}\right)\sqrt{\frac{-m\kappa_0(\omega_0)}{\Lambda^2}} F\left(-\frac{m\kappa_0(\omega_0)}{\Lambda^2}\right)\right]^{-1} \tag{7.30}$$

and reduces to $Z \approx 1/(1+c_2')$ as the detuning vanishes.

In the limit $c_2' \to \infty$ and $\omega_0 \to 0$ the scattering amplitudes $T^1(p)$ and $T^2(p)$ are shown in Fig. 7.6. These are obtained by solving the integral equation (7.8) using the exponential cut-off. The functions are seen to approximately match those obtained in the simplified hard cut-off problem, see Fig. 7.3.

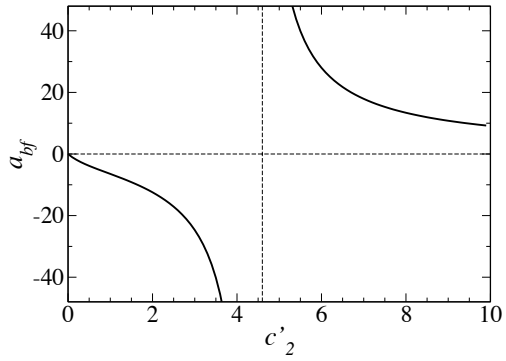

Figure 7.7: Behavior of the scattering length in units of Λ^{-1} under a change of strength of the resonance.

Fig. 7.7 depicts the scattering length as a function of the strength of the resonance. The detuning has here been taken to vanish. The critical strength of the resonance, above which the bound trimer state is present, is found to be

$$c'_{2,\text{crit}} \approx 4.6. \tag{7.31}$$

The results presented above for the hard and exponential cut-offs do not match completely, yet the qualitative behavior is found to be the same. It should be emphasized that the binding energy for strong resonances goes as Λ^2/m and is very large. The binding energy is thus sensitive to the physics at large momenta, i.e. to the specific choice of the regulator $g(|\vec{p}|)$. The question is then, does the existence of the trimer depend on the choices of $g(|\vec{p}|)$ presented above, that is, is it an artifact of the model and not the actual physical phenomena? To answer this question, consider the system close to the formation of the trimer, i.e. c_2 close to $c_{2,\text{crit}}$. Here, the binding energy of the trimer may be arbitrarily small and is a low energy phenomenon, insensitive to the choice of regulator (on the other hand, the precise value of $c_{2,\text{crit}}$, being proportional to Λ, does depend on the choice of $g(|\vec{p}|)$). As c_2 is increased from $c_{2,\text{crit}}$, the binding energy E_3 quickly becomes large. However, once the trimer has formed, changing the

regularization scheme to make the model more realistic at short distances does not make the trimer disappear. Indeed, in order for the trimer to disappear at some $c_2 > c_{2,\mathrm{crit}}$, the binding energy would have to first become large and then again drop to zero. The disappearance of the trimer would then again be a low energy phenomenon and would be predicted by the theory, contrary to what was found above. In this sense, even though the binding energy of the trimer is large, the existence of the trimer is a result of low energy physics. In conclusion, although the precise value of the binding energy of the trimer depends on the choice of regulator, the presence of the trimer state for strong resonances does not.

7.2 Stability of the p-wave superfluid

It is important to estimate the lifetime of the p-wave superfluid. In the strongly resonant BEC regime studied here, one of the main decay channels will be inelastic collisions in which two molecules turn into an atom and a trimer. In the process, the large binding energy of the trimer will be released as kinetic energy and the particles are lost from the system.

As in the case of s-wave collisonal losses studied in section 5.2.1 the loss rate will be written as

$$\dot{n}_{\mathrm{b}} = -\alpha_{\mathrm{in}} n_{\mathrm{b}}^2. \tag{7.32}$$

n_{b} is again the density of bosonic molecules. The inelastic relaxation rate is given by

$$\alpha_{\mathrm{in}} = \frac{2}{m} \langle k_i \sigma_{\mathrm{in}}(k_i) \rangle . \tag{7.33}$$

Here, k_i is defined as the relative momentum of the incident molecules and the average is taken over k_i. The inelastic scattering cross section is given by [44]

$$\sigma_{\mathrm{in}} = \int |f_{\mathrm{in}}|^2 d\Omega \frac{k_f}{k_i}. \tag{7.34}$$

f_{in} is the inelastic scattering amplitude into the final relative momentum k_f and is of order R_e, just like the three-body scattering length above was found to be proportional

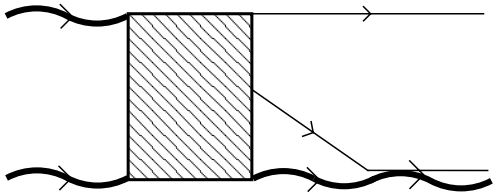

Figure 7.8: The processes which lead to the inelastic losses, Eq. (7.33). The trimer is illustrated as the binding of a fermion and a molecule.

to $1/\Lambda \sim R_e$. This may be seen from estimating the behavior of diagrams of the type shown in Fig. 7.8. These diagrams are similar to the form studied in the s-wave four-fermion problem but in the p-wave formalism. The final relative momentum arises from the kinetic energy released in the binding of three fermionic atoms into a trimer, thus $k_f \sim \Lambda \sim 1/R_e$ and

$$\alpha_{\rm in} \sim \frac{R_e}{m}. \tag{7.35}$$

Additionally, there are inelastic decay channels similar to those studied in section 5.2.1 in which a molecule decays into a deeply bound molecular state in the presence of an additional atom or molecule. Estimates similar to the above show that the decay rate due to these processes are of the same order as $\alpha_{\rm in}$. Note that these are present both for weak and strong resonances, unlike the decay to the trimer state.

Consider the experiment described in Ref. [30] in which it was found that the lifetime of diatomic molecules was quite short, of the order of 2 ms. It is interesting to estimate whether this could be explained by the losses due to the inelastic processes. The decay rate is $\Gamma_{\rm in} \sim \alpha_{\rm in} n$ and is density dependent. The atomic density in the experiment was $n \approx 7 \times 10^{-12}{\rm cm}^{-3}$ and R_e estimated by the size of the molecules to be .02 a_0. Thus the decay rate is of the order of 10 Hz, corresponding to a lifetime of about 100 ms. However, the prefactor to the estimate is uncertain and it is also unknown whether the losses observed in Ref. [30] would depend on the density. In conclusion, it is uncertain whether the observed lifetime of diatomic molecules in Ref. [30] is limited

by inelastic collisions.

Shortly after Ref. [49], containing the work described in this chapter, became available on-line, the paper [41] by Jona-Lasinio *et al* appeared in which similar conclusions were obtained for the p-wave superfluid.

Chapter 8

Conclusions and outlook

In this thesis, the s- and p-wave paired superfluids have been investigated. In the wide-resonance s-wave crossover, properties of the BEC regime were computed in the gas parameter expansion. Higher order corrections were found, and the mass imbalanced BEC was considered. It was studied how p-wave resonances naturally fall into categories of weak and strong depending on the precise details of the Feshbach resonance, and it was demonstrated how the strongly resonant superfluid is unstable towards the formation of strongly bound trimers with angular momentum 1. The rate of losses arising from collisional relaxation was estimated and it was seen how the predicted lifetime of the gas was slightly overestimated compared with the relevant experiment.

A prominent element throughout the thesis has been the constant interplay between few- and many-body physics. This was observed in the s-wave BEC regime, where few-body physics determined the molecule-molecule scattering length a_{b} in terms of the atom-atom scattering length a. Once a_b was known, the many-body physics was derived in terms of this few-body parameter. The decay rate of the superfluid due to collisional relaxation in both the s- and the p-wave superfluids was also demonstrated to depend on few-body physics.

Possible future directions of study in the s-wave case include finite temperature extensions of the work. A study of the excitation spectrum at momenta of the order of the inverse scattering length, for which the underlying structure of the composite bosons

is probed, might prove fruitful. Finally, it would be interesting to compute higher order corrections to the chemical potential and ground state energy which explicitly demonstrate the underlying fermionic structure of the BEC of composite bosons.

An exciting prospect is to restrict the p-wave superfluid to two spatial dimensions. Here, the BCS phase has been shown to be topological and will support vortices with non-Abelian excitations [62, 35], both necessary ingredients for a fault tolerant quantum computer [42]. It remains to be seen whether a stable, two-dimensional p-wave superfluid can be achieved.

Bibliography

[1] A. A. Abrikosov, L. P. Gorkov, and I. E. Dzyaloshinski. Methods of Quantum Field Theory in Statistical Physics. Dover Publications, Cambridge, UK, 1977.

[2] J. O. Andersen. Theory of the weakly interacting Bose gas. Rev. Mod. Phys., 76:599, 2004.

[3] M. H. Anderson, J. R. Ensher, M. R. Matthews, C. E. Wieman, and E. A. Cornell. Observation of Bose-Einstein condensation in a dilute atomic vapor. Science, 269:198, 1995.

[4] A. V. Andreev, V. Gurarie, and L. Radzihovsky. Nonequilibrium dynamics and thermodynamics of a degenerate Fermi gas across a Feshbach resonance. Phys. Rev. Lett., 93:130402, 2004.

[5] J. Bardeen, L. N. Cooper, and J. R. Schrieffer. Microscopic theory of superconductivity. Phys. Rev., 106:162, 1957.

[6] J. Bardeen, L. N. Cooper, and J. R. Schrieffer. Theory of superconductivity. Phys. Rev., 108:1175, 1957.

[7] P. F. Bedaque, H.-W. Hammer, and U. van Kolck. The three-boson system with short-range interactions. Nucl.Phys. A, 646:444, 1999.

[8] S. T. Beliaev. Application of the methods of quantum field theory to a system of bosons. Sov. Phys. JETP, 7:289, 1958.

[9] S. T. Beliaev. Energy-spectrum of a non-ideal Bose gas. Sov. Phys. JETP, 7:299, 1958.

[10] V. B. Berestetskii, E. M. Lifshitz, and L. P. Pitaevskii. Quantum Electrodynamics. Pergamon Press, Oxford, UK, 1982.

[11] S. Bose. Plancks gesetz und lichtquantenhypothese. Z. Phys., 26:178, 1924.

[12] E. Braaten and H.-W. Hammer. Universality in few-body systems with large scattering length. Phys. Rept., 428:259, 2006.

[13] C. C. Bradley, C. A. Sackett, J. J. Tollett, and R. G. Hulet. Evidence of Bose-Einstein condensation in an atomic gas with attractive interactions. Phys. Rev. Lett., 75:1687, 1995.

[14] I. V. Brodsky, M. Yu. Kagan, A. V. Klaptsov, R. Combescot, and X. Leyronas. Bound states of three and four resonantly interacting particles. JETP Letters, 82:273, 2005.

[15] G. Bruun and C. Pethick. Effective theory of Feshbach resonances and many-body properties of Fermi gases. Phys. Rev. Lett., 92:140404, 2004.

[16] Y. Castin. Private communication.

[17] C.-H. Cheng and S.-K. Yip. Anisotropic Fermi superfluid via p-wave Feshbach resonance. Phys. Rev. Lett., 95:070404, 2005.

[18] L. N. Cooper. Bound electron pairs in a degenerate Fermi gas. Phys. Rev., 104:1189, 1956.

[19] F. Dalfovo, S. Giorgini, L. P. Pitaevskii, and S. Stringari. Theory of Bose-Einstein condensation in trapped gases. Rev. Mod. Phys., 71:463, 1999.

[20] G. S. Danilov. On the 3-body problem with short-range forces. Sov. Phys. JETP, 13:349, 1961.

[21] K. B. Davis, M.-O. Mewes, M. R. Andrews, N. J. van Druten, D. S. Durfee, D. M. Kurn, and W. Ketterle. Bose-Einstein condensation in a gas of sodium atoms. Phys. Rev. Lett., 75:3969, 1995.

[22] C. A. R. Sá de Melo and S. S. Botelho. Quantum phase transition in the BCS-to-BEC evolution of p-wave Fermi gases. J. Low Temp. Phys., 140:409, 2005.

[23] B. DeMarco and D. S. Jin. Onset of Fermi degeneracy in a trapped atomic gas. Science, 285:1703, 1999.

[24] D. M. Eagles. Possible pairing without superconductivity at low carrier concentrations in bulk and thin-film superconducting semiconductors. Phys. Rev., 186:456, 1969.

[25] V. N. Efimov. Weakly-bound states of 3 resonantly-interacting particles. Sov. J. Nucl. Phys., 12:589, 1971.

[26] A. Einstein. Quantentheorie des einatomigen idealen Gases. Zweite Abhandlung. Sitzungsber. Preuss. Akad. Wiss., 1925:3, 1925.

[27] H. Feshbach. Unified theory of nuclear reactions. Ann. Phys., 5:357, 1958.

[28] H. Feshbach. A unified theory of nuclear reactions II. Ann. Phys., 19:287, 1962.

[29] A. L. Fetter and J. D. Walecka. Quantum Theory of Many-Particle Systems. Dover, New York, USA, 2003.

[30] J. P. Gaebler, J. T. Stewart, J. L. Bohn, and D. S. Jin. p-wave Feshbach molecules. Phys. Rev. Lett., 98:200403, 2007.

[31] V. M. Galitskii. The energy spectrum of a non-ideal fermi gas. Sov. Phys. JETP, 7:104, 1958.

[32] S. Giorgini, L. P. Pitaevskii, and S. Stringari. Theory of ultracold Fermi gases, 2007. arXiv.org:0706.3360.

[33] M. Greiner, C. A. Regal, and D. S. Jin. Emergence of a molecular Bose-Einstein condensate from a Fermi gas. Nature, 426:537, 2003.

[34] V. Gurarie and L. Radzihovsky. Resonantly-paired fermionic superfluids. Ann. Phys., 322:2, 2007.

[35] V. Gurarie, L. Radzihovsky, and A. V. Andreev. Quantum phase transitions across a p-wave Feshbach resonance. Phys. Rev. Lett., 94:230403, 2005.

[36] T.-L. Ho and R. B. Diener. Fermion superfluids of nonzero orbital angular momentum near resonance. Phys. Rev. Lett., 94:090402, 2005.

[37] M. Holland, S. J. J. M. F. Kokkelmans, M. L. Chiofalo, and R. Walser. Resonance superfluidity in a quantum degenerate Fermi gas. Phys. Rev. Lett., 87:120406, 2001.

[38] N. M. Hugenholtz and D. Pines. Ground-state energy and excitation spectrum of a system of interacting bosons. Phys. Rev., 116:489, 1959.

[39] M. Iskin and C. A. R. Sá de Melo. Mixtures of ultracold fermions with unequal masses. Physical Review A, 76:013601, 2007.

[40] S. Jochim, M. Bartenstein, A. Altmeyer, G. Hendl, S. Riedl, C. Chin, J. Hecker Denschlag, and R. Grimm. Bose-Einstein condensation of molecules. Science, 302:2101, 2003.

[41] M. Jona-Lasinio, L. Pricoupenko, and Y. Castin. Three fully polarized fermions close to a p-wave Feshbach resonance, 2007. arXiv.org:0708.0610.

[42] A. Kitaev. Fault-tolerant quantum computation by anyons. Ann. Phys., 303:2, 2003.

[43] F. R. Klinkhamer and G. E. Volovik. Quantum phase transition for the BEC-BCS crossover in condensed matter physics and CPT violation in elementary particle physics. JETP Lett., 80:343, 2004.

[44] L. D. Landau and E. M. Lifshitz. Quantum Mechanics. Butterworth-Heinemann, Oxford, UK, 1981.

[45] T. D. Lee, K. Huang, and C. N. Yang. Eigenvalues and eigenfunctions of a Bose system of hard spheres and its low-temperature properties. Phys. Rev., 106:1135, 1957.

[46] T. D. Lee and C. N. Yang. Many-body problem in quantum mechanics and quantum statistical mechanics. Phys. Rev., 105:1119, 1957.

[47] A. J. Leggett. In Modern Trends in the Theory of Condensed Matter, pages 13–27. Springer-Verlag, Berlin, Germany, 1980.

[48] A. J. Leggett. Bose-Einstein condensation in the alkali gases: Some fundamental concepts. Rev. Mod. Phys., 73:307, 2001.

[49] J. Levinsen, N. Cooper, and V. Gurarie. Strongly-resonant p-wave superfluids. Phys. Rev. Lett., 99:210402, 2007.

[50] J. Levinsen and V. Gurarie. Properties of strongly paired fermionic condensates. Phys. Rev. A, 73:053607, 2006.

[51] F. London. The λ-phenomenon of liquid helium and the Bose-Einstein degeneracy. Nature, 141:643, 1938.

[52] F. London. On the Bose-Einstein condensation. Phys. Rev., 54:947, 1938.

[53] P. Nozières and S. Schmitt-Rink. Bose condensation in an attractive fermion gas: From weak to strong coupling superconductivity. J. Low Temp. Phys., 59:195, 1985.

[54] H. K. Onnes. On the sudden rate at which the resistance of mercury disappears. Akad. van Wetenschappen, 14:113, 1911.

[55] C. J. Pethick and H. Smith. Bose-Einstein Condensation in Dilute Gases. Cambridge University Press, Cambridge, UK, 2002.

[56] D. S. Petrov. Three-body problem in Fermi gases with short-range interparticle interaction. Phys. Rev. A, 67:010703, 2003.

[57] D. S. Petrov, C. Salomon, and G. V. Shlyapnikov. Weakly bound dimers of fermionic atoms. Phys. Rev. Lett., 93:090404, 2004.

[58] D. S. Petrov, C. Salomon, and G. V. Shlyapnikov. Diatomic molecules in ultracold Fermi gases - Novel composite bosons. J. Phys. B: At. Mol. Opt. Phys., 38:S645, 2005.

[59] D. S. Petrov, C. Salomon, and G. V. Shlyapnikov. Scattering properties of weakly bound dimers of fermionic atoms. Phys. Rev. A, 71:012708, 2005.

[60] P. Pieri and G. C. Strinati. Strong-coupling limit in the evolution from BCS superconductivity to Bose-Einstein condensation. Phys. Rev. B, 61:15370, 2000.

[61] W. H. Press, S. A. Teukolsky, W. T. Vetterling, and B. P. Flannery. Numerical Recipes in Fortran 77: The Art of Scientific Computing. Cambridge University Press, Cambridge, UK, 1996.

[62] N. Read and D. Green. Paired states of fermions in two dimensions with breaking of parity and time-reversal symmetries and the fractional quantum Hall effect. Phys. Rev. B, 61:10267, 2000.

[63] Yu. B. Rumer. A simple model in the theory of superconductivity. Sov. Phys. JETP, 10:409, 1960.

[64] C. A. R. Sá de Melo, M. Randeria, and J. R. Engelbrecht. Crossover from BCS to Bose superconductivity: Transition temperature and time-dependent Ginzburg-Landau theory. Phys. Rev. Lett., 71:3202, 1993.

[65] K. Sawada. Ground-state energy of Bose-Einstein gas with repulsive interaction. Phys. Rev., 116:1344, 1959.

[66] F. Schreck, L. Khaykovich, K. L. Corwin, G. Ferrari, T. Bourdel, J. Cubizolles, and C. Salomon. Quasipure Bose-Einstein condensate immersed in a Fermi sea. Phys. Rev. Lett., 87:080403, 2001.

[67] C. H. Schunck, M. W. Zwierlein, C. A. Stan, S. M. F. Raupach, W. Ketterle, A. Simoni, E. Tiesinga, C. J. Williams, and P. S. Julienne. Feshbach resonances in fermionic ^{6}Li. Phys. Rev. A, 71:045601, 2005.

[68] G. V. Skorniakov and K. A. Ter-Martirosian. 3 body problem for short range forces I. scattering of low energy neutrons by deuterons. Sov. Phys. JETP, 4:648, 1957.

[69] C. Ticknor, C. A. Regal, D. S. Jin, and J. L. Bohn. Multiplet structure of Feshbach resonances in nonzero partial waves. Phys. Rev. A, 69:042712, 2004.

[70] Eddy Timmermans, Kyoko Furuya, Peter W. Milonni, and Arthur K. Kerman. Prospect of creating a composite Fermi-Bose superfluid. Phys. Lett. A, 285:228, 2001.

[71] Eddy Timmermans, Paolo Tommasini, Mahir Hussein, and Arthur Kerman. Feshbach resonances in atomic Bose-Einstein condensates. Physics Reports, 315:199, 1999.

[72] A. G. Truscott, K. E. Strecker, W. I. McAlexander, G. B. Partridge, and R. G. Hulet. Observation of Fermi pressure in a gas of trapped atoms. Science, 291:2570, 2001.

[73] M. Y. Veillette, D. E. Sheehy, and L. Radzihovsky. Large-N expansion for unitary superfluid Fermi gases. Phys. Rev. A, 75:043614, 2007.

[74] G. E. Volovik. Exotic Properties of Superfluid ^{3}He. World Scientific, Singapore, 1992.

[75] J. von Stecher, C. H. Greene, and D. Blume. BEC-BCS crossover of a trapped two-component Fermi gas with unequal masses. Phys. Rev. A, 76:053613, 2007.

[76] T. T. Wu. Ground state of a Bose system of hard spheres. Phys. Rev., 115:1390, 1959.

[77] M. W. Zwierlein, J. R. Abo-Shaeer, A. Schirotzek, C. H. Schunck, and W. Ketterle. Vortices and superfluidity in a strongly interacting Fermi gas. Nature, 435:1047, 2005.

[78] M. W. Zwierlein, C. A. Stan, C. H. Schunck, S. M. F. Raupach, S. Gupta, Z. Hadzibabic, and W. Ketterle. Observation of Bose-Einstein condensation of molecules. Phys. Rev. Lett., 91:250401, 2003.